Dependency of 3D chromatin folding on RNA polymerase II at different cell cycle stages

Dissertation

for the award of the degree
"Doctor rerum naturalium"
of the Georg-August-Universität Göttingen

within the doctoral program
International Max Planck Research School for Genome Science
of the Georg-August University School of Science (GAUSS)

submitted by

Nadine Übelmesser

from Nürnberg

Göttingen 2023

Thesis Advisory Committee

Prof Argyris Papantonis (Supervisor)

Institute of Pathology, University Medical Center Göttingen,

Dr. Ufuk Günesdogan

Department of Developmental Biology, Göttingen Center for Molecular Biosciences

Prof. Matthias Dobbelstein

Institute of Molecular Oncology, University Medical Center Göttingen

Members of Examination Board

1st referee: **Prof Argyris Papantonis**

2nd referee: **Dr. Ufuk Günesdogan**

Further members of Examination Board

Prof. Dr. Heidi Hahn

Department of developmental genetics, University Medical Center Göttingen

Dr. Marieke Oudelaar

Max Planck Institute for Biophysical Chemistry, Göttingen

Prof. Elisabeth Heßmann

Department of Gastroenterology, University Medical Center Göttingen

Date of oral examination: 29.06.2023

Table of Contents

List of abbreviations

3C	Chromosome conformation capture
1D	One-dimensional
3D	Three-dimensional
ABC	ATP binding cassette
AID	Auxin-inducible degron
ATAC-Seq	Assay for Transposase-Accessible Chromatin using sequencing
CDK	Cyclin-dependent kinase
Co-IP	Co-Immunoprecipitation
CTCF	CCCTC-Binding Factor
CTD	Carboxy-Terminal Domain
DNA	Deoxyribonucleic acid
DKO	Double knockout
E-P	Enhancer-Promoter
Fig	Figure
FISH	Fluorescence in situ hybridisation
Kb	kilobase
KD	Knockdown
KO	Knockout
mAID	Mini AID
Mb	megabase
MNase	Micrococcal nuclease
NEBD	nuclear envelope break-down
PIC	Preinitiation Complex
POI	Protein of interest
PTM	post-translational modification
RNAPII	RNA polymerase II
SE	super-enhancers
Ser5P	Phosphorylated RNAPII at Ser5
SMC	Structural maintenance of chromosomes
TAD	Topologically associated domain
TBP	TATA box-binding protein
TF	Transcription factor
TIR1	Transport inhibitor response 1
TSS	Transcription start site

Summary

In human cells, the genetic information is organised in a multilayer fashion. During the cell cycle, chromatin undergoes dramatic structural changes. For proper inheritance, chromatin is compacted to chromosomes in mitosis, followed by reestablishment of the chromatin structure in G1 phase. Advances in technologies have provided insight into the fundamental question what shapes the genome architecture. By now, it is generally accepted that the 3D organisation is developed in a hierarchical manner, which is conserved between species. Moreover, several studies proposed that the 3D organisation could influence transcription. Despite an emerging picture on the 3D organisation, a structural contribution of RNA polymerase II (RNAPII) remains unclear.

This study aims to contribute to this growing area of research by exploring the role of RNAPII in genome organization. I combined methods of molecular biology, transcriptomics, and genomics with the distinct auxin-inducible degradation of the largest RNAPII subunit RPB1 to elucidate its role in spatiotemporal chromatin structure regulation.

In Chapter 1, I show that RNAP II is an important regulator in reestablishing the spatial chromatin structure at the mitosis to G1 transition. On a larger scale RNAPII depletion in G1-sorted cells erases domain structures, weakens local insulation and interactions are lost. At a smaller scale, loops are rewired characterised by the gain of longer loops with stronger insulation. Thereby, the results suggest that active RNAPII can restrain loop extrusion.

In Chapter 2, *in situ* Micro-C reveals transcription-based loops, which arise from *cis*-regulatory contacts at sub-kb resolution. Loss of RNAPII results in weakened loops and affects especially enhancer-anchored loops whereas promoter-anchored loops are more stable. I show that RNAPII is required to establish enhancer-anchored loops.

Taken together the data reveal the importance of RNAPII to reestablish the chromatin architecture following exit from mitosis, as well as its previously unknown impact on loop extrusion.

1. Introduction

The nucleus contains about two meters of DNA, which must be enormously compacted to fit into the nucleus. This accomplishment can only be reached through proper coordinated packaging of DNA in various steps. At the same time, dynamic accessibility of chromatin must be ensured to conduct vital processes in the cell such as transcription and replication.

Advances in the last decade revised the nuclear organisation as dynamic hierarchical model, which is influenced by multiple factors. Presumably, different forces such as architectural proteins and transcription cooperate spatially and temporally to shape this dynamic 3D organisation (Rada-Iglesias, Grosveld and Papantonis, 2018; Rowley and Corces, 2018). How and to what extend these forces shape the nuclear architecture remains unclear. In addition, the role of RNAPII and transcription-related structural changes is heavily debated. Therefore, it is important to understand the interplay between 3D structure and transcriptional landscape.

1.1. The layers of 3D genome organisation

The first organisational layer of the genome is the division into chromosome territories. Microscopic techniques such as fluorescence in situ hybridisation (FISH) allowed the visualisation of chromosome territories and showed the favoured positioning of chromosomes within the nucleus (**Fig 1A**). Gene-poor regions tend to localise at the nuclear periphery whereas gene-rich regions are located conversely in the inner part of the nucleus (Cremer and Cremer, 2001; Meister *et al.*, 2010; Boyle *et al.*, 2011; Yamada *et al.*, 2011; Beliveau *et al.*, 2012).

A milestone in the field of 3D chromatin architecture was the invention of the chromosome conformation capture (3C) technique. There, cross-linked chromatin is digested with restriction enzymes and diluted. This is followed by religation of proximal DNA regions and finally identification by sequencing. In this methodology, interacting DNA regions between two loci which are in close 3D proximity will more likely religate and are thus more frequently detected compared to unspecific religations (Dekker *et al.*, 2002). While FISH can resolve the interaction on the single-cell level, 3C and its derivates improved the resolution and thus the understanding of chromatin organisation. The development of Hi-C increased the resolution to one megabase (Mb) and enabled the depiction of the interactions of the whole genome in a heatmap. Thereby, not only chromosome territories were observed but also their partitioning into the next hierarchical layer, A and B compartments, was revealed (**Fig 1B**). These segregated compartments were previously termed euchromatin and heterochromatin respectively. Thereby, interactions preferentially occur between regions that belong

to the same compartment. The interactions within compartments appear as a plaid pattern in Hi-C contact maps. In general, A compartments were defined as transcriptionally active, GC-rich, and accessible compared to B compartments that are rather transcriptionally inactive, gene-poor and more compacted (Lieberman-Aiden *et al.*, 2009). It has been suggested that compartments are formed by microphase separation which depends on differential biophysical attractive forces between A and B compartments (Hildebrand and Dekker, 2020).

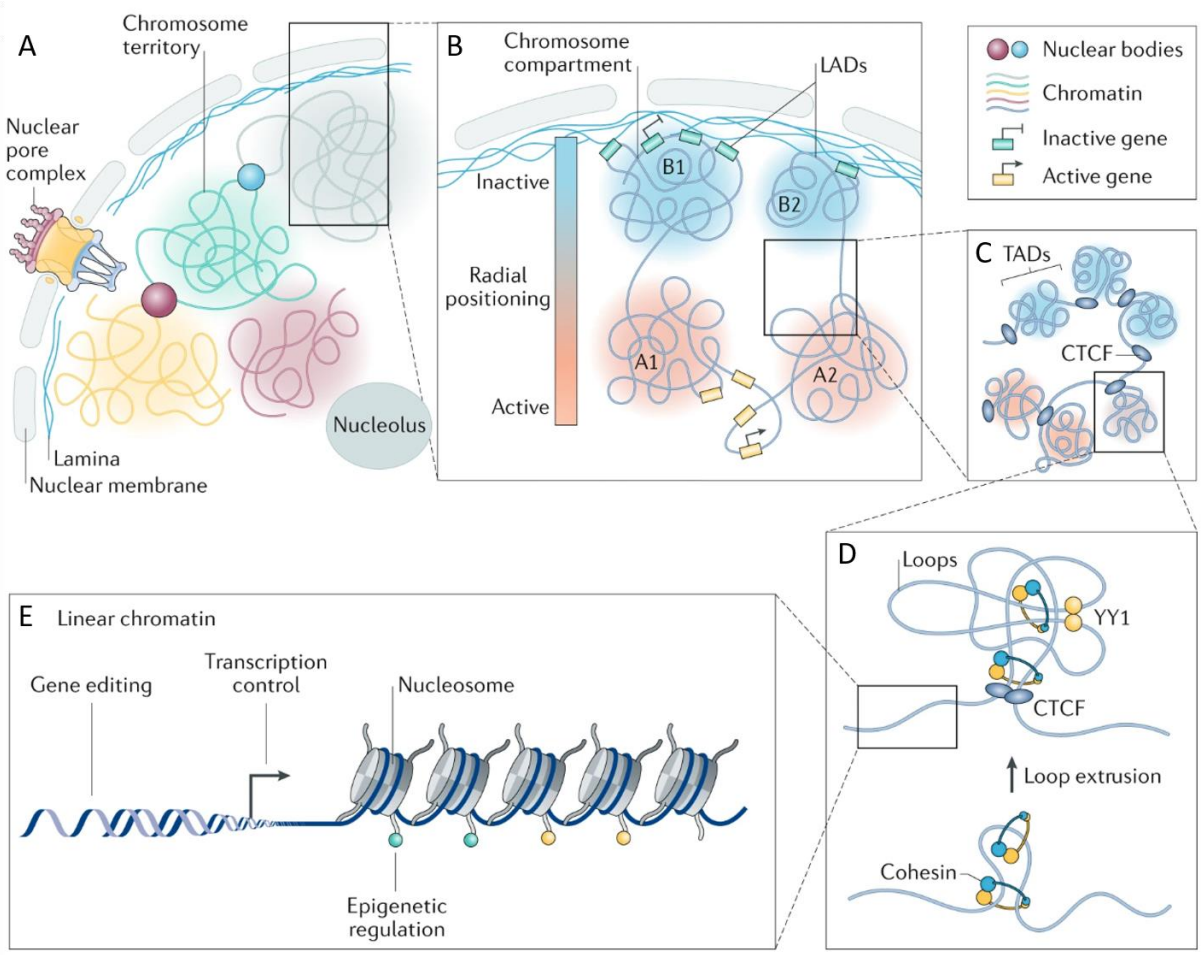

Figure 1: Multiple layers of chromatin organization*. A) Chromosome territories occupy distinct position in the nucleus. B) The genome is partitioned into two different compartments. These A and B compartments are multi-megabase structures, defined as accessible and transcriptionally active vs. closed and transcriptionally inactive respectively. C) Topologically associating domains (TADs) are structures with preferential self-interacting properties insulated by CTCF elements. D) Loops are located within TADs and emerge through a cohesin-mediated process termed loop extrusion. E) Nucleosomes are built by wrapping DNA around the histone octamer. Modifications of the histone tails can epigenetically regulate cellular processes such as transcription (modified from Wang, Han and Qi, 2021).*

Further research identified the division of compartments into smaller domains. These domains termed topologically associated domains (TADs) range from 200 kbp to one Mbp, and are highly conserved amongst mammals (**Fig 1C**) (Vietri Rudan *et al.*, 2015). Regions within one TAD have a higher interaction frequency compared to regions in neighbouring TADs. They are visible as rectangles in Hi-C

maps separated by clear boundaries. This demarcation can be explained by separation of TADs via the boundary element CCCTC-Binding Factor (CTCF) (Dixon *et al.*, 2012; Nora *et al.*, 2012). CTCF binds DNA via its eleven zinc fingers at a conserved consensus motif (Kim *et al.*, 2007). Work by Sexton et al. discovered the existence of TADs in embryonic *Drosophila* genome contact matrices and confirmed the demarcation of active and inactive domains (Sexton *et al.*, 2012). A functional role of TADs is their contribution to increase contact frequency between *cis*-regulatory elements while insulating regions from each other. Their disruption leads to abolished P-E contacts and gene misexpression (Dowen *et al.*, 2014; Lupiáñez *et al.*, 2015; Symmons *et al.*, 2016). Thus, TADs are relevant to bring regulatory elements in close proximity for proper gene regulation.

Rao et al. improved the resolution of Hi-C maps to 1 kb. This enabled the detection of around 10,000 chromatin loops (~ 185 kbp) in human and mouse, anchored by convergent CTCF sites together with the cohesin complex subunits RAD21 and SMC3 (**Fig 1D**). Each TAD contains multiple chromatin loops. Accordingly, CTCF and cohesin are located at TAD boundaries and within TADs anchoring loops. These loops can bring distal regulatory elements to close proximity and often corresponded to enhancer-promoter (E-P) interactions. (Rao *et al.*, 2014; Bonev *et al.*, 2017). The development of loops is discussed in more detail later (see **1.3**).

As a last step of compaction 146 bp of linear DNA is wrapped around the core histone octamer, which is constituted of dimers of each H2A, H2B, H3, and H4 – assembling the nucleosome (**Fig 1E**) (Oudet, Gross-Bellard and Chambon, 1975; Luger *et al.*, 1997). Histones are highly conserved across eukaryotes and represent the most abundant proteins in a cell. Unlike the other histone family members, H1 is not part of the nucleosome but binds the nucleosome surface and the linker DNA to stabilize the complex. Nucleosomes play an important role in gene regulation. The histone tails can be post-translationally modified by enzymes, which alters their interaction with DNA. Most post-translational modifications (PTMs) affect the tails of H3 and H4. Variations in histone isoforms, but also their PTMs impact the DNA compaction states and display the last regulatory layer of 3D organisation (Talbert and Henikoff, 2016). Acetylated histones have a decreased interaction with the DNA leading to a decompacted chromatin state. In contrast, neutralisation of the negative charge of the DNA e.g. by removing acetyl groups from histone tails leads to compaction of the DNA (Widom, 1986; Clark and Kimura, 1990). Thus, PTMs can influence cellular processes such as transcriptional regulation by changing the chromatin conformation. According to that, active marks (e.g. H3K27ac and H3K4me3) are associated with regulatory elements and indicate transcription. On the other hand, decompacted chromatin and repressive marks (e.g. H3K27me3 and H3K9me2/3) display transcriptionally inactive compact chromatin regions and are typically found in heterochromatic regions (Rowley and Corces, 2018; Millán-Zambrano *et al.*, 2022).

1.2. Cell cycle changes in 3D organisation

3D Chromatin organisation during the cell cycle is a dynamic process. The cell cycle is regulated by cyclin-dependent kinases (CDKs) which control the progression through the different cell cycle checkpoints (Lubischer, 2007). During the course of the cell cycle, cells undergo massive structural changes. These cell-cycle dynamics orchestrate multiple cellular processes to adapt the functional needs in the individual phases. In general, two distinct chromatin phases namely interphase and mitosis are distinguished. Interphase is further divided into G1, S, and G2 phase. A characteristic of the interphase chromatin is a decondensed, globular structure with stable compartmentalisation and TADs (Nagano *et al.*, 2017). Here, accessible chromatin allows for transcription. During mitosis, the genetic material is divided into the two daughter cells. For faithful segregation of chromatin, it needs to be highly compacted into rod-shaped chromosomes (Hirano, 2015). Although Walther Flemming detected chromosomes already in 1875, the exact mechanism how the structure is established remains unknown. The high compaction change is likely a result of multiple influences.

Both deacetylation and phosphorylation of histones are hallmarks of mitotic cells and favours DNA compaction (Bradbury, Inglis and Matthews, 1974; Roth and Allis, 1992; Wei *et al.*, 1999; Kruhlak *et al.*, 2001; Wilkins *et al.*, 2014). Mitotic kinases promote nuclear envelope break-down (NEBD) via phosphorylation of lamins and lamin-associated proteins (de Castro, Gokhan and Vagnarelli, 2016). Moreover, many non-histone proteins are phosphorylated upon mitotic entry, which reduces their interaction with DNA. Thus, most transcription factors (TFs) and other proteins are disassociated from chromatin, which correlates with declined transcription on the onset of mitosis (Martínez-Balbás *et al.*, 1995; Kadauke and Blobel, 2013). However, some TFs remain associated with chromosomes to accelerate reactivation of transcription upon G1 reentry (Michelotti, Sanford and Levens, 1997; Kadauke and Blobel, 2013; Yiyuan Liu *et al.*, 2017)**.**

Furthermore, large fractions of the transcription machinery disassociate from chromosomes. The leftover chromatin-bound part of the transcription machinery is phosphorylated during mitosis (Segil *et al.*, 1996; Gottesfeld and Forbes, 1997; Parsons and Spencer, 1997; Prasanth *et al.*, 2003; Liang *et al.*, 2015; Black *et al.*, 2016; Teves *et al.*, 2016). RNAPII itself has several phosphorylation sites (Dahmus, 1995). In addition, it has been shown that phosphorylation by the Cdc2 kinase leads to transcriptional silencing *in vitro* and *in vivo* (Leresche, Wolf and Gottesfeld, 1996; Gebara, Sayre and Corden, 1997). The phosphorylation prevents transcriptional activation and can be reversed by dephosphorylation of RNAPII (Lu *et al.*, 1991; Segil *et al.*, 1996). All these structural changes lead to transcriptional inhibition during mitosis. More recent findings proposed that transcriptional silencing during mitosis is important to reset transcription and regulate gene expression throughout the cell cycle (Ramos-Alonso *et al.*, 2023). One example from Egli et al. showed transcriptional reprogramming of zygotes in somatic cells

was supported by mitotic arrest (Egli *et al.*, 2007; Halley-Stott *et al.*, 2014). At the same time, this unique mitotic structure is completely different from interphase chromatin, which has been visualised in Hi-C contact maps. Mitotic cells showed particularly less interactions (long-range, <10 Mb) and loss of compartmentalisation, TADs, loops and accordingly disassociation of CTCF and cohesin (Nagano *et al.*, 2017; Gibcus *et al.*, 2018; Abramo *et al.*, 2019; Oomen *et al.*, 2019).

The structural maintenance of chromosomes (SMC) proteins condensin and cohesin are essential to shape mitotic chromosomes. One model proposes that chromosome compaction occurs in two steps, which is mediated by two different condensin complexes. First, during prophase the condensin II complex forms consecutive chromatin loops around 100 kbp. This leads to shortening of the chromosomes along the longitudinal axis. The first step is followed by axial compression of structures less than ten Mbp by dividing the chromatin loops into smaller loops by condensin I (Ono *et al.*, 2003; Gibcus *et al.*, 2018). On the other hand, cohesin tethers sister chromatids in *trans* from S phase until the onset of anaphase. Sister chromatid cohesion is important for proper chromosome segregation (**Fig 2, bottom**) (Michaelis, Ciosk and Nasmyth, 1997; Tanaka *et al.*, 2000). However, chromatin can still condense to a small extend upon loss of condensin I, and II even though the cells cannot progress through mitosis. This suggests an additional yet unknown compaction mechanism at the beginning of mitosis (Paulson and Laemmli, 1977; Ono *et al.*, 2003; Naumova *et al.*, 2013; Gibcus *et al.*, 2018).

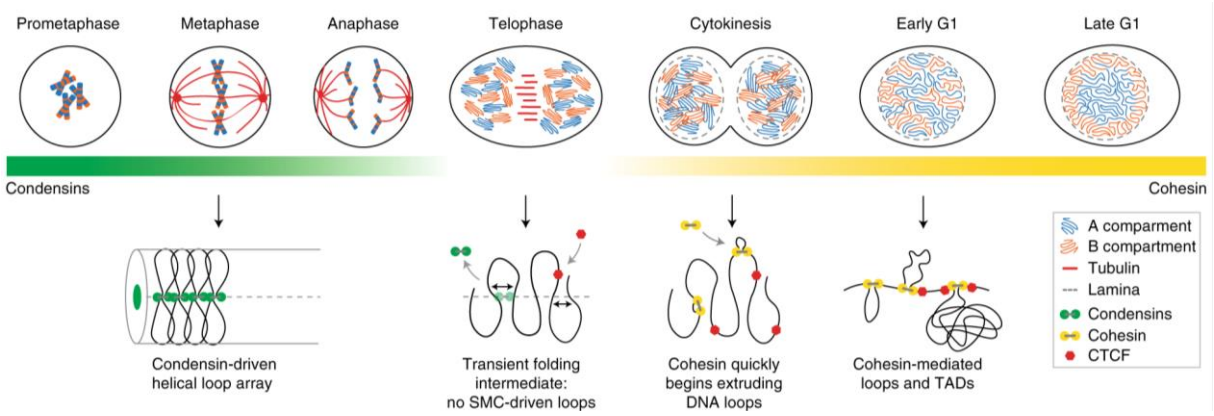

Figure 2: Chromatin dynamics during M-to-G1 transition. *Top) illustration of the chromatin organization from Prometaphase to late G1. A compartments are depicted in blue, B compartments in orange. Red lines represent Tubulin, important for proper chromosome segregation. Bottom) during mitosis, condensin folds chromatin consecutively into smaller loops, which leads to compaction into chromosomes. Upon exit from mitosis, cohesin-mediated loops and TADs are reestablished (From Abramo et al., 2019).*

During telophase the nuclear envelope is rebuild around the chromosomes to separate the divided nuclei and simultaneously condensin-mediated loops are dissolved. Upon exit from mitosis, loops, TADs, compartments, and territories need to be reestablished in the two daughter cells (Nagano *et al.*, 2017; Abramo *et al.*, 2019; Zhang *et al.*, 2019). During ana/telophase increased H3K27ac signals are detected (Kang *et al.*, 2020), followed by chromosome decondensation and a rapid recovery of the

interphase 3D structure. First, short-range interactions such as TADs and loops gradually reestablish even before the cells enter G1 phase. According to several studies, first CTCF followed by cohesin binds to chromatin already in telophase (Abramo *et al.*, 2019; Oomen *et al.*, 2019; Zhang *et al.*, 2019). In addition, during telophase the transcription machinery is present upon nuclear envelope reassembly and RNAPII binds to promoters (Prasanth *et al.*, 2003; Hsiung *et al.*, 2016). This is in line with binding of TFs, E-P contacts, and rapid transcription restart which leads to a spike in transcription involving half of all active genes (Hsiung *et al.*, 2016).

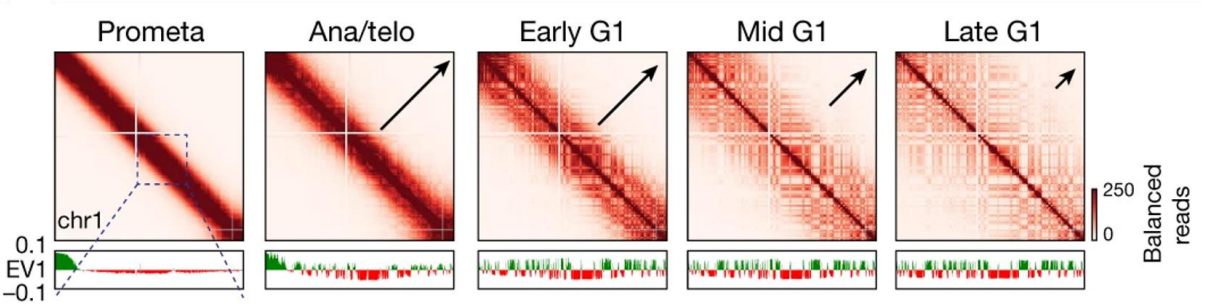

Figure 3: Chromatin structure reestablishment during M-to-G1 transition. *Hi-C heatmaps of chromosome one depict the reestablishment and expansion of A/B compartments from prometaphase until late G1 (From Zhang et al., 2019).*

Even though A compartments decondense during G1 reentry (**Fig 3**), compartmentalisation is still weak and increases progressively until the G2 phase (Hsiung *et al.*, 2016; Nagano *et al.*, 2017; Palozola *et al.*, 2017; Abramo *et al.*, 2019).

The precise reformed 3D organisation raises the question how the structural and transcriptional information is inherited through mitosis and reestablished in G1 reentry. A number of studies have found that some TFs and architectural proteins remain bound during mitosis to mark active regions but also PTMs are key for structural memory (Kadauke and Blobel, 2013; Festuccia *et al.*, 2017). Additionally, histone modifications such as H3K4me3, or H3K27me3 are maintained through M to G1 phase for rapid structural reestablishment (Javasky *et al.*, 2018). This process to mark regions for rapid reactivation is termed 'mitotic bookmarking' (Kadauke *et al.*, 2012; Caravaca *et al.*, 2013; Festuccia *et al.*, 2016; Yiyuan Liu *et al.*, 2017).

1.3. Cohesin-mediated loop formation

The DNA is folded by ring-shaped SMC complexes. SMC complexes are conserved ATP binding cassette (ABC) like ATPases and play a role in chromatin organisation throughout the cell cycle. These ATPases reel DNA in an ATP-dependent manner to generate a consecutively growing DNA loop (Hirano, 2002). Two prominent family members of the SMC complexes are condensin and cohesin (Strunnikov, Larionov and Koshland, 1993; Hirano, 2006; Sedeño Cacciatore and Rowland, 2019).

During mitosis, condensin complexes condense the chromatin to chromosomes, whereas cohesin is involved in sister chromatid cohesion important for proper chromosome segregation (Guacci, Koshland and Strunnikov, 1997; Michaelis, Ciosk and Nasmyth, 1997; Ono *et al.*, 2003; Schalbetter *et al.*, 2017). In interphase, cohesin is a key element in chromatin organisation. It has been shown that the architectural proteins cohesin and CTCF regulate TAD formation (Rao *et al.*, 2014; Flavahan *et al.*, 2015; Merkenschlager and Nora, 2016). TADs facilitate interactions between regulatory elements and further fold into chromatin loops. Chromatin loops are regulatory regions, demarcated by CTCF and cohesin which act as a transcription barrier (Bell and Felsenfeld, 2000; Rao *et al.*, 2014; Bonev and Cavalli, 2016). Notably, cohesin is not only important to form loops but also stabilizes them by capturing DNA in *cis* (Sanborn *et al.*, 2015; Fudenberg *et al.*, 2016; Rao *et al.*, 2017; Davidson *et al.*, 2019; Kim *et al.*, 2019). Cohesin is composed of the subunits STAG1 or STAG2 (yeast homolog Scc3), SMC1, SMC3, and the kleisin member RAD21 (yeast homolog Scc1). The heterodimer SMC1-SMC3 possesses an ATPase activity similar to the ABC protein family (Löwe, Cordell and Van Den Ent, 2001). SMC1-SMC3 are connected both through their hinge and between their heads by RAD21 to form a tripartite ring structure (Hopfner *et al.*, 2000; Haering *et al.*, 2004; Gligoris *et al.*, 2014; Huis In't Veld *et al.*, 2014). RAD21 further interacts with the cohesin subunit STAG1/STAG2, and the cohesin regulators NIPBL, PDS5A, and WAPL (**Fig 4, right**) (Kueng *et al.*, 2006; Kikuchi *et al.*, 2016; Davidson *et al.*, 2019; Kim *et al.*, 2019). Depletion of RAD21 was sufficient to eliminate TADs, loops, and thus impairs gene expression (Rao *et al.*, 2017).

Previous research has established that NIPBL (yeast homolog Scc2) and MAU2 (yeast homolog Scc4) play a role in cohesin loading onto chromatin (**Fig 4, left**). (Ciosk *et al.*, 2000; Tonkin *et al.*, 2004; Watrin *et al.*, 2006; Bermudez *et al.*, 2012; Kikuchi *et al.*, 2016). NIPBL interacts with the cohesin subunit RAD21 and activates the ATPase activity of cohesin which is necessary for the stable association with DNA (Arumugam *et al.*, 2003; Murayama and Uhlmann, 2014; Petela *et al.*, 2018; Kim *et al.*, 2019). SMC3 deacetylation by HDAC8 promotes the interaction between NIPBL and cohesin, and results in longer loops (Petela *et al.*, 2018; van Ruiten *et al.*, 2022). Mutations of the yeast homolog Scc2 were sufficient to prevent the loading of cohesin onto DNA (Rhodes *et al.*, 2017; Petela *et al.*, 2018). Interestingly, the deletion of MAU2 is sufficient to reduce NIPBL levels which resulted in shorter loops (**Fig 5**) (Haarhuis *et al.*, 2017). Consequently, loss of either NIPBL or MAU2 reduced the number of loops, disrupted TADs, and resulted in malformation and developmental disorder (Tonkin *et al.*, 2004; Schwarzer *et al.*, 2017a; Shi *et al.*, 2020).

PDS5A/Pds5 is a competitor of NIPBL/Scc2 for binding cohesin. Its interaction with cohesin has been shown to weaken the Scc2-Scc1 interaction (**Fig 4, left**) (Kikuchi *et al.*, 2016). Conversely, PDS5A binding is achieved by ESCO1/Eco1-mediated acetylation of the SMC3 subunit (**Fig 4, right**). In contrast to NIPBL, PDS5A inhibits the ATPase activity of cohesion, which results in pause and restart of loop

extrusion. Accordingly, inhibition of PDS5A increased the residence time cohesin on chromatin (Wutz *et al.*, 2017; van Ruiten *et al.*, 2022).

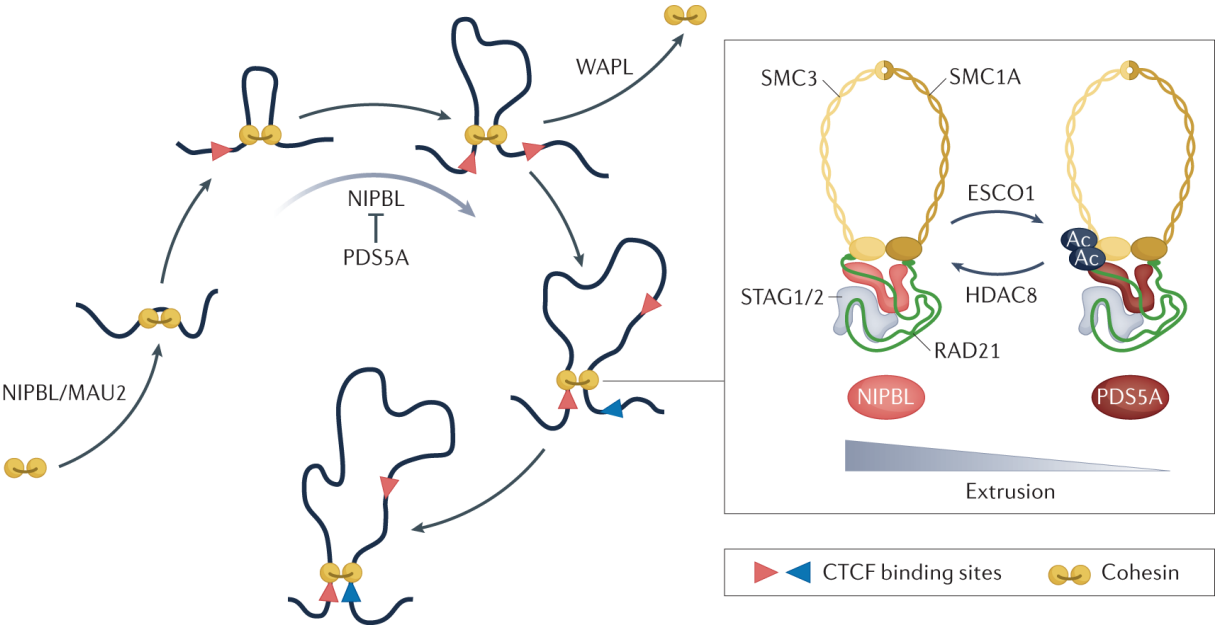

Figure 4: A dynamic loop extrusion model*. Left: Loading of cohesin through NIPBL/MAU2 onto chromatin initiates loop extrusion. PDS5A inhibits the association of NIPBL with cohesin. An initially small loop starts to increase in size by cohesin-mediated loop extrusion until it encounters convergent CTCF molecules. WAPL removes cohesin, which dissolves the loop and thus limits one loop extrusion cycle. Right: The cohesin complex is composed of the subunits SMC3, SMC1A, RAD21, and STAG1 or STAG2. Acetylation of SMC3 by ESCO1 promotes binding of the NIPBL competitor PDS5A and restricts loop extrusion. Conversely, deacetylation of SMC3 by HDAC8 promotes binding of NIPBL and induces loop extrusion (From de Wit and Nora, 2022).*

After cohesin is loaded onto chromatin, it starts to translocate DNA. It has been suggested that cohesin translocates DNA bidirectionally rather than unidirectionally in replicating cells (Kanke *et al.*, 2016). Davidson et al. and Kim et al. showed for the first time that cohesin mediates loop extrusion in a bidirectional manner *in vitro* (Davidson *et al.*, 2019; Kim *et al.*, 2019). Several loop extrusion models have been proposed but the exact mechanism of how DNA is translocated by cohesin remains unknown (Sanborn *et al.*, 2015; Fudenberg *et al.*, 2016; Diebold-Durand *et al.*, 2017; Brackley *et al.*, 2018; Nichols and Corces, 2018; Marko *et al.*, 2019; Ryu *et al.*, 2020; Gerguri *et al.*, 2021; Pradhan *et al.*, 2022).

It is well established, that cohesin is enriched at CTCF binding sites (Parelho *et al.*, 2008; Stedman *et al.*, 2008; Wendt *et al.*, 2008; Dixon *et al.*, 2012; Zuin *et al.*, 2014; Busslinger *et al.*, 2017; Hansen *et al.*, 2017; Li *et al.*, 2020). The current status suggests that cohesin reels DNA until it encounters convergent CTCF sites (Rao *et al.*, 2014; de Wit *et al.*, 2015; Vietri Rudan *et al.*, 2015). Manipulation of CTCF sites disrupted both the recruitment of cohesin, and chromatin loops (de Wit *et al.*, 2015; Guo *et al.*, 2015; Sanborn *et al.*, 2015). Additionally, a loss of TAD insulation through depleted or mutated CTCF leads to

TAD merging which can result in new E-P contacts and thus aberrant gene expression (Zuin *et al.*, 2014; Flavahan *et al.*, 2015; Narendra *et al.*, 2015; Hnisz *et al.*, 2016; Nora *et al.*, 2017; Khoury *et al.*, 2020). Given the role of cohesin and CTCF in loop formation, depletion of CTCF (Nora *et al.*, 2017) or cohesin from chromatin (Schwarzer *et al.*, 2017a) disrupted almost all loops.

Cohesin remains bound to chromatin for about 20 minutes, but takes more than 30 minutes to rebind. In contrast, CTCF has a high turnover with both binding and rebinding for one minute. This illustrates loops as variable and highly dynamic regulatory elements rather than stable entities (Gerlich *et al.*, 2006; Tedeschi *et al.*, 2013; Hansen *et al.*, 2017). As already pointed out, depletion studies of cohesin and CTCF support the model that cohesin is important for loop extrusion. On the other hand, CTCF is required for insulation of TAD boundaries, and to position cohesin for stable chromatin loop formation. Interestingly, A/B compartments were not strongly affected by both cohesin or CTCF depletion (Seitan *et al.*, 2013; Sofueva *et al.*, 2013; Zuin *et al.*, 2014; Gassler *et al.*, 2017; Nora *et al.*, 2017; Rao *et al.*, 2017; Schwarzer *et al.*, 2017b; Wutz *et al.*, 2017; Vian *et al.*, 2018; Richart *et al.*, 2021).

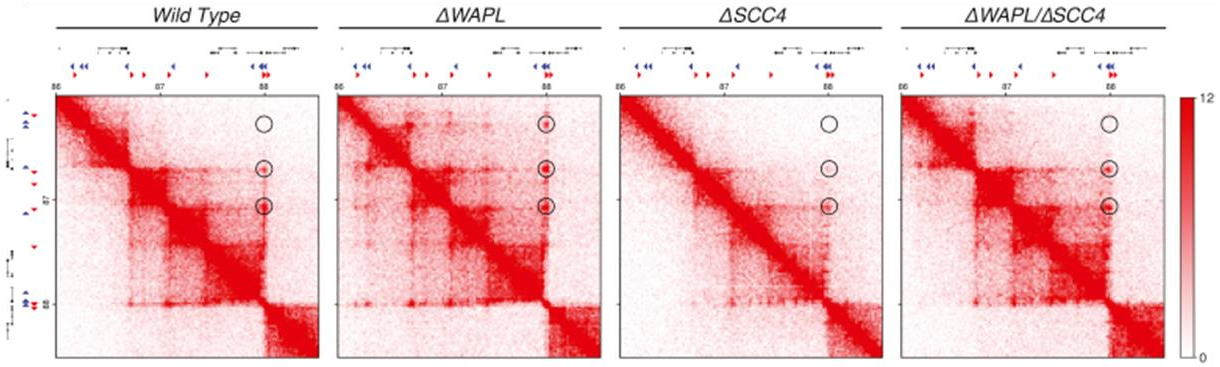

Figure 5: Comparison of ΔWAPL, ΔSCC4, and ΔWAPL/ΔSCC4 contact maps in HAP1 cells*. Exemplary Hi-C heatmaps from a region of chromosome 5, forward CTCF sites are depicted in red, reverse CTCF sites in blue.*

As last step of the loop extrusion model WAPL releases cohesin from chromatin by disrupting the SMC3-RAD21 interaction which dissolves the loop (Gandhi, Gillespie and Hirano, 2006; Kueng *et al.*, 2006). A recent study suggested that CTCF impedes the release of cohesin from chromatin by WAPL to stabilise the loop (Li *et al.*, 2020). Haarhuis et al. reported about a correlation between the residence time of cohesin on chromatin and the respective loop length (Haarhuis *et al.*, 2017). Hence, loss of WAPL increased the residence time of cohesin and resulted in both increased loop length and long-range interactions (**Fig 5**) (Kueng *et al.*, 2006; Tedeschi *et al.*, 2013; Gassler *et al.*, 2017; Haarhuis *et al.*, 2017; Wutz *et al.*, 2017; Rhodes *et al.*, 2020). In addition, WAPL depleted cells displayed the unique Vermicelli formation in mitotic and meiotic cells, and highly compacted chromatin during interphase due to aberrant activity of cohesin (Tedeschi *et al.*, 2013). Previous research has established that decreased WAPL dosage is sufficient to compensate for phenotypes caused in Nipbl$^{+/-}$ mice (Kean *et*

al., 2022). This finding was consistent with correction of the phenotype and restored cohesin levels on chromatin resulting from co-depletion of NIPBL and WAPL (Haarhuis *et al.*, 2017; Luppinoid *et al.*, 2022). This suggests that the balance between NIPBL and WAPL controls the continual loading and unloading of cohesin, which is important for dynamic loop formation and gene regulation.

Even though many aspects of loop formation have already been resolved, the bigger picture is far from complete. For instance, it is still uncertain how many cohesin monomers are necessary for loop formation (Huang, Milutinovich and Koshland, 2005; Matityahu and Onn, 2022). In addition, the loading site of cohesin and its starting point for subsequent translocation is not fully resolved. Since loops are quickly extruded around 0.5 - 2.36 kbp/s current methods are unable to capture cohesin before it encounters CTCF sites (Davidson *et al.*, 2019; Kim *et al.*, 2019; Golfier *et al.*, 2020). Recent evidence suggests that cohesin is loaded at open DNA regions. This is supported by the association of NIPBL and MAU2 with promoter regions upstream of RNAPII (Lopez-Serra *et al.*, 2014; Zuin *et al.*, 2014). Moreover, depletion of CTCF leads to the accumulation of cohesin at transcription start sites (TSSs) of active genes (Wendt *et al.*, 2008; Busslinger *et al.*, 2017). Currently, the exact mechanism is not resolved and future technical approaches are needed to fully understand the principle of loop formation.

1.4. Acute protein depletion

The higher-order nuclear organisation facilitates proper cellular function. In order to understand the mechanism behind cellular processes and principle features of 3D organisation, it is important to gain insight into the functional role of involved proteins. The traditional approach was a loss-of-function study of the endogenous protein of interest (POI) through the generation of knockout (KO) cell lines. However, many proteins are essential for cell survival. Hence, constitutive KO approaches are not suitable for functional studies of critical proteins due to lethality. For instance, a CTCF KO has been shown to induce apoptosis and ultimately lethality (Gomes and Espinosa, 2010; Moore *et al.*, 2012).

Another popular method to study the function of a POI were knockdown (KD) experiments based on small interfering RNAs (Elbashir *et al.*, 2001). Here, the mRNAs are destroyed and the POIs are depleted according to their half-life. The main disadvantage of KDs is an incomplete depletion of the POI which enables the functional retention of the POI. Several proteins have cell-cycle specific functions. With regard to the long duration of KDs and the generation of KO lines, which takes more than one cell cycle, the assessment of direct effects of proteins in a specific cell-cycle stage is impossible. Consequently, phenotypes resulting from KD and KO experiments can be directly associated with the loss of the POI, but may also be caused by secondary effects (Weiss, Taylor and Shokat, 2007).

To overcome these problems a rapid depletion system is required. A rapid degradation of the POI is crucial to elucidate direct cell-cycle specific functions of a protein. Fortunately, new methods with fast degradation kinetics of POIs are emerging. Recently, the concept of degron technologies was groundbreaking to enable the inducible and rapid degradation of a POI.

A widely used tool is the degradation of target proteins by proteolysis targeting chimeras (PROTAC). These molecules contain two domains. One domain binds to the POI and the other recruits an SCF ubiquitin ligase. This leads to ubiquitination and finally degradation of the POI through the proteasome (Sakamoto *et al.*, 2001; Lu *et al.*, 2015; Winter *et al.*, 2015). However, PROTACs require high concentrations, show off-target effects, and their chemical synthesis can be challenging (Bondeson *et al.*, 2018; Liu *et al.*, 2022).

Multiple new degron technologies have been developed that are based on fusion of the endogenous POI to degradation domains by CRISPR-Cas9 genome editing (Cong *et al.*, 2013; Mali *et al.*, 2013). They take advantage of small molecules that bind the degradation domain and rapidly degrade the POI through the proteasome. In general, depletions can be detected after a few minutes up to a few hours (Rao *et al.*, 2017; Wutz *et al.*, 2017; Liu *et al.*, 2021). In contrast to KD and KO experiments the rapid degradation enables the study of cell-cycle specific, primary functions of proteins (Natsume and Kanemaki, 2017).

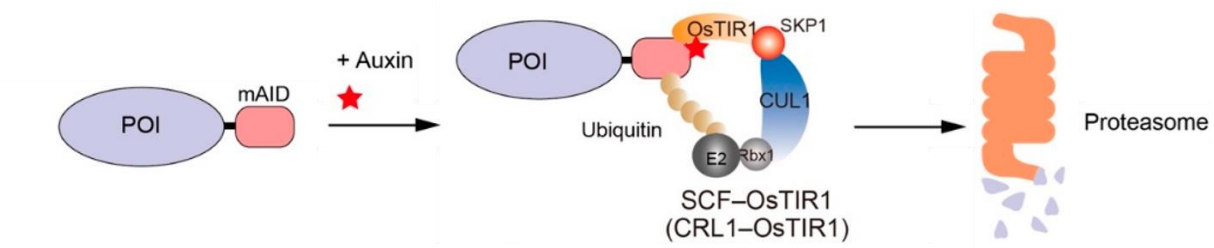

Figure 6: Mechanism of the auxin-inducible degradation*. The target protein POI is tagged with an auxin-inducible degron (mAID). Upon auxin addition, it binds to mAID and recruits the TIR1-SCF E3 ligase complex composed of OsTIR1, SKP1, CUL1 and, Rbx1. Finally, the binding to auxin recruits an E2 ligase, which results in poly-ubiquitylation of mAID and the proteasomal degradation of POI-AID. Adapted* from (Yesbolatova et al., 2020)*.*

One example of a degron technology is the auxin-inducible-depletion system, which uses the small molecule auxin to rapidly deplete the POI. Auxin is a plant hormone which originally regulates plant gene expression (Tan *et al.*, 2007; Nishimura *et al.*, 2009). In brief, the POI is fused to the auxin-inducible degron (AID), which is recognised by auxin. Additionally, the F-box transport inhibitor response 1 (TIR1) protein needs to be integrated in a save harbour locus and expressed in the cell. TIR1 forms the TIR1-SCF complex with the endogenous proteins Skp, Cul1, and the E3 ligase Rbx1 (SCF complex). Upon addition of auxin, SCF-TIR1 binds auxin, which promotes the binding to the degradation domain AID. As a last step, the E2 ligase is recruited to poly-ubiquitylate auxin, which leads

to rapid proteasome-mediated degradation of the POI-AID (**Fig 6**) (Nishimura *et al.*, 2009). The system has been successfully tested in human, mouse, and *Drosophila* which highlights a wide application potential (Nishimura *et al.*, 2009; Natsume *et al.*, 2016). This system has been further improved by the Kanemaki group to increase the efficiency of genome editing and to reduce leakiness (Natsume *et al.*, 2016; Nagashima *et al.*, 2019; Yesbolatova *et al.*, 2019, 2020). For example, a smaller mini AID (mAID) is now widely used to reduce the tag length and thus the probability of non-functional POI (Yesbolatova *et al.*, 2020). Several studies have already explored the impact of proteins on the chromatin architecture. By the usage of the AID system, many structural proteins were successfully degraded in a short time frame evaluating their role in 3D organisation. For instance, Nora et al. depleted CTCF to prove that CTCF is insulating TAD boundaries and is important for loop formation. In their study, no major compartmentalisation changes have been observed (Nora *et al.*, 2017; Wutz *et al.*, 2017). Similarly, depletion of cohesin supported its critical role in TAD and loop formation (Rao *et al.*, 2017; Wutz *et al.*, 2017). In summary, proteins cannot only be rapidly degraded with the AID system but protein levels can also be restored by washout of auxin. In both cases restoring CTCF and cohesin levels lead to recovery of the 3D organisation (Nora *et al.*, 2017; Rao *et al.*, 2017).

By now, these state of the art methods enjoy great popularity and have been widely used to study architectural proteins. A SMC2-mAID cell line verified the function of condensin in chromosome compaction. These methods provided new insight into the impact of RNAPII on chromatin dynamics by tagging the largest subunit RPB1 with mAID (*mAID-POLR2A-mClover*) (Nagashima *et al.*, 2019). In future studies, depletion systems can contribute to a better understanding of chromatin dynamics and the structure-to-function relationship of mammalian genomes.

1.5. The interplay between 3D organisation and transcription

All cells in one organism contain the same set of DNA. A simplistic view where all genes are transcribed in each cell cannot explain the diversity of cell types and differentially expressed genes. In fact, different cellular phenotypes develop from different gene expression patterns. Therefore, to dynamically modulate transcription there must be a way in order to adapt to different physiological demands.

The outdated paradigm of a one-dimensional (1D) view depicted a DNA fibre, which recruits RNAPII, and moves along the DNA during transcription to express genes. This linear transcription model is now replaced by a complex 3D model the so-called transcription factories. Here, RNAPII and other components of the transcription machinery are highly concentrated in focal factories and attract the DNA, which needs to be transcribed (Papantonis and Cook, 2013).

Cell-type specific interactions of *cis*-regulatory elements such as E-P contacts activate target genes and fine-tune transcription (Tolhuis *et al.*, 2002; Amano *et al.*, 2009; Ahmadiyeh *et al.*, 2010; Kagey *et al.*, 2010). Promoters surround the TSS and are the location for preinitiation complex (PIC) assembly. Subsequent recruitment of TFs, RNAPII, TFIIE, and TFIIH completes the PIC assembly. The largest RNAPII subunit RPB1 has a carboxy terminal domain (CTD). The CTD can mediate different protein interactions and contains a Tyr-Ser-Pro-Thr-Ser-Pro-Ser repeated sequence, which is targeted by kinases to control different stages of the transcription cycle. The Mediator complex interacts with unphosphorylated RNAPII (Kim *et al.*, 1994; Zhu *et al.*, 2006). Upon phosphorylation of RNAPII at Ser5 (Ser5P) by the TFIIH kinase Kin28, Mediator releases RNAPII (Søgaard and Svejstrup, 2007), and promoter escape is initiated. This is followed by the process termed elongation where the gene is transcribed (Feaver *et al.*, 1994; Esnault *et al.*, 2008; Jeronimo and Robert, 2014; Wong, Jin and Struhl, 2014; Chen *et al.*, 2021). Additionally, RNAPII binds to enhancer regions (Spicuglia *et al.*, 2002; Koch *et al.*, 2008; de Santa *et al.*, 2010). Enhancers are *cis*-regulatory elements and can be located even more than one Mbp away from their promoter. The association of TFs activate enhancers and recruit chromatin remodellers to increase chromatin accessibility (Gasperini *et al.*, 2019; Vermunt, Zhang and Blobel, 2019). Similar to RNAPII, the Mediator complex binds to promoter regions (Jeronimo and Robert, 2014; Wong, Jin and Struhl, 2014), but also associates with enhancers (Whyte *et al.*, 2013; Petrenko *et al.*, 2016). Mediator is known as transcriptional activator through direct interaction with the CTD of RNAPII (Kim *et al.*, 1994; Zhu *et al.*, 2006). Upon RNAPII release, Mediator can remain bound at the promoter to reinitiate another transcription cycle (Yudkovsky, Ranish and Hahn, 2000). Consequently, loss of Mediator reduced transcription rates. This especially affected genes controlled by super-enhancers (SE) suggesting a regulatory role in gene expression (Kagey *et al.*, 2010; Whyte *et al.*, 2013).

However, the exact mechanism of transcriptional regulation remains unclear. Previous research has shown that transcription is accompanied by structural changes such as the decondensation of the transcribed region (Tumbar, Sudlow and Belmont, 1999; Tsukamoto *et al.*, 2000). Upon mitotic exit chromatin decondenses and the reestablishment of the interphase 3D organisation (Naumova *et al.*, 2013; Nagano *et al.*, 2017) occurs concomitant with a spike in transcription (Hsiung *et al.*, 2016). During differentiation the genome architecture is reorganised in parallel with increased differential gene expression patterns by new intra-TAD E-P contacts (Bonev *et al.*, 2017). Similarly, TAD formation and their boundaries are established simultaneously with transcriptional activation in *Drosophila* zygotes (Hug *et al.*, 2017). In this regard, the fundamental structure-to-function question whether 3D organisation and transcription are interdependent or opposing forces remains intensely debated. New technologies such as the 3C methods and depletion systems (see **1.4**) have shed light into chromatin

organisation. A considerable amount of literature has been published on the potential implication of the chromatin structure on transcription.

One indication of a structure-to-function relationship of mammalian genomes was the observation that A and B compartments correlated with the transcriptional state (Lieberman-Aiden *et al.*, 2009; Rowley *et al.*, 2017). At a smaller scale TADs and their boundaries have been found in regions of active chromatin and expressed genes (Ulianov *et al.*, 2016; El-Sharnouby *et al.*, 2017; Hug *et al.*, 2017). Thereby active genes, especially housekeeping genes, are enriched at the borders together with architectural proteins indicating a relationship between transcription and TAD border formation (Hou *et al.*, 2012; Rao *et al.*, 2014; Van Bortle *et al.*, 2014). This is consistent with stronger TAD demarcation in G1 phase, when transcription reaches its peak (Hsiung *et al.*, 2016; Nagano *et al.*, 2017). In contrast, disruption of TADs changed gene expression presumably due to de novo E-P contacts (Lupiáñez *et al.*, 2015; Nora *et al.*, 2017). Interestingly, the distance between an enhancer and its promoter has been proved less relevant than the location within the same TAD (Symmons *et al.*, 2016).

Hi-C has been widely used to depict distal interactions and to identify continuously formed chromatin loops. Pivotal studies proved that CTCF and cohesin form these loops, restrict enhancer action, and guide E-P contacts to control gene expression (Parelho *et al.*, 2008; Wendt *et al.*, 2008; Dixon *et al.*, 2012; Dowen *et al.*, 2014). Besides, the Mediator complex, and YY1 are located at loop anchors to bridge E-Ps (Rao *et al.*, 2014; Beagan *et al.*, 2017; Weintraub *et al.*, 2017; El Khattabi *et al.*, 2019). Thus, transcription usually occurs within a chromatin loop. Therefore, loss of loops can lead to misregulated transcription. Recent findings verified the binding of CTCF, cohesin, and the cohesin loader NIPBL close to enhancers, active promoter sites, and RNAPII-associated transcription factories (Kagey *et al.*, 2010; Dowen *et al.*, 2014; Swain *et al.*, 2016; Kubo *et al.*, 2021). Inversion or disruption of CTCF binding sites at an enhancer region have already been shown to change chromatin loops and to impair E-P and P-P contacts (Flavahan *et al.*, 2015; Guo *et al.*, 2015; Kubo *et al.*, 2021). A novel MNase-based 3C approach by Aljahani et al. increased the resolution to 20 bp (Aljahani *et al.*, 2022). This enabled the investigation of sub-kb chromatin changes upon cohesin and CTCF depletion, which confirmed their role in precise gene regulation. Promoters and enhancers were previously identified as main elements controlling gene expression. Overall, this suggests that the architectural proteins CTCF and cohesin are additional factors to coordinate transcription besides promoters and enhancers.

Even though RNAPII is able to translocate DNA, its architectural relevance has been debated. In theory, RNAPII mediates physical contacts between distal enhancers and promoters to generate a loop. These E-P interactions are crucial for proper gene expression. Despite new findings in the chromatin organisation field the impact of transcription on 3D organisation is not fully understood. On the one hand, previous research found that active transcription is sufficient to predict the 3D organisation in most eukaryotes (Ulianov *et al.*, 2016; Rowley *et al.*, 2017). As mentioned before, transcription is

accompanied by decondensation of the transcribed region (Tumbar, Sudlow and Belmont, 1999; Tsukamoto *et al.*, 2000). In line with this, RNAPII inhibition (by DRB, or alpha-amanitin) was sufficient to prevent chromatin decondensation and led to chromatin Heterochromatinization (Müller *et al.*, 2001; Naughton *et al.*, 2013). More studies have been published suggesting a role of either RNAPII or transcription in 3D organisation. For example the inhibition of transcription initiation with Triptolide in *Drosophila melanogaster* resulted in decreased domain architecture (Rowley *et al.*, 2017). Transcription has also been reported to relocate cohesin which could impact loop formation (Busslinger *et al.*, 2017). Remarkably, recent findings revealed the role of RNAPII in chromatin dynamics by constraining chromatin movements. In this context, depletion or inhibition of RNAPII promoted dynamic chromatin by loosening these chromatin constraints (Nagashima *et al.*, 2019).
On the other hand, some studies point against a role of transcription in 3D organisation. To name a few, RNAPII inhibition did not affect long-range DNA contacts (Palstra *et al.*, 2008). Mediator degradation or the inhibition of transcriptional elongation did not affect E-P contacts (El Khattabi *et al.*, 2019; Sun *et al.*, 2021), and TAF12 degradation, crucial to direct PIC, and reduced promoter-interacting chromatin loops only slightly (Sun *et al.*, 2021). Ultimately, depletion of the RNAPs I, II, and III revealed only small-scale changes in the 3D organisation (Jiang *et al.*, 2020).

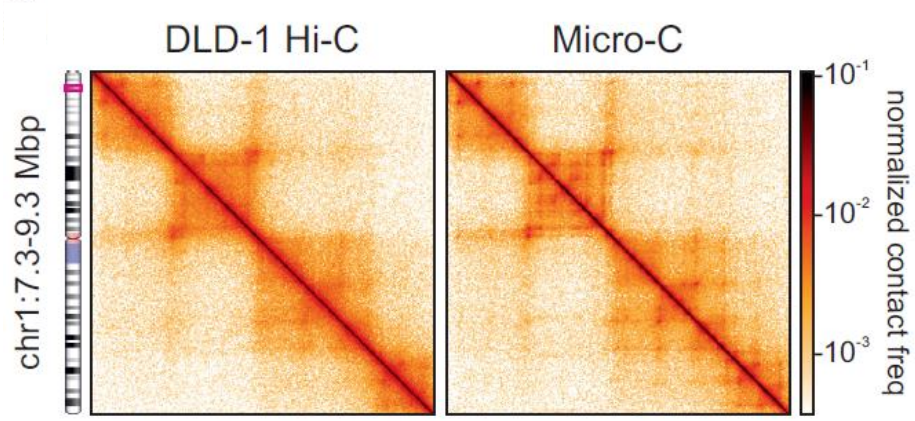

Figure 7: Comparison of Hi-C and Micro-C contact maps. *Left) Hi-C contact map vs. Right) Micro-C contact map at 5kb resolution in DLD1-mAID-RPB1 cells from a two Mbp fragment of chromosome 1 (From Zhang et al. 2021).*

However, the resolution of Hi-C is only sufficient to analyse cohesin/CTCF-mediated loops, but not the chromatin organisation at a finer scale, which rather depicts the impact of RNAPII or transcription. The invention of Micro-C increased the resolution of contact maps to sub-kb scale, by using micrococcal nuclease (MNase) to cut the chromatin (**Fig 7, right**) (Hsieh *et al.*, 2015, 2016). This enabled the detection of several thousand new loops and stripes, which were formed by transcription (Hsieh *et al.*, 2020; Krietenstein *et al.*, 2020). Frequent interactions between gene promoters and *cis*-regulatory elements (P-P, E-P) were discovered that were independent from CTCF, and cohesin. These E-P

interactions were driven by transcription. As a result, transcription inhibition disrupted these newly detected fine-scale P-P contacts, or E-P stripes but did not affect higher-order structures such as TADs and chromatin loops (Hsieh *et al.*, 2020). In addition, Micro-Capture-C identified new contacts between enhancers, promoters, and CTCF sites. Interestingly, increased CTCF contacts were observed when active promoters and enhancers were located between these convergent CTCF sites (Hua *et al.*, 2021). These newly collected data support a model where promoters and enhancers contribute to the highly dynamic and transient loop formation at sub-kb scale. A potential loading of cohesin at enhancers or promoters could lead to fine-scale gene regulation that resembles an interplay between the chromatin structure and transcription. Still, previous studies were unable to encompass the entire role of transcription, and of contributing proteins such as RNAPII on 3D organisation. This highlights the need for further understanding of the structure-to-function relationship of mammalian genomes.

3. Results

3.1. Chapter 1 – RNA polymerase II is required for spatial chromatin reorganization following exit from mitosis

My contribution is reflected by the following experimental outline:

- Culturing DLD1-mAID-mClover-RPB1 cells and HCT116 TOP2B$^{-/-}$-TOP2A-mAID cells
- Cell synchronisation
- FACS sorting and analysis
- Immunofluorescence staining and signal quantification
- Chromatin fractionation, Western blotting and quantification
- ATAC-seq experiment
- ChIP/CUT&Tag experiment
- RNA Factory-seq experiments with N. Josipovic
- Co-Immunoprecipitation

The following figure panels were prepared by myself with data from experiments performed by me:

Figure 1A) Western Blot of DLD1-mAID-mClover-RPB1 cells

Figure 1B) ChIP-seq experiment performed by me, ATAC-seq experiment together with N. Josipovic

Figure 2A) Cell synchronisation and FACS analysis in Control and RNAPII-depleted cells

Figure 2B) FACS analysis of different cell cycle stages in Control and RNAPII-depleted cells

Figure 2C) Chromatin Fractionation Western Blot in Control and RNAPII-depleted cells

Figure 2D) FACS sorting and crosslinking for Hi-C

Figure 3A) Chromatin Fractionation Western Blot in Control and RNAPII-depleted cells

Figure 3B) Immunofluorescence staining and signal quantification

Figure 3C) Fixation of cells for 3D-STORM imaging

Figure 3D) CUT&Tag experiments

Figure 3F+G) ATAC-seq experiment

Figure S1B-C) Immunofluorescence signal quantification

Figure S2A,C) Cell synchronisation

Figure S3A,B) Western Blot of DLD1-mAID-mClover-RPB1 cells

Figure S3C,D Immunofluorescence staining and signal quantification

Figure S3E) EU-labelling, immunofluorescence staining and signal quantification

Figure S3I,K,O) Cell synchronisation, FACS sorting and crosslinking

Figure S4A) Western Blot of HCT116 TOP2B$^{-/-}$-TOP2A-mAID cells

Figure S4B) FACS analysis of different cell cycle stages in HCT116 TOP2B$^{-/-}$-TOP2A-mAID cells

Figure S4C) RNA Factory-seq experiment

Figure S4D, G) Cell synchronisation, FACS sorting and crosslinking

Figure S5A,B) Western Blot/ Chromatin Fractionation Western Blot of DLD1-mAID-mClover-RPB1 cells

Figure S5C) CUT&Tag experiments

Figure S5E,F) Western Blot of Co-Immunoprecipitation experiment with GFP or NIPBL

RESEARCH ARTICLE

RNA polymerase II is required for spatial chromatin reorganization following exit from mitosis

Shu Zhang[1,#], Nadine Übelmesser[1,#], Natasa Josipovic[1,#], Giada Forte[2], Johan A. Slotman[3], Michael Chiang[2], Henrike Gothe[4], Eduardo Gade Gusmao[1], Christian Becker[5], Janine Altmüller[5], Adriaan B. Houtsmuller[3], Vassilis Roukos[4], Kerstin S. Wendt[6], Davide Marenduzzo[2], Argyris Papantonis[1,7,*]

[1] Institute of Pathology, University Medical Center Göttingen, 37075 Göttingen, Germany.
[2] School of Physics and Astronomy, University of Edinburgh, EH9 3FD Edinburgh, United Kingdom.
[3] Optical Imaging Centre, Erasmus Medical Center, 3015 GD Rotterdam, Netherlands.
[4] Institute of Molecular Biology, 55128 Mainz, Germany.
[5] Cologne Center for Genomics, University of Cologne, 50931 Cologne, Germany.
[6] Department of Cell Biology, Erasmus Medical Center, 3015 GD Rotterdam, The Netherlands.
[7] Center for Molecular Medicine Cologne, University of Cologne, 50931 Cologne, Germany.
[#] These authors contributed equally to this work.

*Correspondence: Email: argyris.papantonis@med.uni-goettingen.de; Tel.: +49 551 39 65734 (A.P.)

ABSTRACT

Mammalian chromosomes are three-dimensional entities shaped by converging and opposing forces. Mitotic cell division induces drastic chromosome condensation, but following reentry into the G1 phase of the cell cycle, chromosomes reestablish their interphase organization. Here, we test the role of RNAPII in this transition using a cell line that allows its auxin-mediated degradation. *In situ* Hi-C showed that RNAPII is required for both compartment and loop establishment following mitosis. RNAPs often counteract loop extrusion and, in their absence, longer and more prominent loops arise. Evidence from chromatin binding, super-resolution imaging, and *in silico* modeling elude to these effects being a result of RNAPII-mediated cohesin loading upon G1 reentry. Our findings reconcile the role of RNAPII in gene expression with that in chromatin architecture.

Keywords: chromatin conformation capture; polymerase degron; topoisomerase; transcriptional elongation; loop extrusion; boundary insulation

***One-sentence summary*:** Following exit from mitosis, RNA pol II is required for reestablishing 3D genome folding by loading cohesin complexes onto DNA.

INTRODUCTION

The evolution and expansion of chromosome conformation capture (3C) technologies (*1*) has profoundly renewed our understanding of the spatial organization of eukaryotic chromosomes and of how it underlies their function and maintenance (*2,3*). It is now well accepted that chromosomes are dynamic entities (*4*), and that their dynamics result from converging and opposing forces acting on chromatin (*5*). These forces include tethering to nuclear landmarks like lamina or the nucleolus (*6*), the interplay between transcription factor-bound *cis*-elements (*7*), and the dynamic extrusion of loops via cohesin complexes (*5,8*).

Cohesin-extruded loops, almost invariably anchored at convergent CTCF-bound sites, are found along mammalian chromosomes representing a prominent feature of 3D genome organization. The combination of high-resolution Hi-C with acute and reversible degradation (*9*) of chromatin-organizing factors has shed light on loop emergence. CTCF degradation causes loss of insulation at thousands of topologically-associated domain (TAD) boundaries (*10*). Cohesin depletion leads to the elimination of essentially all CTCF-anchored loops (*11,12*). Depletion of the cohesin-release factor WAPL promotes loop enlargement and aberrant looping by also engaging non-convergent CTCF-bound anchors (*13*). These observations, together with the recently documented ability of cohesin to extrude loops *in* vitro (*14,15*) and the finding that CTCF-STAG interactions protect cohesin from chromatin release (*16,17*), have crystalized a model for how architectural loops form and dissolve.

In addition to cohesin, another molecular motor known for its ability to translocate DNA is the RNA polymerase (*18*). However, its contribution to chromatin folding is still debated. Different lines of evidence point to a connection between RNAPII binding to chromatin and the differential formation of spatial interactions. To cite some recent examples, allele-specific Hi-C showed that the mouse inactive X chromosome lacks active/inactive compartments and TADs, which however form around “escapee” genes and in the active allele (*19*); the transcriptional state of variably-sized domains across eukaryotes, from *C. elegans* and *D. melanogaster* to *A. thaliana* and mammals, is a robust predictor of interactions mapped via Hi-C and explains chromatin partitioning to a great extent (*20,21*); and TAD emergence coincides with transcriptional activation in zygotes (*22*). Pharmacological abrogation of transcription compacts chromatin (*23*), weakens, but does not alleviate, TAD boundaries (*22,24*), and treating native (*25*) or fixed nuclei (*24*) with RNase does not affect TADs, but eliminates specific contacts. Single-nucleosome imaging upon acute RNAPII depletion showed that polymerases act to constrain and direct chromatin movement in 3D space (*26*), compatible with the idea of transcription-based chromatin organization.

In contrast, RNAPII and Mediator-complex components were found to be dispensable for bringing *cis*-elements into spatial proximity (*27*) and inhibition of transcription in parallel with RAD21 reintroduction in cohesin-depleted cells did not affect loop reestablishment (*11*). Nevertheless, CTCF or cohesin depletion from mammalian cells had rather limited impact on gene expression (*10,11*), and upon cohesin elimination, a comparable number of loops formed on the basis of chromatin identity (*11*) or did not dissolve at all (*28*). Most recently, Micro-C, a sub-kbp Hi-C variant, unveiled thousands of fine-scale loops connecting transcriptionally-active loci in mouse and human cells, often without association to CTCF/cohesin (*29*). Thus, the direct effects of active RNAPs on chromatin folding remain unclear.

On top of its potentially direct effects, RNAPs and the act of transcription may remodel genome folding via interplay with cohesin-CTCF complexes. For example, transcription can relocate cohesin by many kilobases (*30*). Such transcription-mediated displacement can even disrupt prominent CTCF loops and rewire spatial interactions (*31,32*). In addition, RNAPs are essential for domain formation

and often counteracted by condensin complexes (*33,34*). This and other data highlight the need to dissect and reconcile the contribution of RNAPII to chromatin organization. To this end, and as pharmacological inhibition of RNAPs is inefficient, we exploited a human cell line that allows rapid and reversible RNAPII depletion (*26*). We combined *in situ* Hi-C and super-resolution imaging of RNAPII with *in silico* models to disentangle the role of RNAPII in gene expression from that in genome architecture to reconcile the aforementioned observations.

RESULTS

Acute RNAPII depletion impacts loop-level interphase chromatin folding

RNAPII is essential for cell viability, so its depletion may only be transient. Thus, we exploited a human DLD-1 colorectal cancer line, in which the largest RNAPII subunit, RPB1, is N-terminally tagged with a mini-AID domain. This allows for its acute and reversible degradation upon addition of auxin (and of doxycycline to activate the plant ubiquitin ligase TIR1 recognizing this mAID domain; see refs *9,26*). In our hands, 2 h of dox/auxin treatment reduce RNAPII protein levels by >60%, while 14 h of treatment result in >80% degradation as assessed by western blotting – without affecting RNAPI or RNAPIII levels (**Figs 1A** and **Fig. S1A**). Degradation is less impactful on chromatin-embedded RNAPs (e.g., those marked by phosphorylated Ser5 residues in their C-terminal domain). Washing out auxin in the presence of its competitive inhibitor, auxinole, largely restores RNAPII-Ser5 levels (**Fig. S1A**), suggesting that soluble (non-phosphorylated) RNAPII is more susceptible to degradation and that any residual polymerases will be chromatin bound (as was the case for CTCF-mAID; see ref. *10*). Thus, quantitative RNAPII removal can be achieved via this system in order to assess its contribution to genome folding.

To further characterize this line, we performed ChIP-seq using an antibody targeting the mClover tag in RPB1. Compared to public RNAPII ChIP-seq data from DLD-1 (GEO: GSM2769059), mClover-tagged polymerases occupied the same positions and could be depleted from chromatin genome-wide upon auxin treatment (**Fig. 1B**). Polymerase degradation was accompanied by a strong decrease in chromatin accessibility at TSSs (**Fig. 1B**), similar to that recently seen using mESCs (*35*). We also queried the H3K27ac (marking active chromatin) and H3K27me3 histone modifications (marking facultative heterochromatin). Upon RNAPII depletion, significant H3K27ac reduction was observed concomitant with increased H3K27me3 levels (**Fig. S1B,C**). Last, we monitored changes in nascent RNA levels using "factory" RNA-seq (*36*). Control and auxin-treated samples separated well in PCA plots, with ~1500 genes changing their transcription levels significantly (**Fig. S1D,E**). Of these, >90% were downregulated and mainly involved in chromatin assembly and gene expression regulation (**Fig. S1F**).

We next asked whether the spatial organization of interphase chromatin is also altered upon RNAPII depletion. We applied *in situ* Hi-C to G1-sorted DLD1-RPB1-mAID cells treated or not with auxin for 14 h or to cells in which auxin was complemented by triptolide treatment (an inhibitor abrogating transcriptional initiation to further enhance RNAPII degradation; see ref. *37*). Using G1 cells removes heterogeneity arising from S-/G2-phase cells to generate Hi-C maps of greater detail (*38*). Following data analysis, we saw only marginal differences in A-/B-compartments (**Fig. 1C,D**). TADs also showed only mild disruptions (**Fig. 1E,F**), with <20% of the 4,110 identified in control Hi-C data changing in cells lacking RNAPII. 227 new TADs could be detected in auxin-/triptolide-treated cells and displayed reinforced insulation at their boundaries (**Fig. 1F**). Average contact profiles in/around TADs, revealed stronger definition of their borders at the expense of intra-TAD interactions (**Fig. 1G**).

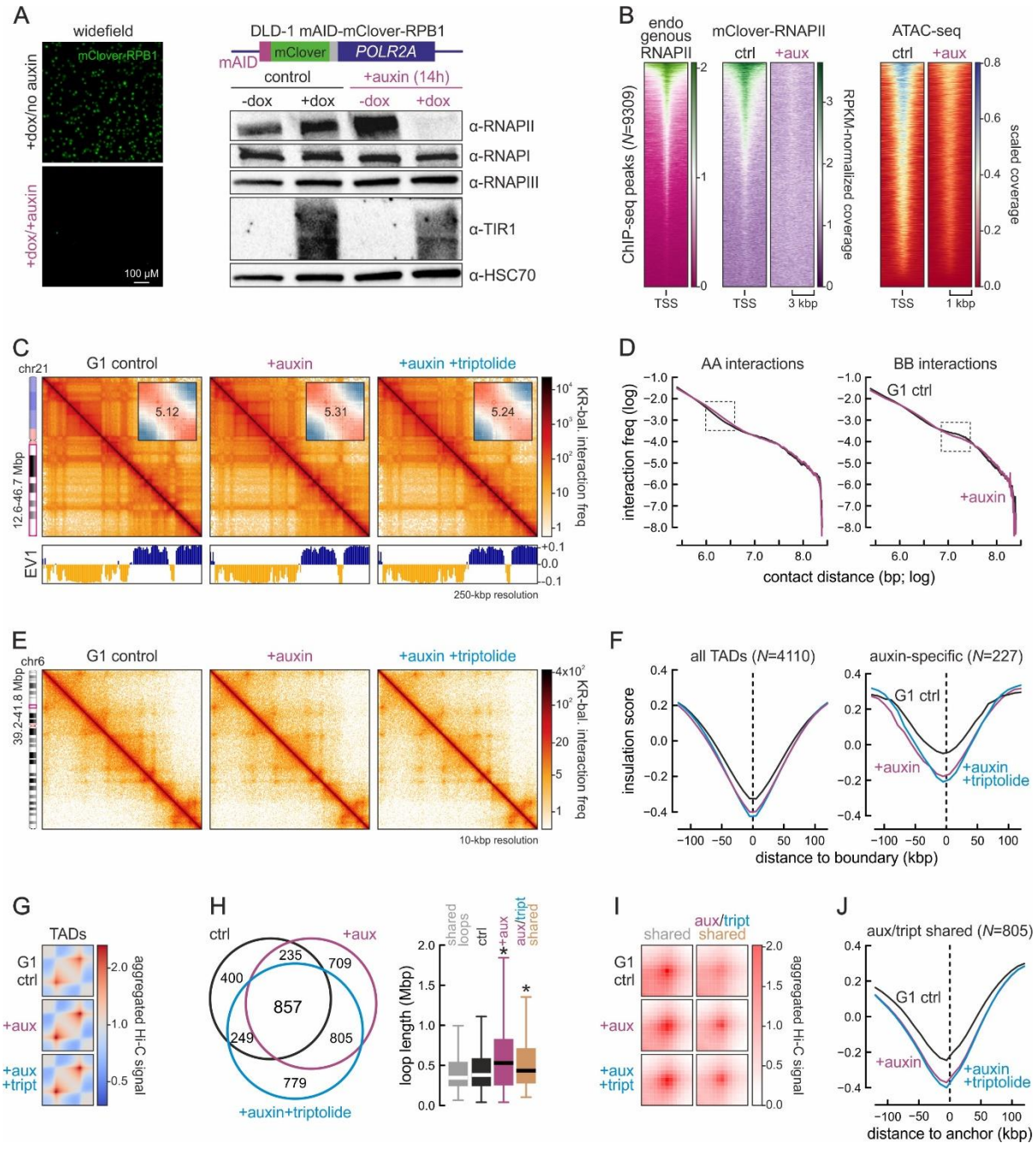

Fig. 1. Effects of acute RNAPII degradation on interphase chromatin folding. (**A**) *Left*: DLD1-mAID-RPB1 cells degrade RNAPII upon 14-h doxycycline/auxin treatment. *Right*: TIR1-mediated RNAPII degradation confirmed by Western blotting; HSC70 levels provide a control. (**B**) Heatmaps of mClover-RNAPII ChIP-seq signal loss upon auxin treatment (middle) overlapping RNAP-bound positions in parental DLD-1 (left) concomitant with decreasing accessibility (right). (**C**) 250-kbp resolution Hi-C from G1-sorted control (left), auxin-treated (middle), and auxin+ triptolide-treated cells (right) aligned to first eigenvector values (EV1). *Insets*: saddle plots showing compartment insulation. (**D**) Plots of Hi-C interaction frequency decay in A- or B-compartments as a function of genomic distance in control (black) or auxin-treated cells (purple). Rectangles: distances where values deviate most. (**E**) 10-kbp resolution Hi-C from control (left), auxin- (middle), and auxin+triptolide-treated cells (right). (**F**) Line plots showing mean insulation from control (black), auxin-treated (purple), and auxin+triptolide-treated

cells (blue) around all or degron-specific TAD boundaries. *N*: number of TADs. (**G**) Heatmaps of aggregated TAD-level interactions in control (top), auxin-treated (middle), and auxin+triptolide-treated cells (bottom). (**H**) *Left*: Venn diagram of shared and unique loops for control (black), auxin-treated (purple), and auxin+triptolide-treated Hi-C (blue). *Right*: Loop lengths displayed as boxplots (right). *: $P<0.01$, Wilcoxon-Mann-Whitney test. (**I**) Plots of aggregated Hi-C signal for loops in panel I. (**J**) As in panel F, but for loop anchors shared by auxin- and auxin+triptolide-treated cells.

Our data so far agreed well with recent observations in mESCs (*35*). However, we also detected >1,500 loops exclusively in auxin-treated cells. These were significantly larger than those in control cells or than those shared between conditions (**Fig. 1H,I**). Of these, 805 loops shared by auxin- and auxin-/triptolide-treated cells were also larger and displayed increased insulation at their anchors (**Fig. 1H-J**). To understand the emergence of these stronger loops, we calculated the cumulative nascent RNA expression levels within the loop domains they form. Compared to all or shared loops from control cells, these 805 were significantly more associated with top-quantile loop domains (F**ig. S1G,H**), suggesting that highly active RNAPII can counteract loop extrusion and its removal leads to stronger loop extrusion. However, although more "stripes" were detected in RNAPII-depleted Hi-C (indicative of loop extrusion; see ref. *39*), these were on average shorter (**Fig. S1I**). In addition almost 10% of these 805 loops also associated with zero-expression domains, but were still enhanced upon RNAPII depletion (**Fig. S1G,H**). We attribute this to Polycomb-mediated interactions that become accentuated upon RNAPII depletion. This is in agreement with the elevated H3K27me3 levels (**Fig. S1C**), the enrichment of H3K27me3 ChIP-seq signal at loop anchors (F**ig. S1J,K**), as well as with recent literature (*40*).

Finally, note that analysis of Hi-C data from mAID-RBP1 cells treated with auxin for 2 h (where 60-70% RPB1 is degraded; **Fig. S1A**), did not reveal changes at any level of spatial genome organization (**Fig. S2A-J**). Together, our data reveal subtle yet discernible effects at the levels of TAD and loop organization occurring upon acute RNAPII depletion in interphase.

Reestablishment of spatial chromatin organization after mitosis requires RNAPII

Since RNAPII depletion did not dramatically affect interphase chromatin organization in asynchronized cell populations, we hypothesized that it may be implicated in reestablishing chromatin folding upon exit from mitosis. This was based on two observations. First, on the detailed description of chromatin refolding dynamics in the mitosis-to-G1 transition, where contacts among *cis*-elements form early and rapidly, often not related to CTCF/cohesin (*41,42*). Second, on the fact that, early in this transition, >50% of all active enhancers and genes exhibit a strong spike in transcription (*43*).

To study chromatin refolding following mitotic exit, we synchronized mAID-RPB1 cells at the G2/M checkpoint using the CDK1 inhibitor RO3306 (blocking ~90% cells in G2; **Fig. 2A,B**), before releasing them via mitosis into G1. 6 h after washing out the inhibitor, >70% cells reentered G1 and were collected by FACS (**Fig. 2A,B**). RNAPII degradation, initiated by adding auxin to cells arrested in G2, was maintained throughout mitosis and G1 reentry without compromising progression past early G1 (as also exemplified by cell cycle markers; **Fig. S3A**). RNAPII degradation was confirmed by fractionation and whole-cell blots (**Fig. 2C** and **Fig. S3B**), immunodetection of Ser5-phosphorylated RNAPs, and EUTP-labeling of nascent RNA (F**ig. S3C,E**). Like in asynchronous cells, the decrease in H3K27ac levels was accompanied by increased H3K27me3 levels in G1-reentry cells depleted of RNAPII (**Fig. S3C,D**). At the same time, the levels of abundant SWI/SNF chromatin remodeler subunits in chromatin were altered, but CTCF incorporation was largely unchanged (**Fig. 2C**).

We next performed Hi-C on G1-reentry cells treated or not with auxin. We obtained >740 million and >1 billion Hi-C contacts from control and auxin-treated samples, respectively (**table S1**). Our first observation was that RNAPII-depleted cells showed increased inter-chromosomal contacts at the expense of intra-chromosomal ones (**Fig. S3F,G**) also confirmed by high throughput 3D-DNA FISH (**Fig. S3H**). At the same time, compartment boundaries were markedly blurred (**Fig. 2D** and **Fig. S3I**), with interactions at distances of >1 Mbp between A- and B-compartment segments becoming stronger (**Fig. 2E**).

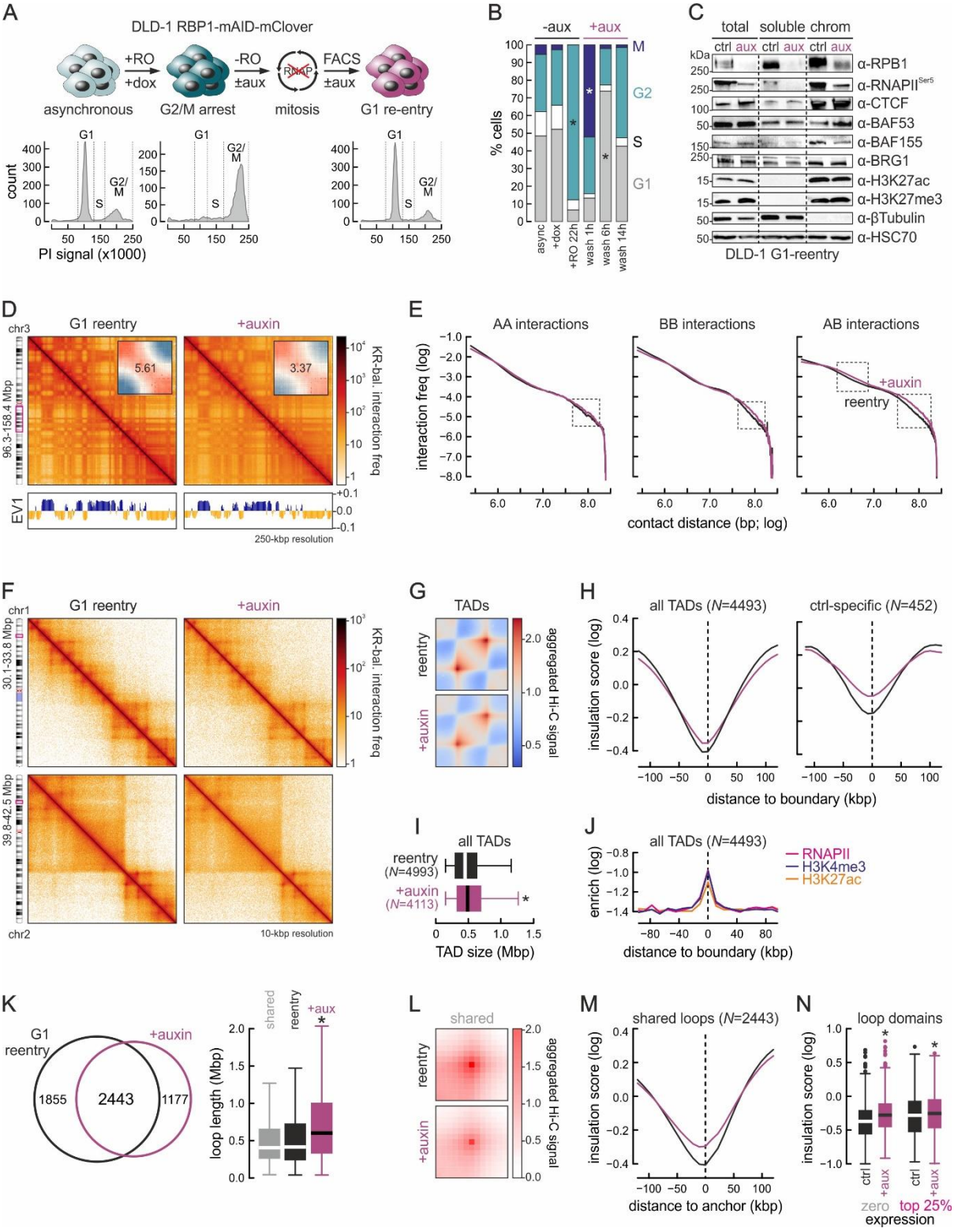

Fig. 2. RNAPII affects genome refolding following mitosis. (**A**) *Top*: DLD1-mAID-RBP1 synchronization. *Bottom*: Propidium iodine FACS profiles. (**B**) Bar plots showing cell percentage in each phase from panel A. *: $P<0.01$, Fischer's exact test. (**C**) Fractionation blots showing RNAPII, chromatin remodeler, and histone mark levels; HSC70 provides a control. (**D**) 250-kbp resolution Hi-C maps from control (left) and auxin-treated cells (right) aligned to first eigenvector values (EV1). *Insets*: saddle plots showing compartment insulation. (**E**) Plots showing interaction frequency decay as a function of genomic distance in control (black) and auxin-treated cells (purple).

Rectangles indicate where values deviate most. (**F**) 10-kbp resolution Hi-C maps from control and auxin-treated cells. (**G**) Heatmaps showing aggregated TAD interactions in control and auxin-treated cells. (**H**) Line plots showing mean insulation from control (black) and auxin-treated cells (purple) around all or control-specific TAD boundaries. *N*: number of TAD boundaries queried. (**I**) Boxplots of TAD sizes in control (black) and auxin-treated cells (purple). *: *P*<0.01, Wilcoxon-Mann-Whitney test. (**J**) Line plot showing RNAPII (magenta), H3K4me3 (blue) and H3K27ac ChIP-seq signal (orange) around control TAD boundaries. (**K**) *Left*: Venn diagram showing shared and unique loops between control (black) and auxin-treated cells (purple). *Right*: Boxplots of loop lengths. *: *P*<0.01, Wilcoxon-Mann-Whitney test. (**L**) Plots of aggregated Hi-C signal for shared loops from panel J. (**M**) As in panel H, but for shared loop anchors. (**N**) Boxplots of loop anchor insulation in control (black) and auxin-treated cells (purple) harboring zero or top-quantile expression levels. *: *P*<0.01, Wilcoxon-Mann-Whitney test.

Loss of interactions at the TAD scale (<1 Mbp) in auxin-treated cells (**Fig. S3J**) led us to analyze 10-kbp resolution Hi-C maps. There, we observed strong and widespread erosion of domain structure, local insulation and loop formation (**Fig. 2F,G** and **Fig. S3K**). Insulation was weakened across all ~4,500 TADs identified in control cells, and even more in the ~10% of TAD boundaries that were not reestablished in the absence of RNAPII (**Fig. 2H**). RNAP-depleted reentry cells also had fewer and larger TADs than control cells (**Fig. 2I**), indicative of boundary collapse and TAD merging. These effects are in line with RNAPII and active histone mark enrichment at TAD boundaries (**Fig. 2J**).

At the loop level, ~1,900 were essentially lost from RNAPII-depleted cells concomitantly with the emergence >1,150 new and significantly longer loops (**Fig. 2K**). Curiously, these longer loops emerged at sites of existing insulation, whereas loops weakened in RNAP-depleted cells showed reduced insulation (**fig. S3L,M**). The 2,443 loops detected in both control and auxin-treated reentry cells were weakened in the absence of RNAPII, while also displaying reduced insulation at their anchors (**Fig. 2K-M**). Again, we compared loop domains of no gene expression to those harboring top-quantile nascent RNA levels. We found that insulation was significantly weakened in both cases (**Fig. 2N**). Finally, looking at stripe formation, we found both accentuated and dissolved ones in RNAP-depleted cells (**fig. S3N,O**).

In summary, our data suggest that RNAPII is implicated in reestablishing both higher-order and fine-scale chromatin folding following exit from mitosis, and its depletion compromises loop formation. Critically, the folding changes that follow polymerase depletion do not simply reflect structures of an earlier G1 time-point (e.g., compared to data from ref. *42*), but rather compromised refolding.

Topoisomerase II depletion does not affect G1-reentry chromatin folding

Transcription enforces supercoiling onto DNA and topoisomerase I (TOP1) is stimulated by RNAPII to resolve supercoils during elongation. However, TOP1 binding alongside initiating polymerases at TSSs was not matched by high TOP1 activity (*44*). In contrast, topoisomerase II has been linked to chromatin organization along the cell cycle and to transcription, with TOP2A affecting RNAPII kinetics (*45*) and marking its pausing sites (*46*). Moreover, TOP2B flanks TAD boundaries in human cells alongside CTCF/cohesin complexes to confine RNAPII (*47*) and preserves domain boundaries in yeast (*48*).

Given that no elongating RNAPs remain in auxin-treated cells, and that TOP2A-mAID cells prolong, but do conclude mitosis (*49*), we asked whether TOP2 depletion from G1-reentry cells explains the effects we observe in RNAPII-depleted cells. To this end, we exploited another colorectal cancer line, HCT116, carrying or not a full knockout of the *TOP2B* gene and homozygously expressing mAID-tagged TOP2A. We verified >70% auxin-induced depletion of TOP2A in TOP2B-knockout cells, and applied the

same synchronization and FACS sorting scheme as before to obtain G1-reentry cells (**Fig. S4A,B**). Using "factory" RNA-seq to compare wild-type cells with those lacking both TOP2A and -B, <400 genes, mostly linked to cell cycle control and cell morphogeneis, were affected by TOP2 elimination (**Fig. S4C**).

Hi-C performed on G1-reentry cells carrying or not TOP2A/B activity revealed marginal changes across all scales of chromatin organization. Compartments were not affected, interactions remained unchanged irrespective of distance, and no increase in *trans* contacts was seen (**Fig. S4D-F**). Negligible changes to TAD boundary insulation were observed, and the mean size of TOP2A/B-depleted TADs did not differ from that in control cells (**Fig. S4G-J**). Finally, although ~600 loops were lost or gained upon TOP2-depletion and condition-specific loops were again larger (**Fig. S3K**), the increase/reduction in Hi-C signal at these loops was significantly less than that recorded upon RNAPII depletion and not followed by changes in insulation at their anchors (**Fig. S4L,M**). In summary, these data suggest that the effects inflicted on chromatin refolding by RNAPII degradation cannot be recapitulated by TOP2A/B depletion, so must rather be polymerase-centric.

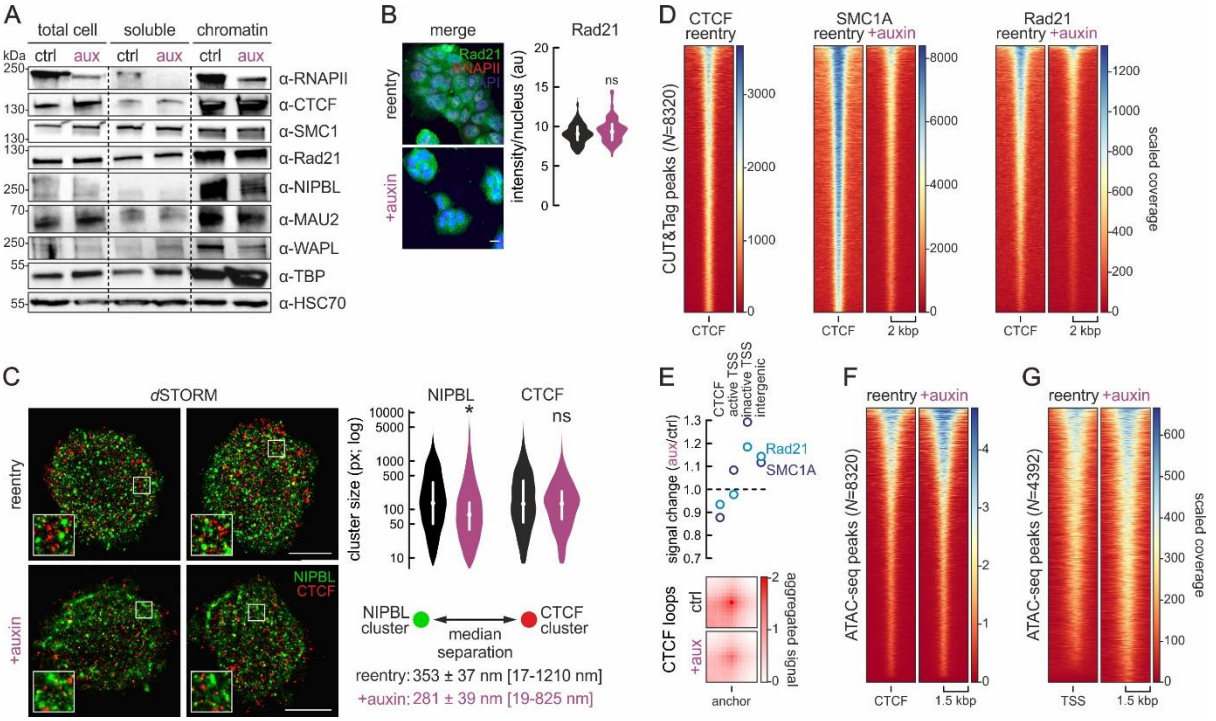

Fig. 3. RNAPII degradation affects CTCF/NIPBL distribution and cohesin loading following mitosis. (**A**) Fractionation blots showing changes in chromatin-bound RNAPII, cohesin loaders NIPBL and MAU2, the WAPL unloader, and TBP; HSC70 provides a loading control. (**B**) RAD21 and RNAPII immunofluorescence in untreated (top) or auxin-treated reentry cells (bottom) and signal quantification (bean plots). Bar: 5 µM. (**C**) *Left*: Rendering of 3D-STORM localizations for NIPBL and CTCF from control (top row) and auxin-treated reentry cells (bottom row). Bar: 5 µM. *Right*: Bean plots showing changes in NIPBL and CTCF cluster sizes. *Bottom right*: Changes in separation between the nearest NIPBL/CTCF clusters (smallest and largest distances shown in square brackets). *: significantly different; $P<0.01$, Wilcoxon-Mann-Whitney test. (**D**) Heatmaps showing SMC1A (middle) and Rad21 CUT&Tag signal (right) in control and auxin-treated G1-reentry cells at CTCF positions (left). (**E**) *Top*: Plot showing changes in SMC1A (dark blue circles) and Rad21 CUT&Tag signal (light blue circles) assigned to CTCF-bound, active/inactive TSSs or intergenic regions in auxin-treated compared to control cells. *Bottom*: Plots

showing aggregate Hi-C signal for loop categories anchored at the CTCF sites in panel D. (**F**) As in panel D, but using ATAC-seq around CTCF-proximal SMC1A/Rad21-bound positions. (**G**) As in panel F, but for active TSSs.

RNAPII removal compromises cohesin chromatin reloading and loop formation

Hi-C data from G1-reentry cells depleted of RNAPII clearly demonstrate A/B-compartment mixing, TAD erosion, and differential loss/gain of loops. Given that loop formation relies on the loading and DNA extrusion by cohesin complexes ending up at CTCF-marked anchors (*10-13,16*), we examined how the levels of CTCF/cohesin subunits change in reentry cells following auxin treatment. Fractionation western blots showed little fluctuation in CTCF, SMC1A or Rad21 levels on chromatin, which was confirmed by quantification of RAD21 levels in individual cells using immunofluorescence (**Fig. 3A,B**). However, the chromatin-bound levels of the two cohesin loaders, NIPBL and MAU2, were markedly reduced, as were the levels of the factor responsible for cohesin unloading, WAPL (concomitant with an increased in its soluble pool titers; **Fig. 3A**). Critically, this is not due to general downregulation of these proteins, because western blots showed that TIR1 activation to degrade RNAPII does not change their abundance in G1-reentry or G2/M-arrested cells (**Fig. S5A,B**).

To understand whether our findings are due to changes in NIPBL and CTCF nuclear distribution, we performed super-resolution localizations of these factors. Dual-color *d*STORM in control and auxin-treated G1-reentry cells led to the following observations. First, NIPBL localizes in clusters of smaller average size upon RNAPII depletion. At the same time, we also observed more localizations in extended and deformed clusters (**Fig. 3C**), exemplified by the shift in "eccentricity" of NIPBL clusters from 0.54 in control to 0.69 in auxin-treated cells (eccentricity of 0 refers to a perfect circle, while eccentricity of 1 to a line). Second, CTCF clusters do not change as regards their mean size, but 50% of all CTCF clusters in control cells lie <129 px^2, while in auxin-treated cells 50% lie <82 px^2 (**Fig. 3C**). Such an increased population of smaller CTCF clusters was also observed via *d*STORM upon cohesin removal in Rad21-mAID cells (*50*) occurring as a result of loop collapse. Last, NIPBL distribution relative to CTCF also changed significantly in the absence of RNAPII. The median separation between NIPBL and its nearest CTCF cluster was reduced from 353 to 281 nm, with the largest recorded distance dropping from >1200 to 825 nm (**Fig. 3C**).

These results, and the changed NIPBL/MAU2/WAPL levels on chromatin, hint to aberrant cohesin loading to (and most likely unloading from) chromatin in the absence of RNAPII, and predict that less cohesin will end up at CTCF-bound sites. To test this prediction, we generated SMC1A and Rad21 CUT&Tag data in control and auxin-treated reentry cells and indeed found cohesin signal significantly reduced at CTCF sites genome-wide (**Fig. 3D**). We quantified the fraction of scaled CUT&Tag signal falling into CTCF-bound regions, active or inactive TSSs, and non-RNAPII-associated intergenic space. We found that the reduced fraction of reads at CTCF sites was accompanied by a 20-30% increase in signal mapping to inactive TSSs in auxin-treated reentry cells, and by a >11% increase in widespread intergenic signal (**Fig. 3E**). It follows that such general reduction of cohesin occupancy at CTCF sites impairs loop formation genome-wide (**Fig. 3E**). Notably, these changes occurred despite no reduction in CTCF-proximal accessibility as judged by ATAC-seq (**Fig. 3F**).

Finally, one could assume that cohesin loading at TSSs (*30,56*) simply results from them being rendered accessible by active RNAPII. Hence, reduced accessibility would readily explain compromised loading. To our surprise, ATAC-seq signal in RNAP-depleted TSSs rather increased (**Fig. 3G**), as did TBP levels on chromatin (**Fig. 3A**). Looking at CUT&Tag signal at >4,000 RNAPII/SMC1A co-occupied TSS, it is drastically reduced upon auxin treatment of reentry cells (**Fig. S5C,D**). This argues in favor of RNAPs recruiting cohesin loaders and unloaders to these sites, while setting up TSS architecture in G1-reentry

cells likely relies on “pioneer” factors (perhaps like TBP) preceding the polymerase. In fact, we used co-immunoprecipitations to show that RNAPII directly interacts with WAPL (**Fig. S5E**), and that NIPBL co-purifies with RNAPII in G1-reentry cells (F**ig. S5F**).

Modeling dissects RNAP contribution to loop extrusion

To dissect the connection between RNAPII and cohesin reloading onto chromatin, we turned to *in silico* modeling of chromatin folding. This allowed us to test scenarios that would be challenging to address experimentally. First, we performed 3D chromatin folding simulations using the established HiP-HoP model (*51*) that accounts for the heteromorphic nature of chromatin, and incorporates transcription factor binding and loop extrusion. We modeled a 10-Mbp region from HUVEC chr14 for which gene expression, histone mark, and CTCF positioning ENCODE data are available (www.encodeproject.org).

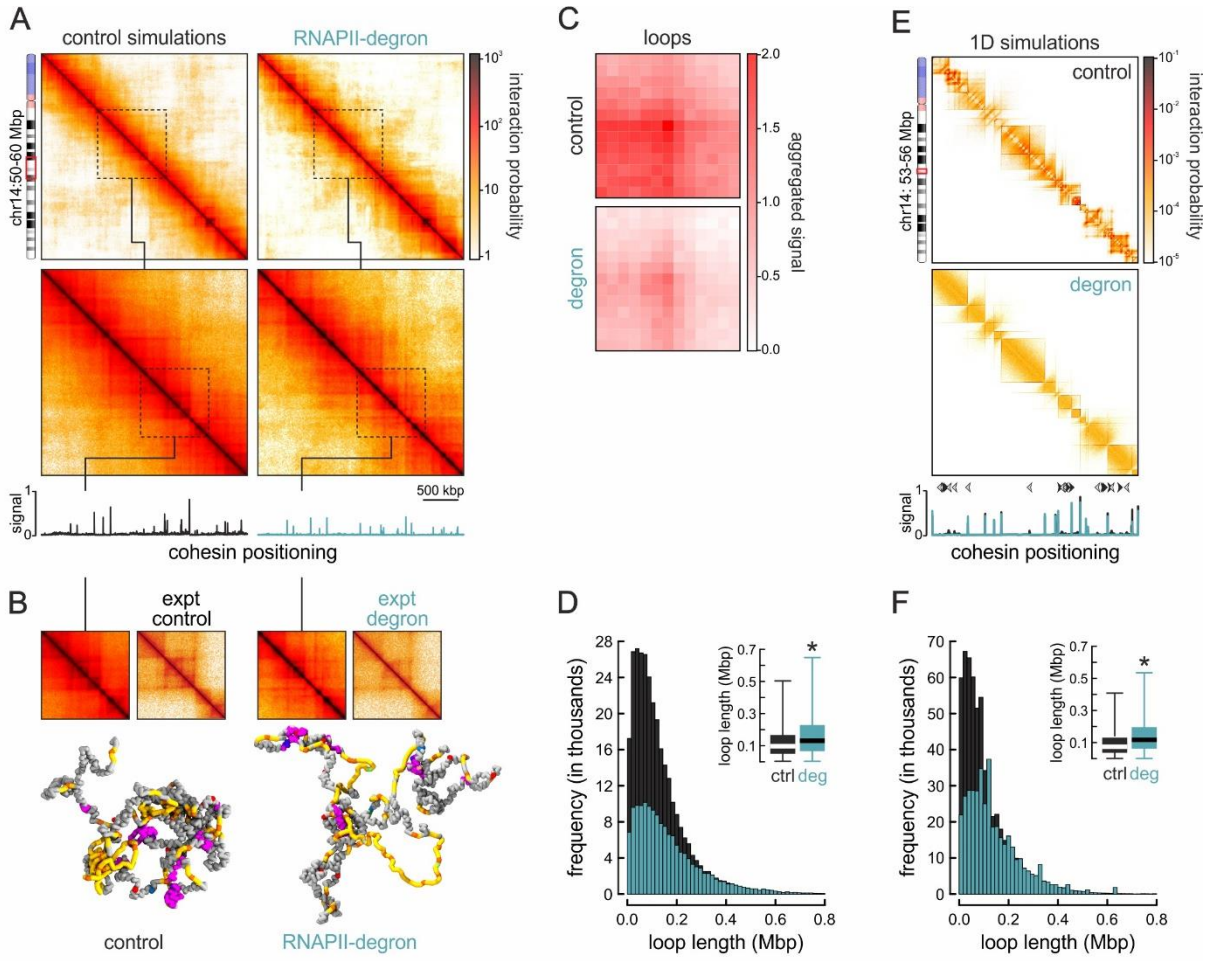

Fig. 4. Computational modeling of RNAPII depletion effects on loop extrusion. (**A**) *Top*: Heatmaps rendered from simulations of wild-type (left) or RNAPII-depleted models (right) of HUVEC chr14:50-60 Mbp. *Bottom*: 10 kbp-resolution heatmaps in the chr14:53-56 Mbp region. Cohesin positioning tracks are aligned below each heatmap. (**B**) Exemplary 3D chromatin folding models of the chr14: 54.5-55.5 Mbp subregion shown in comparison to Hi-C data. (**C**) APA plots showing weakened loops in RNAPII-depleted models. (**D**) Histogram showing looping frequency in the absence of RNAPII (turquoise) compared to wild-type models (black). *Inset*: Boxplots showing larger loops in RNAPII-depleted models (blue). *: significantly different; $P<0.01$, Wilcoxon-Mann-Whitney test. (**E**) Heatmaps rendered from 1D simulations representing wild-type (top) or RNAPII-depleted models (bottom) of the chr14 segment from panel A at 3-kbp resolution. Cohesin positioning (overlaid tracks)

and TSS orientation (arrows) are aligned below. (**F**) As in panel D, but using data from the 1D simulations in panel E.

Control chromatin folding was simulated by assuming that most cohesin loading (90%) occurs at RNAPII-occupied TSSs (with 10% loading randomly). Experimentally-defined cohesin residence times on DNA (~20 min; see ref. *52*) were incorporated into the model. Following multiple iterations, our model produced a mean contact map resembling Hi-C data (**Fig. 4A,B**). To simulate chromatin folding following RNAPII degradation, we eliminated loading at promoters, and only allowed random loading (consistent with low efficacy NIPBL-independent cohesin loading *in vitro*) (*53*). As a result, four major effects were observed. First, a general weakening of interactions and domain insulation across the 10 Mbp modeled (**Fig. 4A,B**), similar to what we saw using Hi-C (**Fig. 2F**). Second, individual models of the fiber displayed obvious unfolding (**Fig. 4B**), likely consistent with the increase in *trans* interactions in our data (**fig. S3F-H**). Third, reduced cohesin occupancy at CTCF sites (**Fig. 4A**), consistent with our CUT&Tag data (**Fig. 3D** and **Fig. S5C,D**). Fourth, markedly weakened loop formation, but with larger loop sizes (**Fig. 4C,D**) matching our experimental results (**Figs 2K,L** and **3E**). Thus, our modeling suggests that inability to load cohesin via RNAPII-bound sites suffices for explaining the major chromatin folding differences observed experimentally.

To interrogate the interplay between RNAPII and loop-extruding cohesin directly, we performed 1D simulations of minimal composition. We modeled a 3-Mbp region of HUVEC chr14 (ch14:53-56 Mbp, hg19) as a coarse-grained fiber carrying CTCF at the appropriate positions, as well as RNAPs transcribing genes in the correct orientation. As before, cohesin was predominantly loaded at RNAPII-bound TSSs in the control scenario, but only randomly in the "degron" model. First, we observed formation of loops and intricate domain compartmentalization under control settings, despite having only two activities operating on the fiber (**Fig. 4E**). Notably, transcription affects cohesin deposition and loop formation in our model, as exemplified by simulations in which all genes in this 3-Mbp segment were modeled as tandemly transcribed (**Fig. S6**). RNAP depletion eliminated compartmentalization and the frequency of looping was again drastically reduced. Cohesin occupancy was decreased at most loop anchors, with loops again becoming larger (**Fig. 4E,F**). This parsimonious model allows us to deduce that the effects observed in experiments can be explained by a simple relationship between cohesin loading at RNAP-occupied sites and the interplay between active transcription and loop extrusion.

DISCUSSION

Following cell division, chromosomes refold in order to establish interphase architecture. At this point, cohesin also needs to be reloaded. Its reloading coincides with the extrusion of CTCF-anchored loops and TAD reestablishment (*41,42*). However, A/B-compartments, driven by homotypic chromatin interactions, reemerge more rapidly, as do contacts amongst *cis*-regulatory elements. Interestingly, the latter display rates that exceed those of extruded loops (*42*). In parallel, the general transcription factor TBP bookmarks mitotic chromatin to facilitate gene reactivation (*54*), and as transcription reinitiates in late telophase, a strong activity spike occurs at most genes and enhancers (*43*). These observations suggest that RNAP activity may play a central role in reestablishing interphase chromatin organization following mitosis.

Here, using an RPB1 "degron" line (*26*), we show that RNAPII presence on chromatin is necessary for both the establishment of compartments and the formation of loops early in G1. The former is intuitively justified by the homotypic interactions that build the "active" A-compartment, and the recent finding that chromatin acetylation can drive compartment formation (*55*). In our RNAPII-

depleted G1-reentry cells, H3K27ac levels are reduced while H3K27me3 levels increase, and this imbalance most probably underlies many of the compartment-level changes, although alleviating H3K27ac bookmarking had little effect on 3D refolding in mESCs (*56*).

The latter effect is more perplexing, but agrees with NIPBL binding at active gene promoters (*30,57,58*) and, thus, raises two key questions. First, how does RNAP depletion promote formation of hundreds of *de novo* loops that are also longer? According to our simulations, and depending on the direction of elongation, RNAPs can reel DNA such that it counters extrusion while also acting as physical blockades to it. This is reminiscent of the condensin-polymerase antagonism reported for bacteria (*34*) and flies (*33*), and inferred by super-resolution imaging in mESCs (*59*). Some of these newly emerging loops form on the basis of strengthened Polycomb interactions, justified by the increase in H3K27me3 levels upon RNAPII degradation. Recent work showing that cohesin removal also resulted in enhancer looping of Polycomb-bound regions (*39*) suggests that RNAPII depletion crosstalks with cohesin loading. As regards increased loop lengths, our simulations argue that this is a consequence of reduced cohesin loading rates to chromatin, as well as of the different loading patterns in control versus RNAP-depleted cells. These translate into fewer cohesin rings acting locally at any given time, and such reduced "crowding" leads to fewer extrusion conflicts allowing longer loops to form. However, when compared to data from *Wapl*-knockout cells showing loop enlargement (*14*), our Hi-C data differ (**Fig. S7A**). But, when compared to Hi-C data from cells undergoing hyperosmotic shock, which affects RNAP as well as cohesin binding to chromatin (*60*), the resulting interaction patterns are much more similar (**Fig. S7B**). These comparisons suggest a distinct and more generalized disruption of the cohesin loading-unloading cycle following RNAPII depletion.

Second, why are the effects of RNAPII depletion more obvious upon G1 reentry? We believe that this is due to a combination of effects. On the one hand, cell synchronization counters the inherent heterogeneity of contacts in individual cells. On the other, early chromatin refolding and transcription bursts in the mitosis-to-G1 transition suggest that RNAPs preempt a central role in establishing a loop-based chromosomal architecture by instructing cohesin loading and compartmentalization. However, we were surprised to find that, in the absence of RNAPII, chromatin accessibility increases following mitotic exit. Although this is counterintuitive, it suggests that the formation of active transcriptional complexes can somehow restrain aberrant accessibility at gene promoters. We speculate that the variable levels of chromatin-bound remodelers (as assessed by western blots in RNAPII-depleted G1-reentry cells) may partly justify this observation. At the same time, this also suggests that pioneer "bookmarking" factors (like TBP, which we find markedly enriched in chromatin in the absence of RNAPII), may have as their default function the "opening up" of chromatin, which is then constrained by preiniatition RNAPs in conjunction with chromatin remodelers recruited at precise stoichiometries.

In summary, we uncovered a dependency of loop extrusion on RNAPII that predominates genome reorganization following exit from mitosis. This dependency may be speak of the significance of mitotic bookmarking, as transcription factor association with mitotic chromatin could dictate RNAP positioning and, in a next step, cohesin loading and loop extrusion. Nonetheless, the precise interplay between polymerases, transcription factors and cohesin subunits during this transition remains to be further elucidated.

MATERIALS AND METHODS

Cell synchronization and sorting

mAID-POLR2A(RPB1)-mClover DLD-1 (*26*) and TO2B-/--TOP2A-mAID HCT116 cells (Roukos lab) were grown in RPMI1640 medium supplemented with 10% FBS under 5% CO_2. Inducible depletion of RPB1

or TOP2A initiated via treatment with doxycycline for 24 h to induce *TIR1* expression, before addition of 500 µM indole-3-acetic acid solution ("auxin", Sigma-Aldrich) for different times to induce RPB1 degradation. For cell synchronization, G2/M arrest was achieved by the addition of 10 µM RO-3306 inhibitor for 21 h. Following this incubation time, cells were washed with PBS, and auxin-supplemented medium was added for up to 6 h to allow cells to quantitatively enter G1. At this point, synchronized or asynchronous cells treated with auxin for up to 14 h were harvested, where applicable resuspended in 1 µg/ml propidium iodide to counterstain DNA, and sorted to isolate G1 cells using a FACS Canto II flow cytometer (Becton Dickinson).

***In situ* Hi-C and data analysis**

All *in situ* Hi-C was performed using the Hi-C+ kit (Arima Genomics) as per manufacturer's instructions. The resulting Hi-C libraries were paired-end sequenced on a NovaSeq6000 platform (Illumina) to >450 million read pairs per replicate (**table S1**). Reads were separately aligned to the reference build of the human genome (hg38) using BWA and Juicer (v. 1.11.09) to generate .hic files (*61*). Only reads with MAPQ >30 were considered for further analysis, and bin-to-bin interactions were extracted from KR-balanced matrices in *.hic* files using the Juicer "dump" utility at different resolutions. A-/B-compartment stratification was performed using the "eigenvector" Juicer utility on 250 kbp-resolution matrices, with both gene and H3K27ac ChIP-seq signal density used to deduce A-compartments. Saddle plots were generated as described previously (*42*). For topologically-associating domains (TADs), KR-balanced matrices we processed via a combination of "directionality index" plus HMM tools at 10 kbp-resolution and in 500-kbp windows. TADs smaller than 150 kbp or found in centromeric regions were filtered out. For a TAD to be considered "shared" between two datasets, boundary positions should not shift by >60 kbp, and their coordinates should overlap should at least 90%. Insulation scores at TAD boundaries were calculated using a sliding 120 kbp x 120 kbp window along the matrix diagonal at 10-kbp resolution as previously described (*62*); squares with a sum of interactions <12 were filtered out. Aggregate TAD plots were generated using *Coolpuppy* (*63*). For loop detection, we used SIP (*64*) and standard parameters: *-res 10000 -mat 2000 -g 2 -d 3 -fdr 0.01 -nbZero 4 -cpu 1 -factor 1 -max 2 -min 2 -sat 0.01 -t 2800 -norm KR -del true*, and an FDR <0.01 to filter the resulting loop lists. Loops specific to a given condition were determined using *pgltools* (with *-d* 29999 due to the smallest allowable loop size of 30 kbp; **table S2**) (https://github.com/billgreenwald/pgltools). Aggregate peak plots were generated via the APA utility in Juicer using standard parameters (*-r 10000 -k KR -q 3 -w 6 -n 15 -u*), before scaling between 0-2 to facilitate comparison. Last, architectural stripes in Hi-C data were detected using *stripenn* (https://github.com/ysora/stripenn). Visualizations and plots were performed using data from merged Hi-C replicates (except for TOP2A-mAID HCT1166 and 2-h RPB1-mAID data); exemplary data from individual Hi-C replicates are shown in **fig. S8** to highlight reproducibility. All code used is available at: https://github.com/shuzhangcourage/HiC-data-analysis.

High throughput 3D-DNA fluorescence in situ hybridization (FISH)

Dual color DNA FISH was performed using the BAC probes targeting different chromosomes (**table S3**) and labeled with Alexa488-dUTP, Alexa568-dUTP or Alexa647-dUTP by nick translation on G1-sorted control and auxin-treated DLD-1 reentry cells seeded on glass slides. Images were acquired using an Opera Phenix High Content Screening System (PerkinElmer), equipped with four laser lines (405 nm, 488 nm, 568 nm, and 640 nm) and two 16-bit CMOS cameras. Images for 3D and radial distances were acquired in confocal mode using a 40X water objective (NA 1.1), and analyzed as described previously to also quantify DNA content and infer cell cycle phase stratification (*65*).

Chromatin immunoprecipitation (ChIP) coupled to sequencing

DLD-1 cells cultured to 80% confluence in 15-cm dishes were crosslinked in 1% PFA/PBS 10 min at room temperature. Cells were processed using the NEXSON ChIP protocol (*66*). In brief, nuclei were isolated via sonication using a Bioruptor Pico (Diagenode; 9 cycles of 10 sec *on* and 30 sec *off*). Chromatin was then sheared in the recommended shearing buffer (27-30 cycles, 30 sec *on* and 30 sec *off*) to a range of 200-500 bp-long fragments, and immunoprecipitation was performed using 4 µg of the appropriate antibody (anti-CTCF: 61311, Active Motif; anti-RAD21: ab88572, Abcam; anti-GFP: ab290, Abcam). Paired-end sequencing was performed on a NovaSeq6000 platform (Illumina) yielding >25 million reads per sample. Raw reads were processed for mapping and peak calling using the ENCODE Data Coordinating Center pipeline (DCC v1.5.0; https://github.com/ENCODE-DCC). Coverage plots and heatmaps were generated via Deeptools (*67*).

Assay for Transposase-Accessible Chromatin using sequencing (ATAC-seq)

Tn5 transposed chromatin was isolated from human DLD-1 mAID-RPB1 cells according to the standard ATAC-seq protocol with a modification (*68*) aiming at quantitative scaling of the resulting data. In brief, 10^5 DLD-1 cells per replicate we "spiked" with 200 *D. melanogaster* S2 cells, washed in 1x PBS and added to lysis buffer (10 mM Tris-HCl pH 7.4, 10 mM NaCl, 3 mM $MgCl_2$, 0.1% NP-40, 0.1% Tween-20, and 0.01% digitonin) for 3 min to isolate nuclei. Nuclei were next washed in washing buffer (10 mM Tris-HCl pH 7.4, 10 mM NaCl, 3 mM $MgCl_2$, 0.1% Tween-20) and pelleted by centrifugation. Isolated nuclei were resuspended in transposase reaction mix (25 µl 2x TD buffer, 16.5 µl 1x PBS, 0.5 µl 10% Tween-20, 0.5 µl 1% digitonin, 2.5 µl Tn5, and 5 µl nuclease-free H_2O) and incubated at 37°C for 30 min under constant shaking at 1000 rpm. The transposition reaction was terminated by the addition of stop buffer (50 mM Tris-HCl pH 8, 10 mM EDTA, 1% SDS), and purified using the DNA Clean & Concentrator kit (Zymo Research). Following standard library generation, samples were sequenced to >40 million reads on a NovaSeq6000 platform (Illumina). Read pairs were mapped to the hg38 and dm6 reference genome builds for human and Drosophila, respectively, using Bowtie 2 (*69*). Unmapped, duplicate, and mitochondrial reads were removed before merging replicates. Finally, ChIPseqSpike was utilized for calculating scaling factors (https://bioconductor.org/packages/release/bioc/html/ChIPSeqSpike.html) to produce RPKM-normalized and scaled coverage.

Cleavage Under Targets and tagmentation (CUT&Tag)

Following lifting from plates using accutase and FACS sorting, 0.5 million G1-phase DLD-1 cells were processed according to manufacturer's instructions (Active Motif). Samples were paired-end sequenced to obtain at least 10^7 reads. Reads were processed according to the standard CUT&Tag pipeline (https://yezhengstat.github.io/CUTTag_tutorial/). Briefly, paired-end reads were trimmed for adapter removal and mapped to the human (hg38) and *E. coli* (ASM584v2) reference genomes using Bowtie 2 (*69*). *E. coli* mapped reads were quantified and used for calibrating human-mapped reads. Peak calling was performed with SEACR (*70*) and using IgG controls for thresholding peak calling. For stringency, cohesin-bound sites were considered those shared by both the SMC1A and Rad21 control datasets, while CTCF-bound those shared by the CUT&Tag and publicly-available CTCF ChIP-seq data (http://chip-atlas.org/view?id=DRX013180). All heatmaps were generated using Deeptools (*67*).

Immunofluorescence and image quantification

DLD-1 cells grown on coverslips were fixed in 4% PFA/PBS for 10 minutes at room temperature. After washing once in PBS, cells were permeabilized with 0.5% Triton-X/PBS for 5 min at room temperature,

washed three times in PBS, blocked using 1% BSA for 1 h, and incubated with the appropriate primary antibody for 1 h at room temperature (anti-RNAPII: 1:500, 61086, Active Motif; anti-H3K27ac: 1:500, 39133, Active Motif; anti-H3K27me3: 1:500, 39155, Active Motif; anti-Rad21: 1:800, ab992, Abcam; anti-Fibrillin: 1:100, sc-393968, Santa Cruz). For visualizing nascent transcripts, cells were pre-incubated with 3 mM 5-ethynyl uridine (EU) for 30 min at 37°C in their growth medium, fixed and processed with the Click-iT EdU chemistry kit (Invitrogen). Images were acquired on a Leica dmi8 microscope using the LASX software. Quantification of nuclear fluorescence were performed by drawing a mask based on DAPI staining, and then calculating the mean intensity per area falling under this mask. Colocalization was assessed using the ImageJ plugin, JACoP (https://imagej.nih.gov/ij/plugins/track/jacop.html).

Chromatin fractionation and western blotting

For assessing protein abundance in different sample preparations, approx. 10^6 cells were gently scraped off 15-cm dishes, and pelleted for 5 min at 600 x *g* at room temperature, supernatants were discarded, and pellets resuspended in 100 µl of ice-cold RIPA lysis buffer (20 mM Tris-HCl pH 7.5, 150 mM NaCl, 1 mM EDTA pH 8.0, 1 mM EGTA pH 8.0, 1% NP-40, 1% sodium deoxycholate) containing 1x protease inhibitor cocktail (Roche). Next, lysates were incubated for 20 min on ice and centrifuged for 15 min at >20,000 x *g* to pellet cell debris to collect the supernatants. The concentration of each protein extract was determined using the Pierce BCA Protein Assay Kit (Thermo Fisher Scientific). For fractionation, the protocol previously described was used (*71*). Following protein separation on precast SDS-PAGE gels (BioRad), proteins were detected using different primary antibodies (**table S4**), and visualized using the Pierce SuperSignal West Pico ECL kit (Thermo Fisher Scientific).

Factory RNA sequencing and data analysis

Nascent RNA from ~10 million mAID-RPB1-mCLover DLD-1 or TO2B$^{-/-}$-TOP2A-mAID HCT116 cells was isolated according to "factory-seq" protocol (*36*). Briefly, cells were gently scraped and lysed in isotonic "physiological buffer" supplemented with 0.5% NP40 buffer. After assessing lysis and nuclei integrity on a hemocytometer microscopy, nuclei were treated with DNase I (Worthington) for 30 min at 33°C, washed, and nuclei were lysed in "native lysis buffer" and treated with caspase group III enzyme mix (PromoKine), pelleted by centrifugation, before the supernatant holding nascent RNA was collected in TRIzol (Invitrogen) and purified using the Direct-Zol RNA purification kit (Zymo). Following standard strand-specific cDNA library preparation using the TruSeq kit (Illumina), sequencing was performed on a NovaSeq6000 platform (Illumina) to >40 million paired-end reads. Raw reads were mapped to human genome (build hg38) using STAR (*72*), quantified using iRNAseq (*73*) and the *-gene* option, before RUVseq normalization (*74*) and differential gene expression analysis. For gene set enrichment, GSEA (http://www.gsea-msigdb.org/gsea/index.jsp) was run on the significantly changing genes (P_{adj}≤0.05; listed in **table S5**).

Dual-color super-resolution dSTORM imaging and analysis

DLD-1 control and auxin-treated reentry cells were seeded onto coverslips, fixed, stained, and imaged as described previously (*50*). In brief, fixed and immunostained cells for NIPBL and CTCF (as described above) were mounted to an Attofluor cell chamber (Thermo Fisher Scientific) and in 1 mL of *d*STORM buffer (25 mM MEA, glucose oxidase, 50 mM NaCl, and 10% glucose in 10 mM Tris-HCl pH 8.0). The chamber is then sealed with a coverslip and left on the microscope at room temperature for 30 min prior to imaging, to minimize drift. Imaging was performed on a Zeiss Elyra PS1 system fitted with an Andor iXon DU 897, 512 × 512 EMCCD camera. Images were made using a 100× 1.49NA TIRF objective

in HiLo mode. Movies of 12,000 frames were recorded with an exposure time of 33 msec. Multichannel images were acquired sequentially from high wavelength to lower wavelengths. *d*STORM movies for each protein target were analyzed via the Zeiss ZEN 2012 software, and any localizations with a precision of >50 nm were discarded. All remaining localizations were drift-corrected using a model-based approach. All additional analysis was done in R (https://www.R-project.org/), localizations from individual nuclei were clustered based on their density using a kernel density estimation (KDE)-based clustering algorithm with the threshold set to 0.05 for all channels. The areas of CTCF or NIPBL clusters were measured using the KDE binary image, and distances between closest neighbors calculated.

Computational modeling

For the 3D simulations, we used our previously described HiP-HoP model (*51*), extended to account for interactions in inactive regions. This model combines our initial "transcription factory" model (*75*) with loop extrusion (*76*), while also accounting for the heteromorphic nature of the chromatin fiber, which means that the local compaction (in DNA base pairs per nanometer) varies along the fiber. Here, we modeled a 10-Mbp region of HUVEC chr14 as a bead-spring polymer containing N beads of diameter σ, each representing 1 kbp of chromatin. We allowed beads in the polymer to interact via three potentials: (i) a Weeks-Chandler-Andersen (WCA) potential, which provides excluded volume interactions; (ii) a finitely-extensible-nonlinear-elastic (FENE) potential accounting for chain connectivity; and (iii) a Kratky-Porod potential describing the flexibility of the chain with parameters set to give a persistence length of 4-5 kbp (in line with that of chromatin *in vivo*). To model the heteromorphic nature of the chromatin fiber in a simple way, we included additional springs (with constants of 200 k_BT/σ^2) between next-to-neighbor chromatin beads along the chain (i.e., beads i and i+2) which are not associated with H3K27ac marks. As H3K27ac marks correlate with active euchromatin regions, these springs cause a local crumpling of the polymer in inactive chromatin fragments, or equivalently a swelling in active regions accounting for their generally more open conformation. Transcription factors (TFs) were simulated as diffusing beads interacting with each other via steric repulsion, again modeled via WCA potentials. We considered three types of TFs: (i) generic active TFs bind strongly (potential depth 7.9 k_BT) to chromatin beads associated with accessible chromatin (defined using ENCODE DHS-seq data), and weakly to beads associated with H3K27ac (potential depth 3.4 k_BT); (ii) HP1-like inactive TFs bind to beads enriched in H3K9me3 marks (potential depth 3.4 k_BT); and (iii) Polycomb-like TFs bind to beads enriched in H3K27me3 marks (potential depth 7.9 k_BT). All of these interactions were modeled via a truncated-and-shifted Lennard-Jones (LJ) potential. To account for post-translational modifications, we allowed each TF type to switch between a binding and a non-binding state at a defined rate ($k_{sw} = 10^{-3}\tau^{-1}$, where τ is the simulation time unit). The binding state was characterized by the aforementioned interaction strengths, whereas the non-binding state only by steric interactions with chromatin beads (via WCA potentials). We considered 250 active TFs, 625 HP1-like TFs, and 125 Polycomb-like TFs in the wild-type simulations, whereas the RNAPII-degron simulations were run without active TFs. We also implemented non-specific interactions between inactive chromatin beads (via a truncated-and-shifted LJ potential with depth 0.45 k_BT) to account for the generic "phase separation" between eu- and hetero-chromatin. Finally, loop extrusion was modeled by representing cohesin dimers as further additional springs. Loop extrusion dynamics were determined by the number density of cohesins (n_c = 0.01/kbp) on the chromatin fiber and two rates: the unbinding rate ($k_{off} = 2.5\times10^{-5}\tau^{-1}$) and the extrusion rate ($v = 4\times10^{-3}$ kbp/τ). Upon binding of cohesin, we introduced an additional spring between two nearby beads along the fiber (i and i+3, since crumpling springs already link i and i+2); the equilibrium length and the spring constant of cohesin bonds were set to 1.5 σ and 40 k_BT/σ^2, respectively. When cohesins were removed

from chromatin, they were instantly repositioned along the fiber. Wild-type conditions were simulated by background random loading (with 10% probability) but with predominant loading at DHS beads (with 90% probability); the RNAPII-degron was simulated by only considering random loading. Finally, a cohesin halted either upon colliding with another extruding complex or upon reaching a CTCF site whose direction was against the direction of extrusion (as shown experimentally; ref. *11*). Note that CTCF sites and orientation were obtained by ENCODE tracks, taking care to include in our simulations only sequences overlapping cohesin (RAD21) peaks – this procedure singles those CTCF binding sites that are relevant to looping. All constituents of the system (chromatin beads and TFs) were allowed to diffuse, and their dynamics were governed by a Langevin equation as described before (*51*) and implemented using Python and the LAMMPS molecular dynamics software package (*77*) as a library.

For the 1D simulations, we considered a 3 Mbp-long chromatin fiber coarse-grained into segments of 1 kbp. Again, we modeled data from a specific subregion of HUVEC chr14. We simulated the dynamics of cohesin rings (total number N_{rings} = 30, comparable to what was used in ref. *76*), each of which could be in one of two states: either bound (i.e., on the fiber) or unbound (i.e., in the diffuse pool). Binding and unbinding were modeled as stochastic processes with rates k_{on} and k_{off}, respectively. When on the fiber, a cohesin molecule was modeled as a dimer, with each monomer undergoing active extrusion at speed v. Each monomer could proceed until it hit a CTCF site with orientation conflicting with its direction of travel, at which point it became immobile (*76*). If a cohesin complex was halted on one side, its other side could continue to move independently. When both monomers in a cohesin dimer became stuck at convergent CTCF sites, the unbinding rate of the dimer was decreased by a factor of 10 to model CTCF-mediated stabilization of extruded chromatin loops, in line with results in ref. *76*. We let monomers in a cohesin dimer interact with each other via steric exclusion so that extrusion would be halted temporarily if another monomer was in their way. Wild-type conditions were simulated by assuming that cohesin was loaded as described above, with 10% background random loading and 90% at DHS sites, whereas RNAPII-degron conditions were simulated by only retaining the random background loading. To simulate feedback of transcription on extrusion, we assumed that the speed of extrusion was reduced by a factor f when the direction of extrusion and that of transcriptional elongation of an active gene were conflicting. Parameters in the simulations were set to $k_{on} = 2\text{x}10^{-2}\ \tau^{-1}$, $k_{off} = 10^{-3}\ \tau^{-1}$, $v = 0.16$ kbt/τ for the wild-type, and to $k_{on} = 2\text{x}10^{-3}\ \tau^{-1}$, $k_{off} = 10^{-3}\ \tau^{-1}$, $v = 0.16$ kbt/τ for the RNAPII-degron. These values can be mapped to $k_{on} = 1$ min^{-1}, $k_{off} = 0.05$ min^{-1}, $v = 0.133$ kbp/s (wild-type, corresponding to a residence time on chromatin ~20 min) or $k_{on} = 0.067$ min^{-1}, $k_{off} = 0.033$ min^{-1}, $v = 0.089$ kbp/s (RNAPII-degron, corresponding to a residence time on chromatin ~30 min). The k_{off} value in simulation units ($k_{off} = 10^{-3}\ \tau^{-1}$) was chosen to be sufficiently small to allow study of extrusion effects. To align simulation times to real times, we consider a residence time on chromatin of ~20 and 30 min for the wild-type and "degron" simulations, respectively. The wild-type value is comparable to that reported previously (*78*). We also set $k_{on} = 1$ min^{-1} (wild-type; while there is no accurate measurements of this rate, it needs to be significantly larger than k_{off}) and reduced its value by a factor 10 in RNAPII-degron simulations in order to have the same rate of random loading both scenarios. Finally, extrusion speed v was chosen such that the chromatin length explored during an extrusion event, $\lambda = v/k_{off}$, was the same for wild-type and "degron", and comparable to that used previously (*76*). For simulations including the feedback of transcription on extrusion, we varied f (which is unknown experimentally) between 0.1 and 0.9 to simulate a variety of scenarios, and presented the case with $f = 0.1$, which led to the most pronounced effects.

Statistical analyses

P-values associated with the Student's t-tests and Fisher's exact tests were calculated using GraphPad (http://graphpad.com/), those associated with the Wilcoxon-Mann-Whitney test using R. Unless otherwise stated, *P*-values <0.01 were deemed significant.

SUPPLEMENTARY MATERIALS

The following supplementary material for this article is available online.

Fig. S1. RNAPII degradation, recovery and its effects on interphase chromatin folding.
Fig. S2. Short-term RNAPII degradation does not affect G1-phase chromatin folding.
Fig. S3. RNAPII degradation affects chromatin refolding in *cis* and in *trans* following mitosis.
Fig. S4. Topoisomerase II depletion marginally affects chromatin refolding following mitosis.
Fig. S5. RNAPII interacts with cohesin complex subunits and its depletion affects their binding to DNA.
Fig. S6. The direction of transcription can affect loop extrusion.
Fig. S7. Comparison of RNAPII-depletion to Wapl/Mau2-depletion or hyperosmotic stress Hi-C data.
Fig. S8. Exemplary Hi-C data from individual replicates.
Table S1. General statistics of all Hi-C datasets.
Table S2. Lists of loops called from Hi-C data.
Table S3. Targets of 3D-DNA FISH probes.
Table S4. Antibodies used in Western blots.
Table S5. Significantly differentially-regulated genes in auxin-treated DLD-1 or HCT116 cells.

REFERENCES

1. S. J. Tjalsma, W. de Laat, Novel orthogonal methods to uncover the complexity and diversity of nuclear architecture. *Curr Opin Genet Dev*. **67**, 10-17 (2020).
2. C. Marchal, J. Sima, D. M. Gilbert, Control of DNA replication timing in the 3D genome. *Nat Rev Mol Cell Biol*. **20**, 721-737 (2019).
3. Q. Szabo, F. Bantignies, G. Cavalli, Principles of genome folding into topologically associating domains. *Sci Adv*. **5**, eaaw1668 (2019).
4. A. S. Hansen, C. Cattoglio, X. Darzacq, R. Tjian, Recent evidence that TADs and chromatin loops are dynamic structures. *Nucleus* **9**, 20-32 (2018).
5. A. Rada-Iglesias, F. G. Grosveld, A. Papantonis, Forces driving the three-dimensional folding of eukaryotic genomes. *Mol Syst Biol*. **14**, e8214 (2018).
6. A. Canat, A. Veillet, A. Bonnet, P. Therizols, Genome anchoring to nuclear landmarks drives functional compartmentalization of the nuclear space. *Brief Funct Genomics* **19**, 101-110 (2020).
7. S. Kim, J. Shendure, Mechanisms of interplay between transcription factors and the 3D genome. *Mol Cell* **76**, 306-319 (2019).
8. J. Nuebler, G. Fudenberg, M. Imakaev, N. Abdennur, L. A. Mirny, Chromatin organization by an interplay of loop extrusion and compartmental segregation. *Proc Natl Acad Sci USA* **115**, E6697-E6706 (2018).
9. A. Yesbolatova, T. Natsume, K. I. Hayashi, M. T. Kanemaki, Generation of conditional auxin-inducible degron (AID) cells and tight control of degron-fused proteins using the degradation inhibitor auxinole. *Methods* **164-165**, 73-80 (2019).
10. E. P. Nora, A. Goloborodko, A. L. Valton, J. H. Gibcus, A. Uebersohn, N. Abdennur, J. Dekker, L. A. Mirny, B. G. Bruneau, Targeted degradation of CTCF decouples local insulation of chromosome domains from genomic compartmentalization. *Cell* **169**, 930-944 (2019).

11. S. S. P. Rao, S. C. Huang, B. Glenn St Hilaire, J. M. Engreitz, E. M. Perez, K. R. Kieffer-Kwon, A. L. Sanborn, S. E. Johnstone, G. D. Bascom, I. D. Bochkov, X. Huang, M. S. Shamim, J. Shin, D. Turner, Z. Ye, A. D. Omer, J. T. Robinson, T. Schlick, B. E. Bernstein, R. Casellas, E. S. Lander, E. Lieberman-Aiden, Cohesin loss eliminates all loop domains. *Cell* **171**, 305-320 (2017).
12. W. Schwarzer, N. Abdennur, A. Goloborodko, A. Pekowska, G. Fudenberg, Y. Loe-Mie, N. A. Fonseca, W. Huber, C. H. Haering, L. Mirny, F. Spitz, Two independent modes of chromatin organization revealed by cohesin removal. *Nature* **551**, 51-56 (2017).
13. J. H. I. Haarhuis, R. H. van der Weide, V. A. Blomen, J. O. Yáñez-Cuna, M. Amendola, M. S. van Ruiten, P. H. L. Krijger, H. Teunissen, R. H. Medema, B. van Steensel, T. R. Brummelkamp, E. de Wit, B. D. Rowland, The cohesin release factor WAPL restricts chromatin loop extension. *Cell* **169**, 693-707 (2017).
14. I. F. Davidson, B. Bauer, D. Goetz, W. Tang, G. Wutz, J. M. Peters, DNA loop extrusion by human cohesin. *Science* **366**, 1338-1345 (2019).
15. Y. Kim, Z. Shi, H. Zhang, I. J. Finkelstein, H. Yu, Human cohesin compacts DNA by loop extrusion. *Science* **366**, 1345-1349 (2019).
16. Y. Li, J. H. I. Haarhuis, S. C. Ángela, O. Roel, M. S. van Ruiten, L. Willems, H. Teunissen, K. W. Muir, E. de Wit, B. D. Rowland, D. Panne, The structural basis for cohesin-CTCF-anchored loops. *Nature* **578**, 472-476 (2020).
17. G. Wutz, R. Ladurner, B. Glenn St Hilaire, R. R. Stocsits, K. Nagasaka, B. Pignard, A. Sanborn, W. Tang, C. Varnai, M. P. Ivanov, S. Schoenfelder, P. van der Lelij, X. Huang, G. Durnberger, E. Roitinger, K. Mechtler, I. Finley Davidson, P. Fraser, E. Lieberman-Aiden, J. M. Peters, ESCO1 and CTCF enable formation of long chromatin loops by protecting cohesin^{STAG1} from WAPL. *eLife* **9**, e52091 (2020).
18. A. Papantonis, P. R. Cook, Fixing the model for transcription: the DNA moves, not the polymerase. *Transcription* **2**, 41-44 (2011).
19. L. Giorgetti, B. R. Lajoie, A. C. Carter, M. Attia, Y. Zhan, J. Xu, C. J. Chen, N. Kaplan, H. Y. Chang, E. Heard, J. Dekker, Structural organization of the inactive X chromosome in the mouse. *Nature* **535**, 575-579 (2016).
20. S. V. Ulianov, E. E. Khrameeva, A. A. Gavrilov, I. M. Flyamer, P. Kos, E. A. Mikhaleva, A. A. Penin, M. D. Logacheva, M. V. Imakaev, A. Chertovich, M. S. Gelfand, Y. Y. Shevelyov, S. V. Razin, Active chromatin and transcription play a key role in chromosome partitioning into topologically associating domains. *Genome Res*. **26**, 70-84 (2016).
21. M. J. Rowley, M. H. Nichols, X. Lyu, M. Ando-Kuri, I. S. M. Rivera, K. Hermetz, P. Wang, Y. Ruan, V. G. Corces, Evolutionarily conserved principles predict 3D chromatin organization. *Mol Cell* **67**, 837-852 (2017).
22. C. B. Hug, A. G. Grimaldi, K. Kruse, J. M. Vaquerizas, Chromatin architecture emerges during zygotic genome activation independent of transcription. *Cell* **169**, 216-228 (2017).
23. C. Naughton, N. Avlonitis, S. Corless, J. G. Prendergast, I. K. Mati, P. P. Eijk, S. L. Cockroft, M. Bradley, B. Ylstra, N. Gilbert, Transcription forms and remodels supercoiling domains unfolding large-scale chromatin structures. *Nat Struct Mol Biol*. **20**, 387-395 (2013).
24. A. R. Barutcu, B. J. Blencowe, J. L. Rinn, Differential contribution of steady-state RNA and active transcription in chromatin organization. *EMBO Rep*. **20**, e48068 (2019).
25. L. Brant, T. Georgomanolis, M. Nikolic, C. A. Brackley, P. Kolovos, W. van Ijcken, F. G. Grosveld, D. Marenduzzo, A. Papantonis, Exploiting native forces to capture chromosome conformation in mammalian cell nuclei. *Mol Syst Biol*. **12**, 891 (2016).

26. R. Nagashima, K. Hibino, S. S. Ashwin, M. Babokhov, S. Fujishiro, R. Imai, T. Nozaki, S. Tamura, T. Tani, H. Kimura, M. Shribak, M. T. Kanemaki, M. Sasai, K. Maeshima, Single nucleosome imaging reveals loose genome chromatin networks via active RNA polymerase II. *J Cell Biol*. **218**, 1511-1530 (2019).
27. L. El Khattabi, H. Zhao, J. Kalchschmidt, N. Young, S. Jung, P. Van Blerkom, P. Kieffer-Kwon, K. R. Kieffer-Kwon, S. Park, X. Wang, J. Krebs, S. Tripathi, N. Sakabe, D. R. Sobreira, S. C. Huang, S. S. P. Rao, N. Pruett, D. Chauss, E. Sadler, A. Lopez, M. A. Nóbrega, E. Lieberman-Aiden, F. J. Asturias, R. Casellas, A pliable mediator acts as a functional rather than an architectural bridge between promoters and enhancers. *Cell* **178**, 1145-1158 (2019).
28. M. J. Thiecke, G. Wutz, M. Muhar, W. Tang, S. Bevan, V. Malysheva, R. Stocsits, T. Neumann, J. Zuber, P. Fraser, S. Schoenfelder, J. M. Peters, M. Spivakov, Cohesin-dependent and -independent mechanisms mediate chromosomal contacts between promoters and enhancers. *Cell Rep*. **32**, 107929 (2020).
29. T. H. S. Hsieh, C. Cattoglio, E. Slobodyanyuk, A. S. Hansen, O. J. Rando, R. Tjian, X. Darzacq, Resolving the 3D landscape of transcription-linked mammalian chromatin folding. *Mol Cell* **78**, 539-553 (2020).
30. G. A. Busslinger, R. R. Stocsits, P. van der Lelij, E. Axelsson, A. Tedeschi, N. Galjart, J. M. Peters, Cohesin is positioned in mammalian genomes by transcription, CTCF and Wapl. *Nature* **544**, 503-507 (2017).
31. S. Heinz, L. Texari, M. G. B. Hayes, M. Urbanowski, M. W. Chang, N. Givarkes, A. Rialdi, K. M. White, R. A. Albrecht, L. Pache, I. Marazzi, A. García-Sastre, M. L. Shaw, C. Benner, Transcription elongation can affect genome 3D structure. *Cell* **174**, 1522-1536 (2018).
32. I. Olan, A. J. Parry, S. Schoenfelder, M. Narita, Y. Ito, A. S. L. Chan, G. S. C. Slater, D. Bihary, M. Bando, K. Shirahige, H. Kimura, S. A. Samarajiwa, P. Fraser, M. Narita, Transcription-dependent cohesin repositioning rewires chromatin loops in cellular senescence. *Nat Commun*. **11**, 6049 (2020).
33. M. J. Rowley, X. Lyu, V. Rana, M. Ando-Kuri, R. Karns, G. Bosco, V. G. Corces, Condensin II counteracts cohesin and RNA polymerase II in the establishment of 3D chromatin organization. *Cell Rep*. **26**, 2890-2903 (2019).
34. H. B. Brandão, P. Paul, A. A. van den Berg, D. Z. Rudner, X. Wang, L. A. MirnY, RNA polymerases as moving barriers to condensin loop extrusion. *Proc Natl Acad Sci USA*. **116**, 20489-20499 (2019).
35. Y. Jiang, J. Huang, K. Lun, B. Li, H. Zheng, Y. Li, R. Zhou, W. Duan, C. Wang, Y. Feng, H. Yao, C. Li, X. Ji, Genome-wide analyses of chromatin interactions after the loss of Pol I, Pol II, and Pol III. *Genome Biol*. **21**, 158 (2020).
36. M. Caudron-Herger, P. R. Cook, K. Rippe, A. Papantonis, Dissecting the nascent human transcriptome by analysing the RNA content of transcription factories. *Nucleic Acids Res*. **43**, e95 (2015).
37. Y. Wang, J. J. Lu, L. He, Q. Yu, Triptolide (TPL) inhibits global transcription by inducing proteasome-dependent degradation of RNA polymerase II (Pol II). *PLoS One* **6**, e23993 (2011).
38. S. Sati, B. Bonev, Q. Szabo, D. Jost, P. Bensadoun, F. Serra, V. Loubiere, G. L. Papadopoulos, J. C. Rivera-Mulia, L. Fritsch, P. Bouret, D. Castillo, J. L. Gelpi, M. Orozco, C. Vaillant, F. Pellestor, F. Bantignies, M. A. Marti-Renom, D. M. Gilbert, J. M. Lemaitre, G. Cavalli, 4D genome rewiring during oncogene-induced and replicative senescence. *Mol Cell* **78**, 522-538 (2020).
39. L. Vian, A. Pekowska, S. S. P. Rao, K. R. Kieffer-Kwon, S. Jung, L. Baranello, S. C. Huang, L. El Khattabi, M. Dose, N. Pruett, A. L. Sanborn, A. Canela, Y. Maman, A. Oksanen, W. Resch, X. Li, B. Lee, A. L. Kovalchuk, Z. Tang, S. Nelson, M. Di Pierro, R. R. Cheng, I. Machol, B. Glenn St Hilaire, N.

C. Durand, M. S. Shamim, E. K. Stamenova, J. N. Onuchic, Y. Ruan, A. Nussenzweig, D. Levens, E. Lieberman-Aiden, R. Casellas, The energetics and physiological impact of cohesin extrusion. *Cell* **173**, 1165-1178 (2018).

40. J. D. P. Rhodes, A. Feldmann, B. Hernandez-Rodriguez, N. Diaz, J. M. Brown, N. A. Fursova, N. P. Blackledge, P. Prathapan, P. Dobrinic, M. K. Huseyin, A. Szczurek, K. Kruse, K. A. Nasmyth, V. J. Buckle, J. M. Vaquerizas, R. J. Klose, Cohesin disrupts polycomb-dependent chromosome interactions in embryonic stem cells. *Cell Rep*. **30**, 820-835 (2020).
41. K. Abramo, A. L. Valton, S. V. Venev, H. Ozadam, A. N. Fox, J. Dekker, A chromosome folding intermediate at the condensin-to-cohesin transition during telophase. *Nat Cell Biol*. **21**, 1393-1402 (2019).
42. H. Zhang, D. J. Emerson, T. G. Gilgenast, K. R. Titus, Y. Lan, P. Huang, D. Zhang, H. Wang, C. A. Keller, B. Giardine, R. C. Hardison, J. E. Phillips-Cremins, G. A. Blobel, Chromatin structure dynamics during the mitosis-to-G1 phase transition. *Nature* **576**, 158-162 (2019).
43. C. C. S. Hsiung, C. R. Bartman, P. Huang, P. Ginart, A. J. Stonestrom, C. A. Keller, C. Face, K. S. Jahn, P. Evans, L. Sankaranarayanan, B. Giardine, R. C. Hardison, A. Raj, G. A. Blobel, A hyperactive transcriptional state marks genome reactivation at the mitosis-G1 transition. *Genes Dev*. **30**, 1423-1439 (2016).
44. L. Baranello, D. Wojtowicz, K. Cui, B. N. Devaiah, H. J. Chung, K. Y. Chan-Salis, R. Guha, K. Wilson, X. Zhang, H. Zhang, J. Piotrowski, C. J. Thomas, D. S. Singer, B. F. Pugh, Y. Pommier, T. M. Przytycka, F. Kouzine, B. A. Lewis, K. Zhao, D. Levens, RNA polymerase II regulates topoisomerase 1 activity to favor efficient transcription. *Cell* **165**, 357-371 (2016).
45. S. Thakurela, A. Garding, J. Jung, D. Schübeler, L. Burger, V. K. Tiwari, Gene regulation and priming by topoisomerase IIα in embryonic stem cells. *Nat Commun*. **4**, 2478 (2013).
46. S. Singh, K. Szlachta, A. Manukyan, H. M. Raimer, M. Dinda, S. Bekiranov, Y. H. Wang, Pausing sites of RNA polymerase II on actively transcribed genes are enriched in DNA double-stranded breaks. *J Biol Chem*. **295**, 3990-4000 (2020).
47. L. Uusküla-Reimand, H. Hou, P. Samavarchi-Tehrani, M. V. Rudan, M. Liang, A. Medina-Rivera, H. Mohammed, D. Schmidt, P. Schwalie, E. J. Young, J. Reimand, S. Hadjur, A. C. Gingras, M. D. Wilson, Topoisomerase II beta interacts with cohesin and CTCF at topological domain borders. *Genome Biol*. **17**, 182 (2016).
48. Y. J. Achar, M. Adhil, R. Choudhary, N. Gilbert, M. Foiani, Negative supercoil at gene boundaries modulates gene topology. *Nature* **577**, 701-705 (2020).
49. C. F. Nielsen, T. Zhang, M. Barisic, P. Kalitsis, D. F. Hudson, Topoisomerase IIα is essential for maintenance of mitotic chromosome structure. *Proc Natl Acad Sci USA* **117**, 12131-12142 (2020).
50. V. Casa, M. M. Gines, E. G. Gusmao, J. A. Slotman, A. Zirkel, N. Josipovic, E. Oole, W. F. J. Van Ijcken, A. B. Houtsmuller, A. Papantonis, K. S. Wendt, Redundant and specific roles of cohesin STAG subunits in chromatin looping and transcriptional control. *Genome Res*. **30**, 515-527 (2020).
51. A. Buckle, C. A. Brackley, S. Boyle, D. Marenduzzo, N. Gilbert, Polymer simulations of heteromorphic chromatin predict the 3D folding of complex genomic loci. *Mol Cell* **72**, 786-797 (2018).
52. A. S. Hansen, I. Pustova, C. Cattoglio, R. Tjian, X. Darzacq, CTCF and cohesin regulate chromatin loop stability with distinct dynamics. *eLife* **6**, e25776 (2017).
53. I. F. Davidson, D. Goetz, M. P. Zaczek, M. I. Molodtsov, P. J. Huis In 't Veld, F. Weissmann, G. Litos, D. A. Cisneros, M. Ocampo-Hafalla, R. Ladurner, F. Uhlmann, A. Vaziri, J. M. Peters, Rapid movement and transcriptional re-localization of human cohesin on DNA. *EMBO J*. **35**, 2671-2685 (2016).

54. S. S. Teves, L. An, A. Bhargava-Shah, L. Xie, X. Darzacq, R. Tjian. A stable mode of bookmarking by TBP recruits RNA polymerase II to mitotic chromosomes. eL*ife* **7**, e35621 (2018).
55. C. D. Rosencrance, H. N. Ammouri, Q. Yu, T. Ge, E. J. Rendleman, S. A. Marshall, K. P. Eagen, Chromatin hyperacetylation impacts chromosome folding by forming a nuclear subcompartment. *Mol Cell* **78**, 112-126 (2020).
56. B. Pelham-Webb, A. Polyzos, L. Wojenski, A. Kloetgen, J. Li, D. C. Di Giammartino, T. Sakellaropoulos, A. Tsirigos, L. Core, E. Apostolou, H3K27ac bookmarking promotes rapid post-mitotic activation of the pluripotent stem cell program without impacting 3D chromatin reorganization. *Mol Cell* **81**, 1732-1748 (2021).
57. J. Zuin, V. Franke, W. F. J. van IJcken, A. van der Sloot, I. D. Krantz, M. I. J. A. van der Reijden, R. Nakato, B. Lenhard, K. S. Wendt, A cohesin-independent role for NIPBL at promoters provides insights in CdLS. *PLoS Genet*. **10**, e1004153 (2014).
58. Y. Zhu, M. Denholtz, H. Lu, C. Murre, Calcium signaling instructs NIPBL recruitment at active enhancers and promoters via distinct mechanisms to reconstruct genome compartmentalization. *Genes Dev*. **35**, 65-81 (2021).
59. B. Gu, C. J. Comerci, D. G. McCarthy, S. Saurabh, W. E. Moerner, J. Wysocka, Opposing effects of cohesin and transcription on CTCF organization revealed by super-resolution imaging. *Mol Cell* **80**, 699-711 (2020).
60. R. Amat, R. Böttcher, F. Le Dily, E. Vidal, J. Quilez, Y. Cuartero, M. Beato, E. de Nadal, F. Posas, Rapid reversible changes in compartments and local chromatin organization revealed by hyperosmotic shock. *Genome Res*. **29**, 18-28 (2019).
61. N. C. Durand, M. S. Shamim, I. Machol, S. S. P. Rao, M. H. Huntley, E. S. Lander, *Cell Syst*. **3**, 95-98 (2016).
62. E. Crane, Q. Bian, R. P. McCord, B. R. Lajoie, B. S. Wheeler, E. J. Ralston, S. Uzawa, J. Dekker, B. J. Meyer, Condensin-driven remodelling of X chromosome topology during dosage compensation. *Nature* **523**, 240-244 (2015).
63. I. M. Flyamer, R. S. Illingworth, W. A. Bickmore, Coolpup.py: versatile pile-up analysis of Hi-C data. *Bioinformatics* **36**, 2980-2985 (2020)
64. M. J. Rowley, A. Poulet, M. H. Nichols, B. J. Bixler, A. L. Sanborn, E. A. Brouhard, K. Hermetz, H. Linsenbaum, G. Csankovszki, E. Lieberman-Aiden, G. Corces, Analysis of Hi-C data using SIP effectively identifies loops in organisms from *C. elegans* to mammals. *Genome Res.* **30**, 447-458 (2020).
65. V. Roukos, G. Pegoraro, T. C. Voss, T. Misteli, Cell cycle staging of individual cells by fluorescence microscopy. *Nat Protoc.* **10**, 334-348 (2015).
66. L. Arrigoni, A. S. Richter, E. Betancourt, K. Bruder, S. Diehl, T. Manke, U. Bonisch, Standardizing chromatin research: a simple and universal method for ChIP-seq. *Nucleic Acids Res*. **44**, e67 (2016).
67. F. Ramírez, F. Dündar, S. Diehl, B. A. Grüning, T. Manke, DeepTools: A flexible platform for exploring deep-sequencing data. *Nucleic Acids Res.* **42**, W187-191 (2014).
68. M. R. Corces, A. E. Trevino, E. G. Hamilton, P. G. Greenside, N. A. Sinnott-Armstrong, S. Vesuna, A. T. Satpathy, A. J. Rubin, K. S. Montine, B. Wu, A. Kathiria, S. W. Cho, M. R. Mumbach, A. C. Carter, M. Kasowski, L. A. Orloff, V. I. Risca, A. Kundaje, P. A. Khavari, T. J. Montine, W. J. Greenleaf, H. Y. Chang, An improved ATAC-seq protocol reduces background and enables interrogation of frozen tissues. *Nat Methods* **14**, 959-962 (2017).
69. B. Langmead, S. L. Salzberg, Fast gapped-read alignment with Bowtie 2. *Nat Methods* **9**, 357-359 (2012).

70. M. P. Meers, D. Tenenbaum, S. Henikoff, Peak calling by Sparse Enrichment Analysis for CUT&RUN chromatin profiling. *Epigenetics Chromatin* **12**, 42 (2019).
71. E. Watrin, A. Schleiffer, K. Tanaka, F. Eisenhaber, K. Nasmyth, J. M. Peters, Human Scc4 is required for cohesin binding to chromatin, sister-chromatid cohesion, and mitotic progression. *Curr Biol*. **16**, 863-874 (2006).
72. A. Dobin, C. A. Davis, F. Schlesinger, J. Drenkow, C. Zaleski, S. Jha, P. Batut, M. Chaisson, T. R. Gingeras, STAR: ultrafast universal RNA-seq aligner. *Bioinformatics* **29**, 15-21 (2013).
73. J. G. S. Madsen, S. F. Schmidt, B. D. Larsen, A. Loft, R. Nielsen, S. Mandrup, iRNA-seq: computational method for genome-wide assessment of acute transcriptional regulation from total RNA-seq data. *Nucleic Acids Res*. **43**, e40 (2015).
74. D. Risso, J. Ngai, T. P. Speed, S. Dudoit, Normalization of RNA-seq data using factor analysis of control genes or samples. *Nat Biotech.* **32**, 896-902 (2014).
75. C. A. Brackley, J. Johnson, S. Kelly, P. R. Cook, D. Marenduzzo, Simulated binding of transcription factors to active and inactive regions folds human chromosomes into loops, rosettes and topological domains. *Nucleic Acids Res*. **44**, 3503-3512 (2016).
76. G. Fudenberg, M. Imakaev, C. Lu, A. Goloborodko, N. Abdennur, L. A. Mirny, Formation of chromosomal domains by loop extrusion. *Cell Rep*. **15**, 2038-2049 (2016).
77. S. Plimpton, Fast parallel algorithms for short-range molecular dynamics. *J Comp Phys.* **1**, 1-19 (1995).
78. A. S. Hansen, I. Pustova, C. Cattoglio, R. Tjian, X. Darzacq, CTCF and cohesin regulate chromatin loop stability with distinct dynamics. *eLlife* **6**, e25776 (2017).

Acknowledgements: We thank Peter Cook, Nick Gilbert, and Juanma Vaquerizas for critical reading of the manuscript, the Maeshima lab (NIG, Japan) for gifting us the DLD-1 mAID-RPB1 cells, and the NGS Integrative Genomics UMG unit for ATAC library sequencing. **Funding:** Work in the lab of A.P. is funded by the Deutsche Forschungsgemeinschaft (DFG) via a Basic module grant (Project Nr.: 290613333) and the SPP2202 (422389065) and TRR81 programs (109546710). S.Z. is supported by a CSC fellowship. S.Z., N.Ü., and N.J. are further supported by the International Max Planck Research School for Genome Science. Work in the lab of D.M. is supported by an ERC Consolidator grant (THREEDCELLPHYSICS), work in the lab of K.S.W. was supported by the project GENOMETRACK (737.016.014) NWO-BBOL research programme financed by the Dutch Research Council (NWO), and in the lab of V.R. by the DFG via the SFB1361 (393547839) and SPP2202 programs (402733153). **Author contributions:** S.Z., N.Ü., and N.J. performed experiments. S.Z., N.J., and E.G.G. performed bioinformatics analyses. G.F., M.C., and D.M. performed computational modeling. H.G. and V.R. performed 3D DNA FISH. J.S., A.B.H., and K.S.W. performed super-resolution STORM imaging. C.B. and J.A. performed all next-generation sequencing. A.P. conceived and supervised the study, and compiled the manuscript with input from all coauthors. **Competing interests:** The authors have no competing interests to declare. **Data availability:** NGS data generated in this study are available via the NCBI Gene Expression Omnibus (GEO) repository under accession number GSE160321. All data needed to evaluate the conclusions in this paper are present in the main text and Supplementary Materials.

Science
AAAS

Supplementary Materials
for

RNA polymerase II is required for spatial chromatin reorganization following exit from mitosis

S. Zhang[1,#], N. Übelmesser[1,#], N. Josipovic[1,#], G. Forte[2], J. A. Slotman[3], M. Chiang[2], H. Gothe[4], E. G. Gusmao[1], C. Becker[5], J. Altmüller[5], A. B. Houtsmuller[3], V. Roukos[4], K. S. Wendt[6], D. Marenduzzo[2], A. Papantonis[1,7,*]

[1] Institute of Pathology, University Medical Center Göttingen, 37075 Göttingen, Germany.
[2] School of Physics and Astronomy, University of Edinburgh, EH9 3FD Edinburgh, United Kingdom.
[3] Optical Imaging Centre, Erasmus Medical Center, 3015 GD Rotterdam, Netherlands.
[4] Institute of Molecular Biology, 55128 Mainz, Germany.
[5] Cologne Center for Genomics, University of Cologne, 50931 Cologne, Germany.
[6] Department of Cell Biology, Erasmus Medical Center, 3015 GD Rotterdam, The Netherlands.
[7] Center for Molecular Medicine Cologne, University of Cologne, 50931 Cologne, Germany.
[#] These authors contributed equally to this work.

*Correspondence: argyris.papantonis@med.uni-goettingen.de (A.P.)

This PDF file includes:

Figures S1 to S8
Tables S1, S3 and S4
Captions for Tables S2 and S5

Other Supplementary Materials for this manuscript include:

Tables S2 and S5 (provided online as *.xlsx* files)

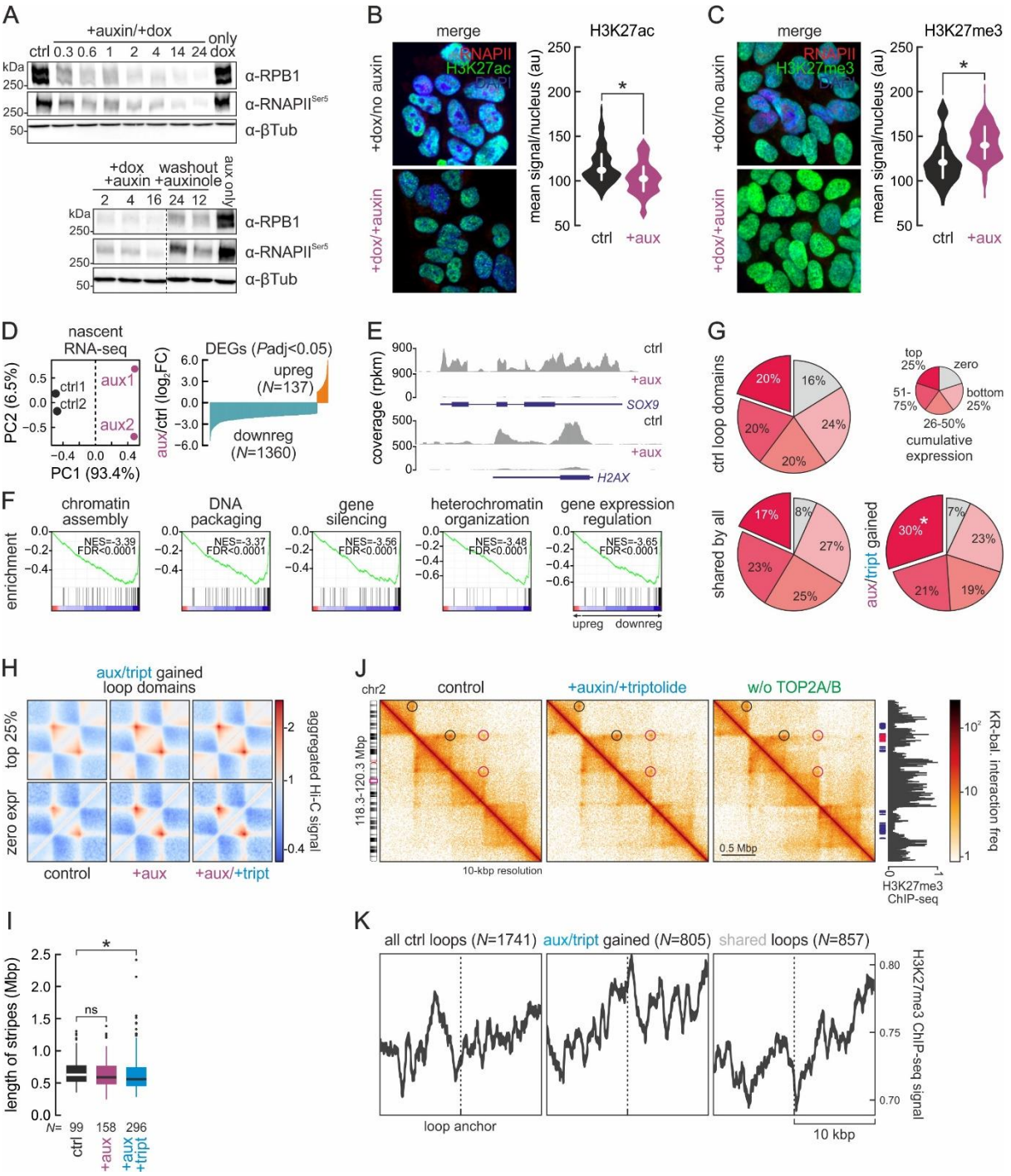

Fig. S1. RNAPII degradation, recovery and its effects on interphase chromatin folding. (**A**) Western blots showing depletion of total cell RPB1 or phospho-Ser5-RNAPII on increasing exposure to doxycycline plus auxin (top) or RNAPII recovery following auxin washout in the presence of auxinole (bottom); β-tubulin provides a loading control. (**B**) Representative H3K27ac immunofluorescence from untreated (top) or 14-h auxin-treated cells (bottom) and signal quantification (bean plots). *: significantly different; *P*<0.01, Wilcoxon-Mann-Whitney test. Bar: 5 µM. (**C**) As in panel B, but for H3K27me3 levels. (**D**) *Left*: PCA plot for G1-sorted control (black) and 14-h auxin-treated nascent RNA-seq data (purple). *Right*: Nascent RNA changes (log_2 fold-change compared to control; P_{adj}<0.05) in 1497 genes upon auxin treatment. (**E**) Genome browser examples of nascent RNA reduction at two typical gene loci. (**F**) Gene set enrichment analysis of data in panel D; top five enriched pathways. (**G**)

Pie charts showing distribution of all (top), shared (bottom left) and auxin/triptolide-shared loops (bottom right) according to their cumulative gene expression levels (no expression – grey; four nonoverlapping quantiles – shades of red). *: significantly different; $P<0.05$, Fisher's exact test. (**H**) Heatmaps showing mean loop domain interactions in control (top), auxin- (middle) and auxin-/triptolide-treated cells (bottom) for the auxin/triptolide-shared loops of panel G. (**I**) Boxplots showing changes in the length of stripes detected in Hi-C data from control (black), auxin-treated (purple) or auxin/triptolide-treated Hi-C data (blue). *: significantly different to control; $P<0.05$, Wilcoxon-Mann-Whitney test. (**J**) Hi-C maps from control (left), auxin/triptolide-treated (middle) or TOP2A/B-depleted cells (right) in the chr2 subregion encompassing the *HOXD* gene cluster. H3K27me3 ChIP-data from control cells are aligned to the maps, and emerging H3K27me3-anchored loops are denoted (red circles). (**K**) Line plots showing mean H3K27me3 ChIP-seq signal enrichment in the 20 kbp around all (left), auxin-/triptolide-gained loops (middle) or loops shared between RNAPII-depleted and control cells (right). The number of loops in each group (*N*) is indicated. The Hi-C data presented and analyzed in panels H-K come from individual Hi-C replicates (see Table S1).

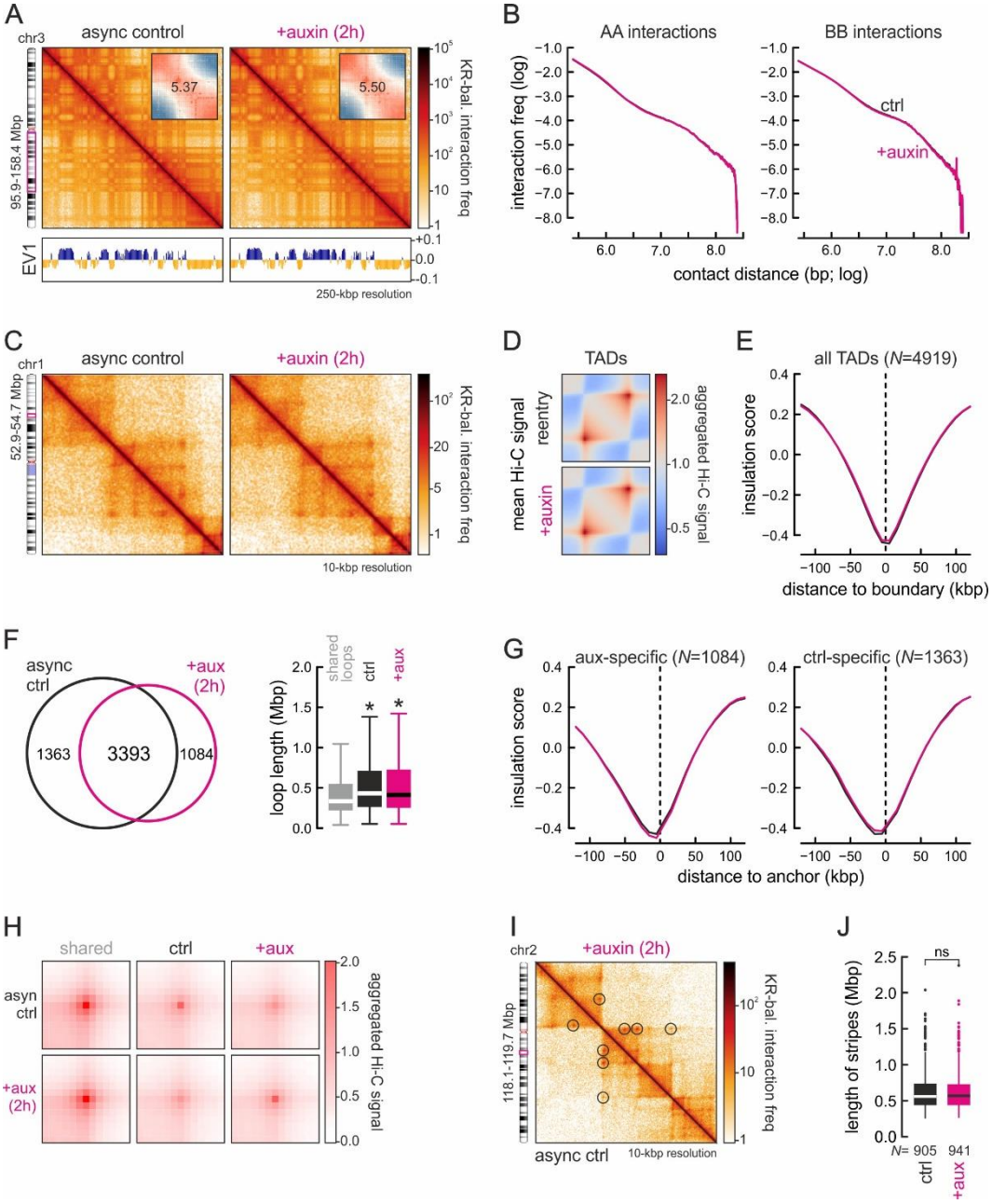

Fig. S2. Short-term RNAPII degradation does not affect G1-phase chromatin folding. (**A**) Exemplary Hi-C maps of a subregion of chr3 from asynchronous control (left) and 2-h auxin-treated DLD1-mAID-RPB1 cells (right) at 250-kbp resolution aligned to first eigenvector values (EV1; below). *Insets*: saddle plots showing no change in A/B-compartment insulation. (**B**) Decay plots showing Hi-C interaction frequency between A- (left) or B-compartments (right) as a function of genomic distance (log) in control (black line) and 2-h auxin-treated cells (magenta line). (**C**) Exemplary Hi-C maps of a subregion of chr1 from control (left) and auxin-treated cells (right) at 10-kbp resolution. (**D**) Heatmaps showing aggregated TAD-level interactions in control (top) and auxin-treated cells (bottom). (**E**) Line plots showing mean insulation score from control (black line) and auxin-treated cells (magenta line) in the 240 kbp around all TAD boundaries in control cells. The number of TAD boundaries queried (*N*) is indicated. (**F**) *Left*: Venn diagram showing shared and unique loops in control (black) and auxin-treated Hi-C data (magenta). *Right*: Loop lengths displayed as boxplots. *: significantly different; *P*<0.01, Wilcoxon-Mann-Whitney test. (**G**) As in panel E, but for the anchors of control- (left) and degron-specific loops

(right; from panels H,I). (**H**) Aggregate plots showing mean Hi-C signal at shared (left), control- (middle), and degron-specific loops (right) from panel F. (**I**) Composite Hi-C map showing little change in loop emergence (circles) between control (bottom half) and auxin-treated cells (top half). (**J**) Boxplots showing no significant change in the length of stripes detected in Hi-C data from control (black) or auxin-treated cells (magenta). The Hi-C data presented and analyzed in panels A-J come from individual Hi-C replicates (see Table S1).

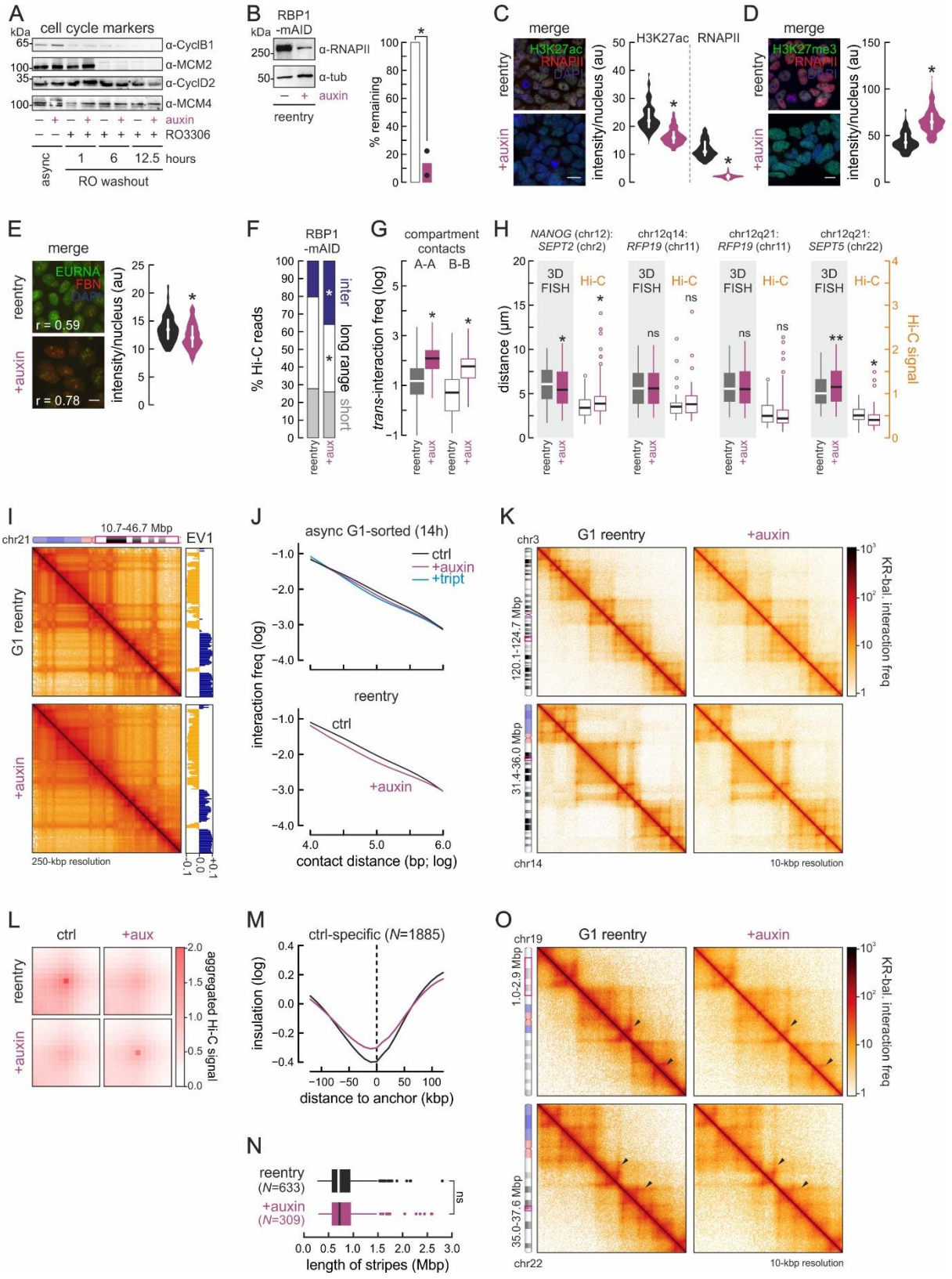

Fig. S3. RNAPII degradation affects chromatin refolding in *cis* and in *trans* following mitosis. (**A**) Western blots of selected cell cycle markers in cells treated or not with auxin at different times after release from the G2/M block. (**B**) *Left*: Western blot of RNAPII (RPB1) in G1-reentry cells treated or not with auxin; β-tubulin provides a loading control. *Right*: Quantification of such western blot data from two independent replicates. *: significantly different mean; $P<0.01$, unpaired two-tailed Student's t-

test. (**C**) *Left*: Exemplary widefield immunofluorescence images of DLD1-mAID-RPB1 G1-reentry cells treated with doxycycline plus auxin (bottom) or not (top) and stained for H3K27ac and RNAPII (RPB1); nuclei were counterstained with DAPI. *Right*: Bean plots showing mean fluorescence intensity per nucleus. *: significantly different; *P*<0.01, Wilcoxon-Mann-Whitney test. (**D**) As in panel C, but stained for RNAPII and H3K27me3, and quantifying H3K27me3 levels. (**E**) As in panel C, but stained for fibrillin and EU-labeled nascent RNA, and quantifying EU-RNA levels. The correlation of signal from the two fluorescent channels (r) is also indicated. (**F**) Bar plots showing percent of Hi-C reads in inter- (blue), long-range (>20 kbp) or short-range intra-chromosomal contacts (white) across datasets. *: significantly different; *P*<0.01, Fisher's exact test. (**G**) Boxplots showing inter-chromosomal interactions between A-A and B-B compartments in auxin-treated versus control reentry cells. *: significantly different; *P*<0.01, Wilcoxon-Mann-Whitney test. (**H**) Boxplots comparing interchromosomal distance changes for the loci indicated assessed using high throughput 3D-DNA FISH (grey background) or Hi-C data at 0.5-Mbp resolution. *: significantly different; *P*<0.01, Wilcoxon-Mann-Whitney test. (**I**) Additional Hi-C examples of a subregion of chr3 from control (top) and auxin-treated reentry cells (bottom) at 250-kbp resolution aligned first eigenvector values (right). (**J**) Decay plots showing Hi-C interaction frequency as a function of genomic distance (log) at the scale of TADs (0.01-1 Mbp) in control (black line) or auxin-treated reentry cells (purple/blue lines). (**K**) Additional Hi-C examples of subregions in chr3 and 14 from control (left) and auxin-treated reentry cells (right) at 10-kbp resolution. (**L**) Plots showing aggregate Hi-C signal for loops lost/gained in control (left) and auxin-treated reentry cells (right). (**M**) Line plots showing mean insulation scores in the 240 kbp around control- (top) or degron-specific loops (bottom) from control (black line) and auxin-treated cells (purple line). The number of anchors queried (*N*) is indicated. (**N**) Boxplots showing no significant change in the length of stripes detected in Hi-C data from control (black) or auxin-treated cells (purple). (**O**) Hi-C maps showing typical changes in "stripes" (arrowheads) between control (left) and auxin-treated reentry cells (right) at 10-kbp resolution. The Hi-C data presented and analyzed in panels I-O come from two merged Hi-C replicates (see Table S1).

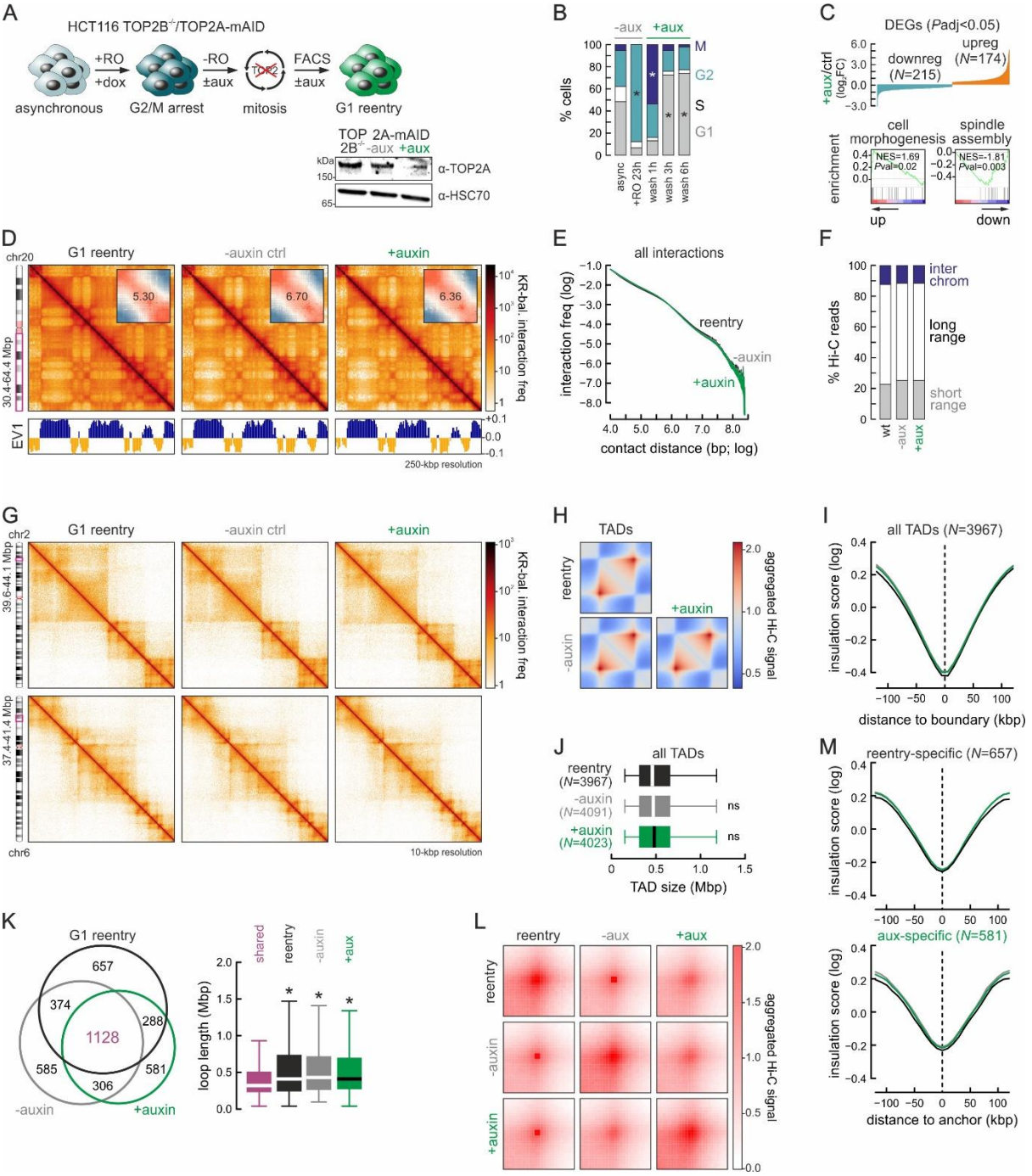

Fig. S4. Topoisomerase II depletion marginally affects chromatin refolding following mitosis. (**A**) *Top*: Overview of the experimental scheme for HCT116-TOP2B$^{-/-}$-TOP2A-mAID cell synchronization and release. *Bottom right*: Western blots showing auxin-mediated TOP2A degradation; HSC70 provides a loading control. (**B**) Bar plots showing the percent of cells in each phase from panel A. *: significantly different; P<0.01, Fisher's exact test. (**C**) *Top*: Graph showing nascent transcription changes ($\log_2$ fold-change compared to control, P_{adj}<0.05) upon TOP2-depletion. *Bottom*: Gene set enrichment analysis. (**D**) Exemplary Hi-C maps of a subregion of chr20 from control (left), TOP2B$^{-/-}$-untreated and TOP2B$^{-/-}$-auxin-treated G1-reentry cells (right) at 250-kbp resolution aligned to first eigenvector values (below). *Insets*: saddle plots showing compartment insulation. (**E**) Decay plots showing interaction frequency as a function of genomic distance (log) in the Hi-C data from panel D. (**F**) Bar plots showing the percentage of Hi-C reads in interchromosomal (blue), long- (>20 kbp; white) and short-range intra-chromosomal

contacts (grey) in the Hi-C data from panel D. (**G**) Exemplary 10-kbp resolution Hi-C maps of subregions in chr1 and 6 from the same conditions as in panel D. (**H**) Heatmaps showing aggregated TAD-level interactions in control (top), TOP2B$^{-/-}$-untreated (bottom left) and TOP2B$^{-/-}$-auxin-treated reentry cells (bottom right). (**I**) Line plots showing mean insulation scores in the 240 kbp around TAD boundaries from panel H. The number of TADs queried (*N*) is indicated. (**J**) Boxplots showing size changes in the TAD groups from panel H. (**K**) *Left*: Venn diagram showing shared and unique loops between the Hi-C datasets from panel D. *Right*: Loop lengths displayed as boxplots. *: significantly different to shared loops; $P<0.01$, Wilcoxon-Mann-Whitney test. (**L**) Plots showing aggregate Hi-C signal for the loop categories from panel K. (**M**) As in panel I, but for the anchors of loop from panels K,L. The Hi-C data presented and analyzed in panels A-M come from individual Hi-C replicates (see Table S1).

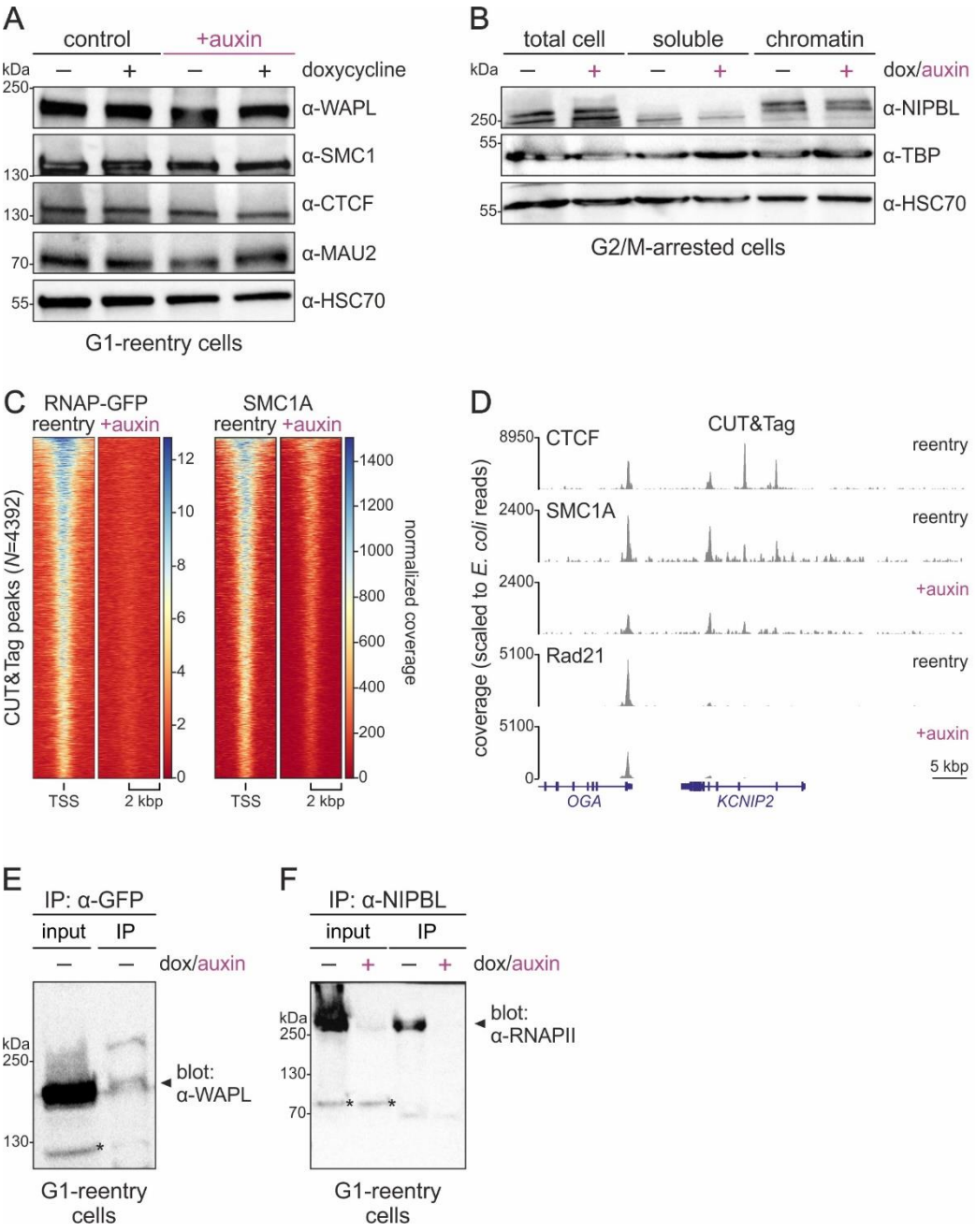

Fig. S5. RNAPII interacts with cohesin complex subunits and its depletion affects their binding to DNA. (**A**) Western blots showing unchanged cohesin components (SMC1A, MAU2, WAPL) and CTCF levels upon RNAPII degradation in G1-reentry cells; HSC70 provides a control. (**B**) Fractionation blots for NIPBL and TBP in G2/M-arrested cells treated or not with auxin; HSC70 provides a control. (**C**) Heatmaps showing scaled RNAPII (left) and SMC1A (right) CUT&Tag signal from control and auxin-treated G1-reentry cells in the 4 kbp around active TSSs. (**D**) Typical browser views of CTCF, SMC1A, and Rad21 CUT&Tag data from G1-reentry cells treated or not with auxin (merge of two replicates). (**E**) Western blot showing WAPL co-immunoprecipitating with mClover-mAID-RPB1 in G1-reentry cells. (**F**) As in panel E, but showing RNAPII (RPB1) co-immunoprecipitating with NIPBL only in untreated G1-reentry cells. *: unspecific bands.

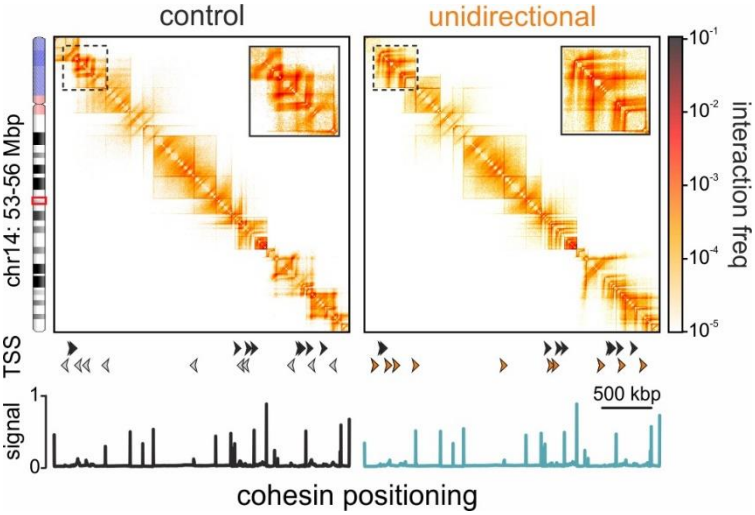

Fig. S6. The direction of transcription can affect loop extrusion. Heatmaps rendered from loop extrusion 1D simulations representing wild-type chromatin (left) or chromatin where all TSS are transcribed in the same direction (right) in the HUVEC chr14:53-56 Mbp segment. Profiles of cohesin positioning and TSS orientations are aligned below each heatmap (reoriented TSSs are indicated in orange).

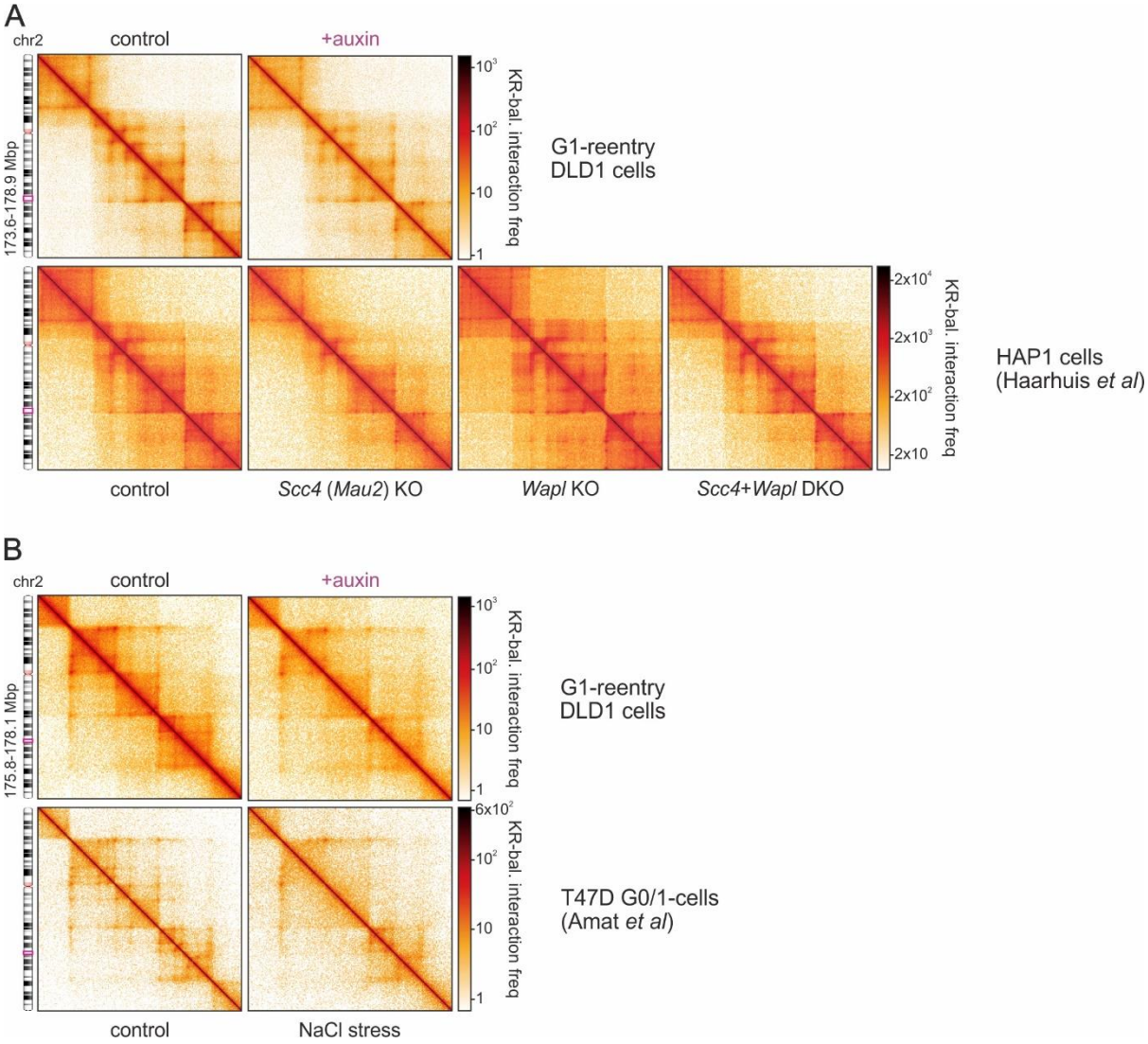

Fig. S7. Comparison of RNAPII-depletion to Wapl/Mau2-depletion or hyperosmotic stress Hi-C data. (**A**) Exemplary Hi-C heatmaps from a subregion for chr2 (ideogram) derived from G1-reentry DLD-1 (top row) compared to heatmaps from wild-type, *Scc4*-KO, *Wapl*-KO, and *Scc4*/*Wapl*-DKO HAP1 cells (bottom row; data from ref. *13*). (**B**) As in panel A, but comparing Hi-C from G1-reentry DLD-1 (top row) to data from T47D cells before and after NaCl stress (bottom row; data from ref. *60*). All Hi-C data presented here are from merged Hi-C replicates (see Table S1 and refs *13* and *60*).

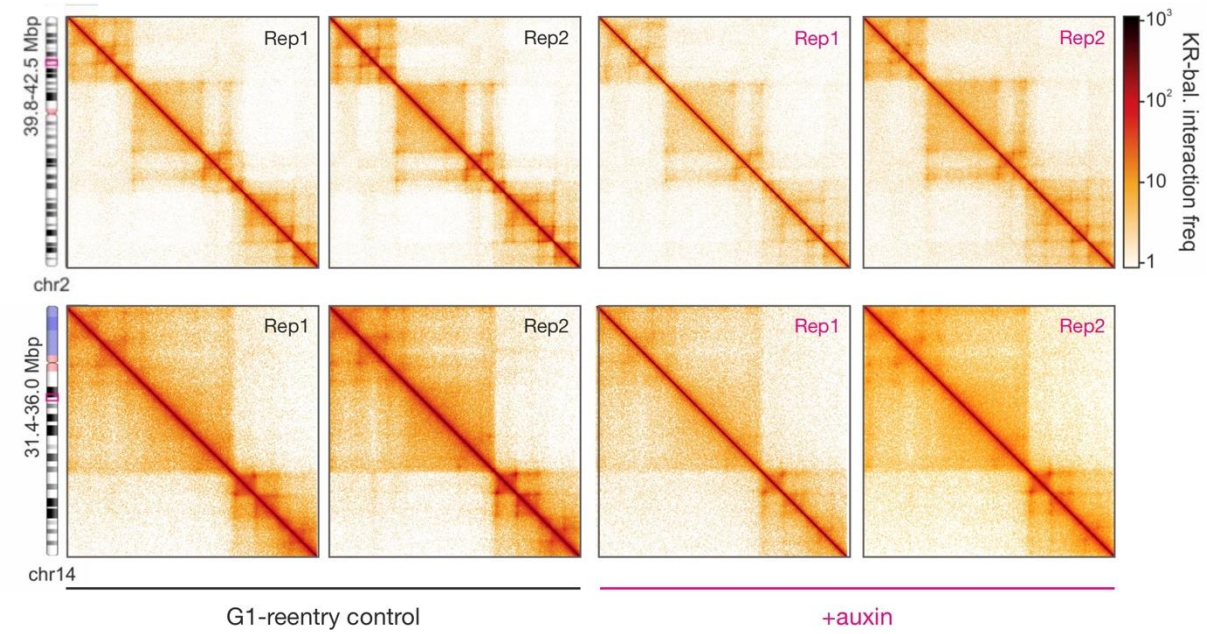

Fig. S8. Data from individual G1-reentry Hi-C replicates are reproducible. Representative Hi-C heatmaps from subregions of chr2 and 14 (ideograms) derived from independent replicates generated using G1-reentry DLD-1 cells treated (+auxin) or not with auxin (control). Details for each replicate can be found in Table S1.

Table S1. General statistics of all Hi-C datasets.

Hi-C dataset:	total reads	% aligned	Hi-C contacts	% inter-chromo	% intra-chromo	% short-range	% long-range
2h control	570,638,421	89.91	387,244,720	10.44	57.42	21.94	35.47
2h +auxin	521,206,158	91.46	361,994,319	10.84	58.62	22.43	36.17
G1 control, r1	512,551,503	89.70	339,693,791	16.49	49.78	16.75	33.03
G1 control, r2	617,136,578	89.46	400,421,522	12.40	52.48	18.77	33.70
14h +aux/+tript	461,569,471	90.67	313,489,486	16.87	51.04	19.88	28.67
14h +auxin	516,427,195	89.04	338,221,913	17.69	47.80	17.65	30.14
reentry +aux, r1	538,423,263	90.05	355,346,372	24.38	41.61	16.90	24.70
reentry +aux, r2	1,153,253,737	89.37	714,520,317	22.96	39.00	15.78	23.21
TOP2 control	705,232,509	88.87	462,507,451	12.44	53.14	22.59	30.55
TOP2 -auxin	541,077,797	88.39	364,665,469	10.32	57.07	23.96	33.11
TOP2 +auxin	546,798,121	88.24	368,526,565	10.08	57.32	24.49	32.83

Table S3. Targets of 3D-DNA FISH probes.

probe target:	genomic coordinates (hg19)
Nanog	chr12:7,696,106-7,696,694
chr12q14	chr12:60,211,422-60,211,814
chr12q21	chr12:83,646,182-83,815,279
PRPF19	chr11:60,677,496-60,677,988
SEPT2	chr2:242,097,006-242,097,495
SEPT5	chr22:19,578,750-19,579,058

Table S4. Antibodies used in Western blots.

antibody:	cat. No., provider	working dilution
anti-CTCF	61311 Active Motif	1:2,000
anti-GFP	ab290, Abcam	1:1,000
anti-H3K27ac	39133, Active Motif	1:1,000
anti-H3K27me3	39155, Active Motif	1:1,000
anti-HSC70	sc-7298, Santa Cruz	1:2,000
anti-MAU2	ab183033, Abcam	1:1,000
anti-NIPBL	A301-779A, Bethyl	1:10,000
anti-Rad21	ab992, Abcam	1:1,000
anti-RPB1	ab817, Abcam	1:500
anti-RNAPI	sc-48385, Santa Cruz	1:200
anti-RNAPIII	ab88243, Abcam	1:1,000
anti-RNAPII^{Ser5}	61086, Active Motif	1:1,000
anti-SMC1A	ab9262, Abcam	1:4,000

anti-WAPL	16370-1-AP, Proteintech	1:1,000
anti-βTubulin	T0198, Sigma-Aldrich	1:2,000

3.2. Chapter 2 – Enhancer-promoter contact formation requires RNAPII and antagonizes loop extrusion

My contribution is reflected by the following experimental outline:

- Culturing DLD1-mAID-mClover-RPB1 cells
- Cell synchronisation
- FACS sorting
- Chromatin fractionation and Western blotting
- Western Blot quantifications
- CUT&Tag experiments
- ATAC-seq experiments

The following figure panels were prepared by myself with data from experiments performed by me:

Figure 1A) Cell synchronisation, FACS sorting and crosslinking

Figure 2A,3A) CUT&Tag experiment

Figure S1A,D) Chromatin fractionation and Western blotting

Figure S1B,C) CUT&Tag experiment

Figure S1D) ATAC Seq experiment

Figure S2A,S3A) CUT&Tag experiment

LETTER

Enhancer-promoter contact formation requires RNAPII and antagonizes loop extrusion

Shu Zhang[1,#], Nadine Übelmesser[1,#], Mariano Barbieri[1] and Argyris Papantonis[1,*]

[1] Institute of Pathology, University Medical Center Göttingen, 37075 Göttingen, Germany.
[#] These authors contributed equally to this work.

*Correspondence: A.P., argyris.papantonis@med.uni-goettingen.de

Abstract

Homotypic chromatin interactions and loop extrusion are thought to be two main drivers of mammalian chromosome folding. Here, we tested the role of RNAPII across different scales of interphase chromatin organization in a cellular system allowing for its auxin-mediated degradation. We combined Micro-C and computational modeling to characterize subsets of loops differentially gained or lost upon RNAPII depletion. Gained loops, extrusion of which was antagonized by RNAPII, almost invariably formed by engaging new or rewired CTCF anchors. Lost loops selectively concerned contacts between enhancers and promoters anchored by RNAPII explaining the repression of most genes. Surprisingly, promoter-promoter interactions remained essentially unaffected by polymerase depletion and sustained cohesin occupancy in its absence. Together, our findings reconcile the role of RNAPII in transcription with a role in setting-up regulatory 3D chromatin architectures genome-wide, while also revealing a direct impact on cohesin loop extrusion.

Keywords: chromosome conformation capture; RNA polymerase; loop extrusion; Polycomb complex

Word count (excl. abstract, references, and methods): 4,057

Introduction

Genomic functions like gene expression and DNA replication require a tunable three-dimensional (3D) architecture of interphase chromatin[1,2]. Work in the last decade, combining genome-wide chromosome conformation capture assays with the removal of different chromatin components, has attributed key hallmarks of this 3D architecture to the interplay between the insulator factor CTCF and the ring-shaped cohesin complex[3,4]. 3D chromatin domains (from Mbp-sized "topologically associating domains" or TADs[5] to kbp-sized "loop domains"[6]) are insulated from one another via CTCF-demarcated boundaries, while the chromatin in these domains is actively extruded into loops by cohesin[7-9]. Removing CTCF from chromatin leads to insulation loss at domain boundaries[10], while cohesin removal eliminates CTCF-anchored loops[6,11]. The physical interaction of an extruding cohesin complex with two convergently-oriented CTCF-bound sites determines loop length of its stabilization together with STAG proteins[12-14].

Loops anchored at CTCF-bound sites appear as prominent dot-like features off the diagonal of high-resolution Hi-C contact maps[14]. These dots disappear in cells where the cohesin-loading factor, NIPBL, is eliminated[15], but multiply in cells lacking the cohesin-release factor WAPL[16]. Thus, loop formation arises from regulated cohesin "load-unload" cycles. However, recent live-cell imaging of the mouse *Fbn2* locus showed that full looping is rarely achieved and that, most of the time, cohesin-extruded loops within an active domain form without bridging both CTCF boundaries[17]. This can be explained by the notion that 3D genome architecture results from the antagonistic interplay of loop extrusion with homotypic (i.e., active-to-active or inactive-to-inactive) compartmentalization of chromatin domains [18,19]. Then, one would predict that RNA polymerase II (RNAPII), a potent molecular motor capable of translocating and bridging DNA[20,21], influences 3D genome architecture via both physical interactions[22] and transcription[23].

Earlier studies in this direction have shown that pharmacological inhibition of transcription could neither dissolve nuclear subcompartments formed by active RNAPII[24] nor long-range contacts between genes and enhancers in select loci[25]. Similarly, TAD formation in zygotes does not rely on transcriptional genome activation[26] and RNase A treatment of cell nuclei does not compromise TAD structure, but does eliminate specific enhancer-promoter interactions[27,28]. On the other hand, Hi-C maps generated upon depletion of Mediator complex subunits or inhibition of RNAPII elongation while re-expressing cohesin in RAD21-depleted cells had no discernible effect on CTCF loop formation[6,29]. This also held true when depleting the basal transcription factor TAF12 or RNAPII and using promoter-capture Hi-C or Hi-C, respectively[30,31]. Moreover, haploid human cells depleted of Mediator could not sustain a transcription-permissive chromatin architecture[32]. However, even kbp-resolution Hi-C contact maps do not prominently feature loops other than those anchored by CTCF. This was remedied by the introduction of Micro-C, a Hi-C variant using micrococcal nuclease (MNase) to fragment chromatin and reveal tens of thousands of transcription-based loops along mammalian chromosomes[33,34]. In fact, its capture-based adaptation, Micro-Capture-C (MCC), allowed mapping of 3D contacts between different *cis*-regulatory elements at near-base-pair resolution[35]. Still, pharmacological inhibition of transcription coupled to Micro-C did not affect looping and only reduced "gene stripe" signal by 1.25-fold[33].

This and other such data highlight the need for a conclusive dissection of whether and how core components of the transcriptional apparatus, like RNAPII and Mediator[36,37], contribute to the formation of 3D chromatin contacts. To this end, we applied Micro-C to a diploid human cell line allowing for the near-complete auxin-mediated degradation of the largest subunit of RNAPII, RPB1[38,39]. We identified thousands of transcription-anchored and CTCF loops changing upon RNAPII depletion. We combined experiments with *in silico* models to interpret the interplay between cohesin loop extrusion and RNAPII-mediated looping.

Results

Transcription-based architecture of human chromosomes

Previously, we used *in situ* Hi-C to identify changes in 3D genome architecture upon RNAPII depletion from human diploid cells[39]. For these Hi-C experiments, we used asynchronous G1-sorted DLD-1 cells allowing for the quantitative degradation of RNAPII upon auxin addition for 14 h[37,39]. Effects at the level of TADs and compartments were small (as also seen after RNAPII depletion in asynchronous mESCs[30]), but we did identify ~800 CTCF loops that emerged in RNAPII-depleted cells and were significantly larger than the loops in untreated cells[39]. However, interactions between RNAPII-bound sites were scarce in that data, hence our incomplete understanding of how RNAPs contribute to 3D chromatin folding.

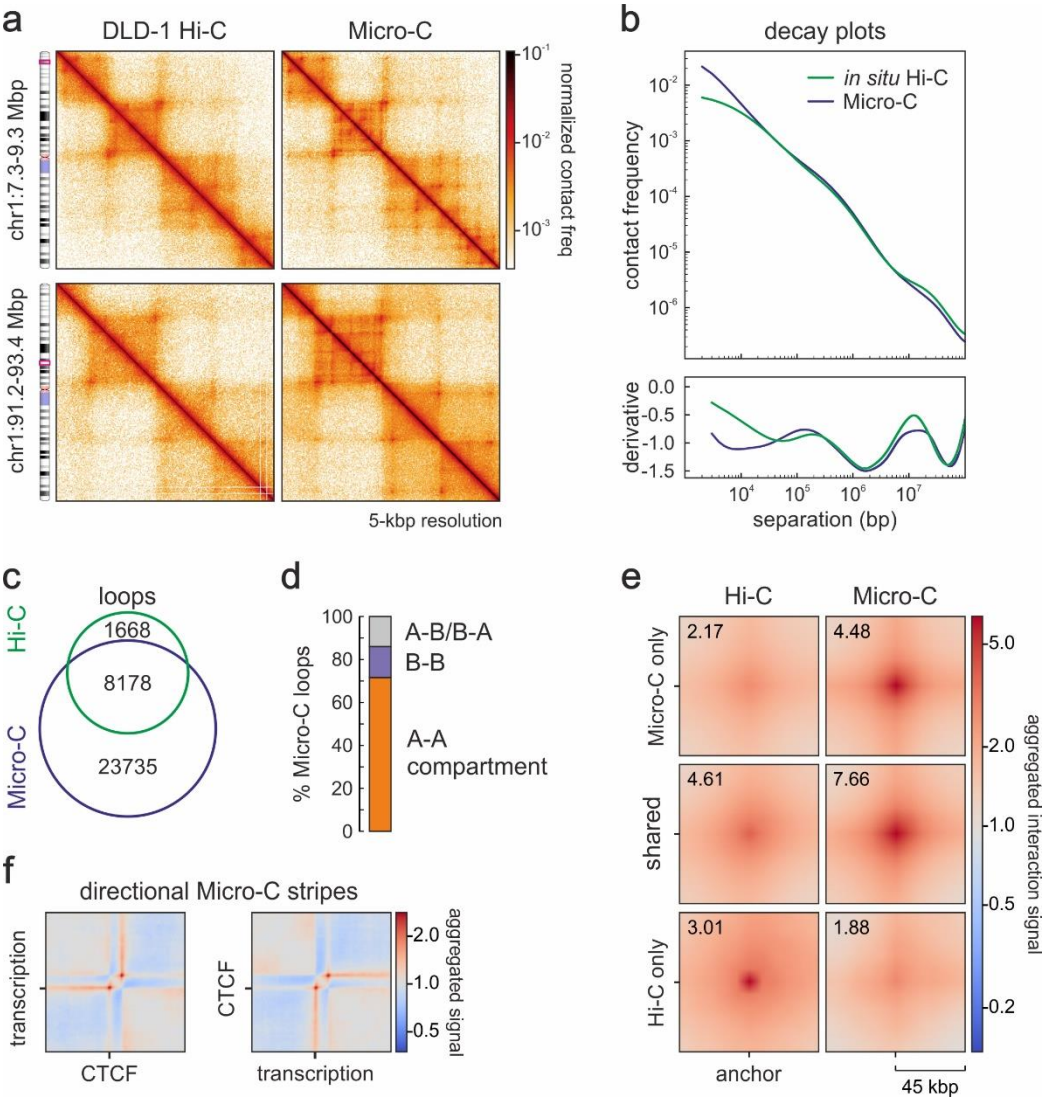

Fig. 1. Micro-C enhances high-resolution views of 3D genome folding. a, Comparison of Hi-C (left) and Micro-C 5-kbp resolution contact maps (right) from DLD1-mAID-RPB1 cells. **b,** Hi-C (green) and Micro-C (blue) interaction frequencies decaying as a function of genomic distance (top) and their first derivative (bottom). **c,** Venn diagram showing overlap of loops detected in Hi-C (green) and Micro-C contact maps (blue). **d,** Bar plot showing per cent of Micro-C loops with anchors in the A- or B-compartment. **e,** Aggregate plots showing Hi-C (left) and Micro-C signal (right) around shared and unique loops. **f,** Aggregate Micro-C signal of stripes with one CTCF and one transcriptional anchor.

To address this and obtain a comprehensive view of the transcription-based architecture of human cells, we performed Micro-C. We generated contact maps containing >1.25 billion pairwise interactions (Supplementary Table 1), which revealed fine intra-domain architecture compared to matching Hi-C data (of comparable sequencing depth; Fig. 1a,b). This detailed view of 3D chromatin folding allowed detection of >31,000 loops, encompassing >80% of the loops detected by Hi-C (Fig. 1c). The anchors of these loops mapped predominantly to the A (active) compartment, suggesting that multiple RNAPII-anchored loops could be detected (Fig. 1d). Indeed, when we stratified these ~31,000 loops by the presence or absence of RNAPII and/or H3K27ac or CTCF at their anchors, ~25% could be classified as transcription-anchored. This increases to 40% once we consider anchors that have CTCF in addition to RNAPII/H3K27ac. Moreover, the ~8,200 loops that are shared between Hi-C and Micro-C are featured more prominently in Micro-C contact maps (Fig. 1e). Finally, our highly resolved contact maps allowed detection of thousands of cases where directional loop extrusion gives rise to stripes emanating by a CTCF and a transcriptional anchor (Fig. 1f). Thus, Micro-C allowed us to study how transcription-anchored 3D interactions are remodeled upon RNAPII depletion.

New CTCF-anchored loops emerge after RNAPII depletion

To ask how RNAPs affects 3D interactions, we used the 14-h auxin treatment determined previously[39] and generated Micro-C data in the presence or absence of RNAPII. Under these conditions, the vast majority of RNAPII was depleted from chromatin and led to decreased H3K27ac and cohesin levels genome-wide (assessed using CUT&Tag; Extended Data Fig. 1a,b). We first used our Micro-C data to assess changes in nucleosome positioning after RNAPII depletion. For example, nucleosomes around CTCF sites became markedly more ordered; this did not come at the expense of CTCF binding to its cognate motifs, but did result in more focal ATAC-seq signal, i.e. to locally constrained accessibility (Extended Data Fig. 1c). Decrease in chromatin accessibility was also observed at gene promoters and enhancers genome-wide (Extended Data Fig. 1d). Notably, these changes were not a result of reduced availability of proteins like CTCF or cohesin as their levels on chromatin remained unaffected (Extended Data Fig. 1e).

We next surveyed Micro-C contact maps to discover widespread emergence of new and longer loops (Fig. 2a). These new loops typically arose in and around domains with active genes that became silenced upon RNAPII depletion. More than 11,000 loops were gained or strengthened to surpass the detection threshold in RNAPII-depleted data. These were significantly longer than either transcription-or CTCF-anchored loops of control cells (Fig. 2b), and involved at least one CTCF-bound anchor in ~75% of cases, as well as increased local insulation (Fig. 2c-e). Looking into loops that have one "CTCF only" anchor (e.g., the left one) and one "RNAPII only" (e.g., the right one), we found that they specifically rewired the latter. From a total of 1134 such loops, 74% rewired to a new anchor further downstream that almost invariably contained a CTCF-bound site (Fig. 2f). Rewiring often gave rise to nested loop structures (i.e., 795 unchanged CTCF anchors gave rise to 1134 new loops; Fig. 2a,f). The orientation of CTCF motifs in the new anchors was convergent in respect to that in the unchanged anchor (Fig. 2f). Interestingly, new CTCF anchors were disproportionately located at the TSSs and bodies of genes that were longer than average (Extended Data Fig. 1f) and became depleted of active RNAPs (Fig. 2g). In the absence of RNAPII and transcription, these anchors obtained more canonically spaced nucleosomes around them (Fig. 2h), but showed less reduction in SMC1A occupancy (Fig. 2i) than what was seen genome-wide (see Fig. 2a and Extended Data Fig. 1b,c,e).

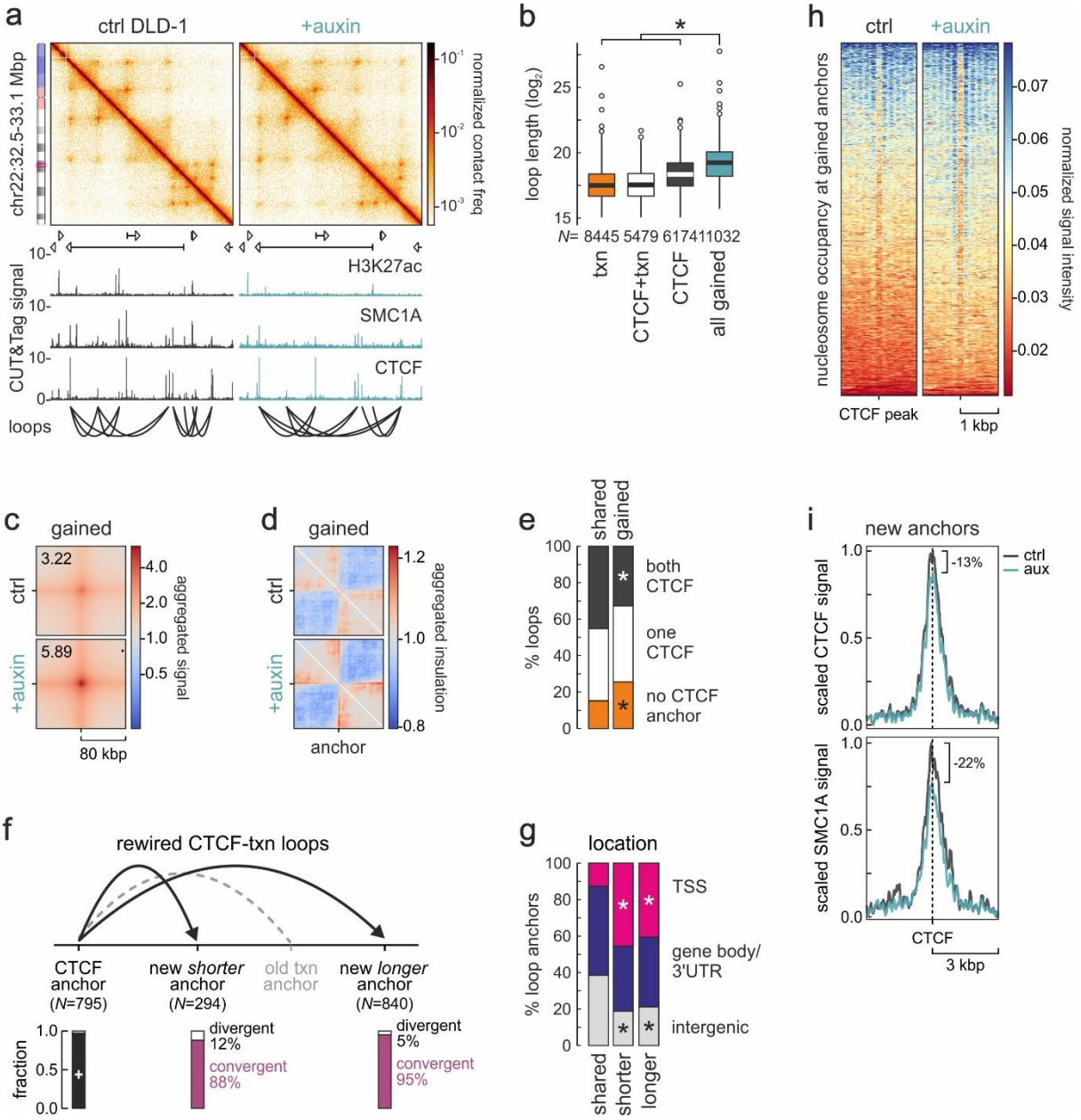

Fig. 2. Loops forming upon RNAPII degradation engage new CTCF anchors. a, Micro-C contact maps from control (left) and auxin-treated cells (right) showing emerging loop at 2-kbp resolution in an exemplary genomic region of chr22 aligned to H3K27ac, CTCF, and SMC1A CUT&Tag tracks. Loops for each condition are depicted by spider plots (bottom). **b,** Box plots of the lengths of control loops with transcription- (orange), CTCF- (black) or transcription/CTCF-anchors (white), and loops gained upon auxin treatment (green). **P*<0.01, Wilcoxon-Mann-Whitney test. **c,** Aggregate plots for loops gained in auxin-treated cells. **d,** Plots of mean insulation at the anchors of loops gained in auxin-treated cells. **e,** Bar plots showing per cent of loops with no (orange), one (white) or two CTCF anchors (black) that are shared or gained by auxin-treated cells. **P*<0.01, Fischer's exact test. **f,** Bar plots showing the fraction of convergent versus divergent CTCF motifs in gained loop anchors (*N*). **g,** Bar plots showing per cent of gained loop anchors located in different genomic locations. **P*<0.01, Fischer's exact test. **h,** Heatmaps of nucleosome occupancy around gained CTCF anchors from panel f. **i,** Line plots of mean CTCF and SMC1A signal in the 6 kbp around gained loop anchors from panel f.

Finally, we asked whether any loops gained after RNAPII depletion form via H3K27me3-mediated interactions (there were hints of ~200 such loops in our previous Hi-C data[39]). Despite no discernible

changes of H3K27me3 levels in CUT&Tag (**Extended Data Fig. 2a**) and chromatin fractionation blots in control and auxin-treated cells (**Extended Data Fig. 1e**), >2,200 new loops with H3K27me3 peaks in at least one anchor arose. This increased to 3,184 if we consider anchors with H3K27me3 peaks in the next 5-kbp bin (**Extended Data Fig. 2b,c**). Such new loops typically emerged in bundles within facultative heterochromatin domains, often without CTCF association (**Extended Data Fig. 2a**). Therefore, our Micro-C data now explain that thousands of new and longer loops emerge after RNAPII depletion via CTCF- and Polycomb-driven interactions.

RNAPII depletion leads to selective loss of enhancer-anchored loops

Next, we asked which loops and contacts are lost or weakened below the detection threshold upon RNAPII depletion. Lost loops were almost always found within CTCF loop-domain or TAD structures (**Fig. 3**a and **Extended Data Fig. 3a**). This is in line with transcription-anchored loops being the smallest (**Fig. 3b**); with the overall reduced contact frequency of loci separated by <1 Mbp upon RNAPII depletion (**Extended Data Fig. 3b**); and with gene regulatory domains being encompassed by CTCF loops[14]. The anchors of these 5,332 lost loops were significantly less likely to contain CTCF than those of unchanged loops (<25% have CTCF at both anchors; **Fig. 3c**). Following stratification into promoter-promoter (P-P) and enhancer-enhancer/-promoter loops (E-E/E-P), we discovered that enhancer-anchored ones were most sensitive to RNAPII depletion (**Fig. 3d**). Moreover, E-P loops that did not contained CTCF in either anchors were almost fully lost, compared to those that did (**Extended Data Fig. 3c**). This selective loss was reflected in the reduced cohesin occupancy at E-P compared to P-P loop anchors (that was even more pronounced at the 590 super-enhancers; Fig. **3e** and **Extended Data Fig. 3d**). Surprisingly, much like their looping propensity, H3K27ac levels around promoters remained unaffected, while those at enhancers dropped by >50% (Extended Data Fig. 3e). In total, ~900 E-P loop domains (together spanning >700 Mbp) dissolved upon RNAPII depletion, which involved >40% (557/1360) of all genes significantly downregulated upon auxin treatment ($|\log_2 FC|>2$, $P_{adj}<0.05$; RNA-seq data from ref. 39).

We also stratified loops not according to the type of elements in their anchors (i.e., enhancers *vs* promoters), but on whether their anchors were marked by CTCF, transcription or both. 59% of loops lost upon RNAPII depletion were anchored solely by RNAPII/H3K27ac at both anchors, while CTCF-only loops were only 18% of the total number lost (**Fig. 3f**). For an additional 1,675 loops, where only one anchor could be annotated, transcription anchors also predominated. Notably, CTCF-bound anchors displayed less reduction in cohesin occupancy than transcription-only anchors (i.e., 28-35% compared to 48%; **Fig. 3g**). Together, we found that transcription-anchored loops are most sensitive to RNAPII depletion. This is selective for loops involving enhancers in at least one anchor and not influenced much by CTCF presence.

Finally, even Micro-C features that at first appeared unaffected by auxin treatment, did respond to RNAPII depletion. For instance, loop-like signal at the edges of stripes was enhanced in the absence of RNAPII (**Extended Data Fig. 3f**), likely due to weakening of transcription in one of the anchors. Also, looking more carefully into loops that did not seem to change between the two conditions, we discovered that many rewired one anchor by <20 kbp (i.e., by <4 bins in a 5 kbp-resolution contact map). When we used control loop coordinates and auxin-treated Micro-C signal to plot aggregate plots, signal appeared weaker. However, when we used matching auxin-treated coordinates (i.e., shifted by <4 bins for the rewired anchor) and auxin-treated Micro-C signal, we noticed strengthening of these loops too (**Extended Data Fig. 3g**). This suggests that RNAPII depletion from chromatin also allows for such fine-scale changes, presumably due to the absence of engaged polymerases that influence anchor selection.

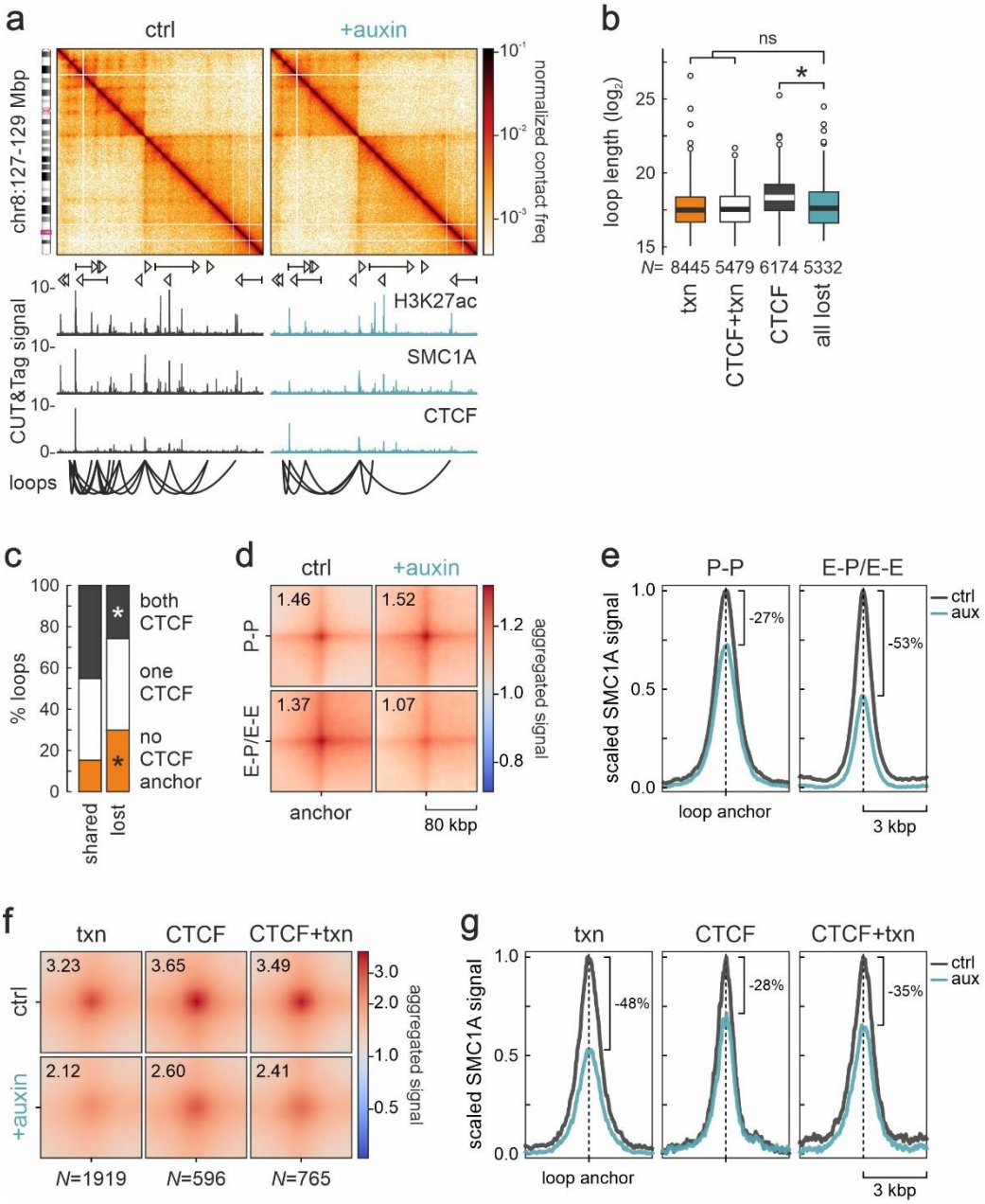

Fig. 3. RNAPII depletion selectively affects enhancer-promoter/-enhancer loops. a, Micro-C contact maps from control (left) and auxin-treated cells (right) showing loop loss in an exemplary genomic region on chr8 at 4-kbp resolution aligned to H3K27ac, CTCF, and SMC1A CUT&Tag tracks. Loops called for each condition are depicted by spider plots (bottom). **b,** Box plots of lengths of control loops with transcription- (orange), CTCF- (black) or transcription/CTCF-anchors (white) and of loops lost upon auxin treatment (green). **P*<0.01, Wilcoxon-Mann-Whitney test. **c,** Bar plot showing per cent of loops with no (orange), one (white) or two CTCF anchors (black) shared or lost by auxin-treated cells. **P*<0.01, Fischer's exact test. **d,** Aggregate plots for promoter- (P-P) or enhancer-anchored loops (E-P/E-E) before (ctrl) and after RNAPII depletion (+auxin). **e,** Line plots of mean SMC1A signal around the loop anchors from panel d. **f,** As in panel d, but for loops with transcriptional (txn), CTCF or both anchors (CTCF+txn). **g,** As in panel e, but for loop anchors from panel f.

Modeling the interplay between loop extrusion and RNAPII

A key observation in our data was the overall reduced cohesin occupancy at RNAPII loop anchors (**Fig. 3a,e,g**), which nevertheless coincided with the emergence of new prominent CTCF-anchored loops (**Fig. 2a-g**). To test the interplay between RNAPII engaged to chromatin and cohesin loop extrusion, which would be challenging to do experimentally, we used computational modeling of 3D chromatin folding.

We first considered a synthetic 460 kbp-long polymer containing two genes transcribed in the sense direction, a cluster of eight enhancers between the genes, plus three CTCF binding sites (two encompassing the genes/enhancers, and one located inside the downstream gene; **Fig. 4a**). Each bead in the polymer represented 2 kbp of chromatin, and we implemented two scenarios using established Molecular Dynamics approaches[40,41]. The first model approximated conditions in untreated DLD-1 cells (control), where RNAPs have specific affinity for promoters and enhancers, and can also transverse gene bodies at expected speeds to simulate transcription. In parallel, the model considers cohesin complexes able to bind the polymer and extrude loops at experimentally-deduced speeds (see **Methods** and **Supplementary Table 2**). Based on the documented co-association of cohesin and RNAPII[39,42], we introduced a weak interaction potential between cohesin and polymerases. Thus, cohesin is allowed to bind any position in the polymer with a probability of 0.1, but binds promoters or enhancers with a 0.9 probability when in its vicinity (as recently suggested[39,45-47]). In the model meant to approximate RNAPII depletion (like in auxin-treated cells), all RNAPs are removed from the simulation and cohesin can now bind any position in the polymer with equal probability.

Control contact maps displayed a ~300 kbp-long CTCF loop that encompasses the two genes, and compartment-like interactions between the genes and enhancer cluster (**Fig. 4a,b**). Cohesin occupancy in this model showed the expected accumulation at the two distal, but not at the intragenic CTCF site (in line with transcribing RNAPs relocating cohesins[42-44]; **Fig. 4a**). Interestingly, and despite loading being equally favored at promoters and enhancers, cohesin loading rates are highest at the enhancer cluster (**Fig. 4a**, bottom). This agrees with what has been recently experimentally deduced[45-47]. RNAP depletion in our model leads to elimination of all contacts between genes and enhancers, and to the emergence of a new CTCF loop anchored at the intragenic CTCF site (**Fig. 4a,**b). This matches our Micro-C findings of intragenic CTCF sites being engaged in *de novo* looping following RNAPII depletion (**Fig. 2e-g**). These simulations also allow us to monitor the flow of cohesin along the polymer. We saw that RNAP presence on the polymer hindered cohesin-driven extrusion, especially around promoters. This was alleviated in the RNAP-depletion model (**Fig. 4c**; also suggested by recent preprints[48,49]).

Finally, we used the same parameters to simulate the folding of a 1.2-Mbp locus on chr2 containing a number of enhancers and variously oriented CTCF sites, as well as two convergent active genes. *In silico* generated contact maps showed good agreement to Micro-C data (Fig. 4d; SCC>0.6) and allowed us to simulate different extents of RNAP depletion. In the presence of RNAPs, the intragenic CTCF site overlapping the two gene bodies did not engage in loop formation *in vivo* or *in silico*. Upon depletion of 75% of RNAPs, diffuse interaction signal was observed, but full depletion was needed in order for a focal looping interaction to form (**Fig. 4d**). This was accompanied by increased cohesin occupancy at that CTCF anchor, and by reduced occupancy at active promoters. As before, the net flow of cohesin along the polymer was markedly less obstructed. Interestingly, under conditions of 75% RNAP depletion the effects on cohesin loading and flow are not closer to the full depletion than to the control model (**Fig. 4d**, bottom). This suggests that the near-complete RNAP depletion from chromatin is required to obtain experimentally discernible changes. Taken together, the competition between active RNAPs and cohesin loaded preferentially, but not exclusively, at promoters and enhancers was what gave rise to most contact patterns seen by Micro-C.

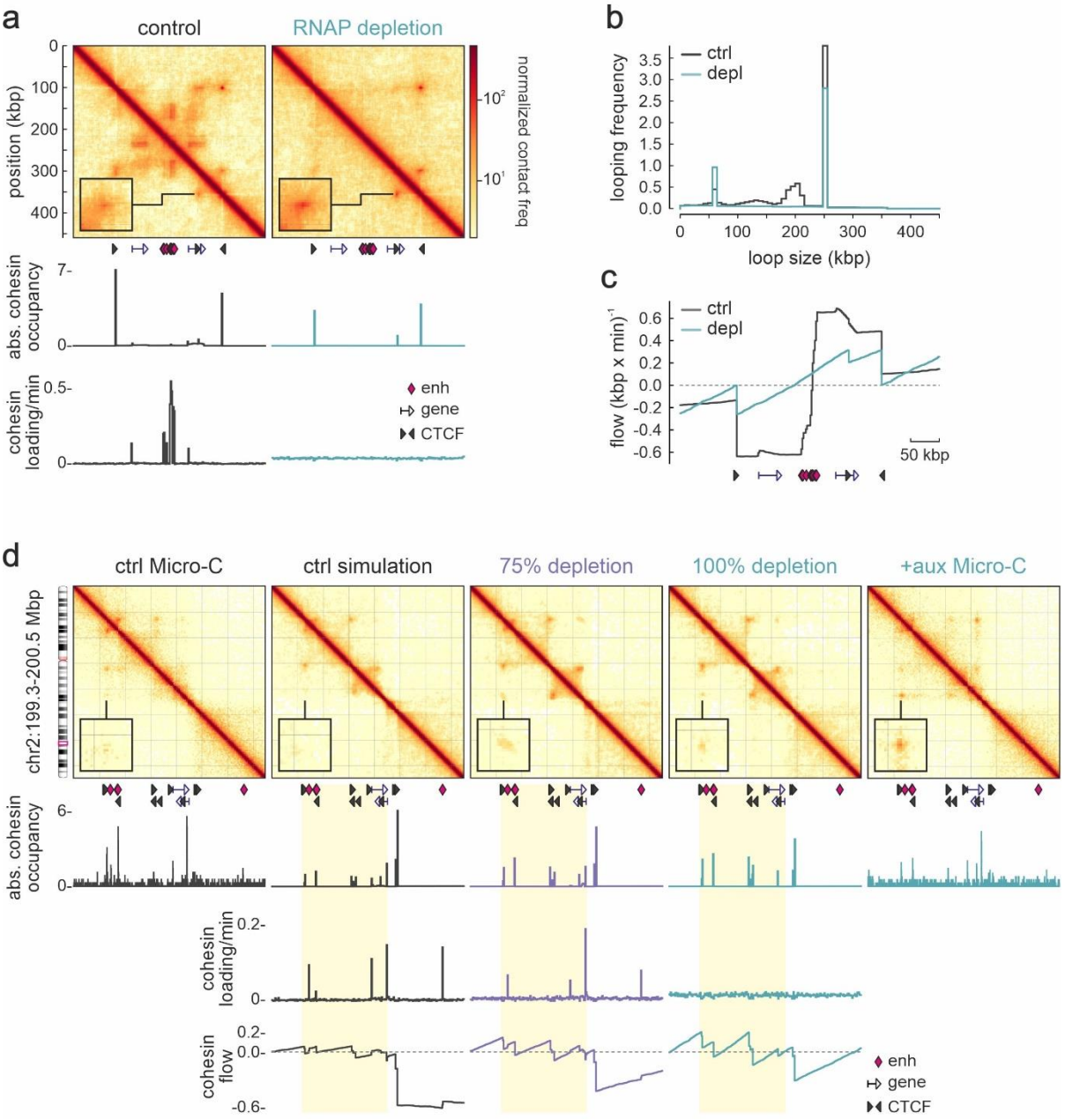

Fig. 4. Models of 3D chromatin folding in the presence or absence of RNAPII. a, Average contact maps from 800 configurations of a toy model including (control) or not polymerases (RNAP depletion) are shown aligned to plots of absolute cohesin occupancy and loading. The positions of enhancers (diamonds), genes (arrows), and CTCF-bound site orientations are denoted (arrowheads). **b,** Plot of looping frequency per configuration as a function of distance in the models from panel a. **c,** Plot of the net flow of cohesin molecules along the polymer in each scenario. Positive and negative values represent extrusion in the sense and antisense direction, respectively. **d,** Average contact maps from 800 configurations of models simulating the presence (ctrl) or absence of RNAPs (75% or 100% depletion) in a 1.2-Mbp locus on chr2 compared to Micro-C data (far left and far right) aligned to plots of absolute cohesin occupancy, loading, and flow.

Discussion

In previous work, we established the necessity of RNAPII for reestablishing interphase chromatin folding after exit from mitosis by a human cell line. We did not only show domain and compartment erosion in the absence of RNAPII, but also a dependency for cohesin loading onto chromatin[39]. However, in that same study, we could not identify 3D architecture changes of comparable magnitude by Hi-C applied to

non-synchronized cells. This remained perplexing until we obtained the Micro-C data analyzed here. Our highly-resolved contact maps show that the transcription-based 3D architecture of interphase chromatin is markedly perturbed by RNAPII depletion. We could document both loss/ weakening and gain/strengthening of specific loop-like interactions that beg the following questions.

First, how do longer and more pronounced CTCF loops arise in the absence of RNAPII? The data we present here, as well as recent preprinted work[49], see RNAPs as physical "moving" barriers to loop extrusion. Along the same lines, recent studies found that transcribing RNAPII complexes can reposition cohesin complexes[42-44] or give rise to new spatial interactions[50]. Thus, depletion of the RNAPII barriers should allow for a more efficient extrusion of loops anchored at CTCF-bound sites, and facilitate the *de novo* engagement of CTCF anchors located inside of previously-active promoters and gene bodies (as also corroborated by our simulations). In parallel, a subset of loops that involved interactions between Polycomb-bound regions emerged in the absence of RNAPII. H3K27me3-marked regions are considered transcriptionally inert, but often bind "poised" RNAPII[51], removal of which might contribute directly or indirectly to the observed effects. Directly by a competitive interplay of RNAPII with Polycomb proteins, and indirectly by RNAPs affecting cohesin loading (as cohesin depletion was shown to enhance contacts between Polycomb-bound regions[52]). A somewhat similar effect is now described in a preprint for promoter-proximal paused RNAPs maintaining local 3D chromatin architecture in erythrocytes[53].

Second, why did promoter- and enhancer-anchored interactions respond differently to RNAPII depletion? Here, we recorded two unforeseen events. H3K27ac levels dropped genome-wide following RNAPII depletion, but were significantly more reduced at enhancers compared to promoters. At the same time, enhancer-anchored loops were selectively weakened upon RNAPII depletion, but promoter-promoter ones remained essentially unaffected. This was independent of whether these interactions involved or not CTCF at their anchors, and showed decreased cohesin occupancy in a pattern similar to H3K27ac. This was striking, given that promoters and enhancers are thought to be variants of a single class of *cis*-elements[54]. Nevertheless, our data suggest that spatial communication between promoters relies on a different set of factors (perhaps STAG1 *vs* -2[55]) than that between enhancers and their target promoters. Which these factors and their attributes are represents the next challenge in the field.

Third, how is cohesin chromatin occupancy affected by the absence of RNAPII? In the M-to-G1 transition, reduced cohesin loading correlated with the depletion of RNAPII from chromatin despite the fact that chromatin accessibility was not reduced (and, thus, could not be solely responsible for any reduction in cohesin loading[39]). Here, we documented a similar reduction of chromatin-associated NIPBL and cohesin levels following RNAPII depletion from interphase cells. This was most apparent at enhancers-promoter loops and in line with (i) the binding of cohesin loaders at promoters[42] (although the specificity of some of this data is now debated[49]); (ii) the fact that the loader NIPBL and unloader WAPL co-purify with RNAPII complexes[39]; (iii) recent work pointing to enhancers as cohesin-loading sites for the formation of 3D interactions[45-47]. Moreover, we should revisit studies where pioneer transcription factors (like OCT4 and SOX2[56]) and chromatin remodelers (like SNF2h[57]) affected the loading/unloading cycles of cohesin onto chromatin. Still, distinguishing between cohesin loading or stalling at a given position remains challenging *in vivo*, due to the processive nature of extruding complexes. However, our simulations show that, by introducing a weak interaction between RNAPII and cohesin, the latter is predominantly directed to active promoters and enhancers. Disfavoring cohesin loading at promoters (by competition with RNAPII), generates contacts rarely seen by Micro-C.

Cohesin, its loader NIPBL, and the Mediator complex were proposed to co-associate in order to physically and functionally connect active enhancers and promoters[58]. Hi-C studies that followed this work found Mediator and RNAPII to be dispensable for 3D chromatin folding[29,30]. This is now challenged by our data, by MCC data showing loss of enhancer-promoter contacts following acute depletion of

Mediator[37], and by decreased cohesin binding to RNAPII-transcribed genes following depletion of the yeast Med14 subunit[59]. Together, these new observations put the still-debated role of RNAPII in 3D chromatin folding under a different light: they provide definitive evidence for the necessity of RNAPII in sustaining enhancer-promoter interactions, as well as for direct antagonism during the formation of CTCF loops. The former appears to require the presence of RNAPII on chromatin, whereas the latter likely also implicates ongoing transcription. Nonetheless, there remain aspects of polymerase-based 3D chromatin architecture to be elucidated, like the differential dependency of promoter- compared to enhancer-anchored interactions or the mechanistic details of RNAPII influence on cohesin loading.

Data availability

NGS data generated in this study are available via the NCBI Gene Expression Omnibus repository under accession number GSE178593.

Code availability

All custom code used for Micro-C in this study is available at: https://github.com/shuzhangcourage/HiC-data-analysis.

References

1. Aboelnour, E. & Bonev, B. Decoding the organization, dynamics, and function of the 4D genome. *Dev. Cell* **56**, 1562-1573 (2021).
2. Razin, S.V. & Kantidze, O.L. The twisted path of the 3D genome: where does it lead? *Trends Biochem. Sci*. **47**, 736-744 (2022).
3. Xiang, J.F. & Corces, V.G. Regulation of 3D chromatin organization by CTCF. *Curr. Opin. Genet. Dev*. **67**, 33-40 (2021).
4. van Ruiten, M.S. & Rowland, B.D. On the choreography of genome folding: A grand pas de deux of cohesin and CTCF. *Curr. Opin. Cell Biol*. **70**, 84-90 (2021).
5. Beagan, J.A. & Phillips-Cremins, J.E. On the existence and functionality of topologically associating domains. *Nat*. *Genet*. **52**, 8-16 (2020).
6. Rao, S.S.P. et al. Cohesin loss eliminates all loop domains. *Cell* **17**, :305-320 (2017).
7. Fudenberg, G., Imakaev, M., Lu, C., Goloborodko, A., Abdennur, N. & Mirny, L.A. Formation of chromosomal domains by loop extrusion. *Cell Rep*. **15**, 2038-2049 (2016).
8. Davidson, I.F., Bauer, B., Goetz, D., Tang, W., Wutz, G. & Peters, J.M. DNA loop extrusion by human cohesin. *Science* **366**, 1338-1345 (2019).
9. Kim, Y., Shi, Z., Zhang, H., Finkelstein, I.J. & Yu. H. Human cohesin compacts DNA by loop extrusion. *Science* **366**,1345-1349 (2019).
10. Nora, E.P. et al. Targeted degradation of CTCF decouples local insulation of chromosome domains from genomic compartmentalization. *Cell* **169**, 930-944 (2017).
11. Wutz, G. et al. Topologically associating domains and chromatin loops depend on cohesin and are regulated by CTCF, WAPL, and PDS5 proteins. *EMBO J*. **36**, 3573-3599 (2017).
12. Wutz, G. et a;. ESCO1 and CTCF enable formation of long chromatin loops by protecting cohesin^{STAG1} from WAPL. *eLife* **9**, e52091 (2020).
13. Li, Y. et al. The structural basis for cohesin-CTCF-anchored loops. *Nature* **578**, 472-476 (2020).
14. Rao, S.S. et al. A 3D map of the human genome at kilobase resolution reveals principles of chromatin looping. *Cell* **159**, 1665-1680 (2014).
15. Schwarzer. W. et al. Two independent modes of chromatin organization revealed by cohesin removal. *Nature* **551**, 51-56 (2017).
16. Haarhuis, J.H.I. et al. The cohesin release factor WAPL restricts chromatin loop extension. *Cell* **169**, 693-707 (2017).
17. Gabriele, M. et al. Dynamics of CTCF- and cohesin-mediated chromatin looping revealed by live-cell imaging. *Science* **376**, 496-501 (2022).

18. Nuebler, J., Fudenberg, G., Imakaev, M., Abdennur, N. & Mirny, L.A. Chromatin organization by an interplay of loop extrusion and compartmental segregation. *Proc. Natl. Acad. Sci. U.S.A*. **115**, E6697-E6706 (2018).
19. Rada-Iglesias, A., Grosveld, F.G. & Papantonis, A. Forces driving the three-dimensional folding of eukaryotic genomes. *Mol. Syst. Biol*. **14**, e8214 (2018).
20. Papantonis, A. & Cook, P.R. Fixing the model for transcription: the DNA moves, not the polymerase. *Transcription* **2**, 41-44 (2011).
21. Lee, K. & Blobel, G.A. Chromatin architecture underpinning transcription elongation. *Nucleus* **7**, 1-8 (2016).
22. Cook, P.R. & Marenduzzo, D. Transcription-driven genome organization: a model for chromosome structure and the regulation of gene expression tested through simulations. *Nucleic Acids Res*. **46**, 9895-9906 (2018).
23. Racko, D., Benedetti, F., Dorier, J. & Stasiak, A. Transcription-induced supercoiling as the driving force of chromatin loop extrusion during formation of TADs in interphase chromosomes. *Nucleic Acids Res*. **46**, 1648-1660 (2018).
24. Mitchell, J.A. & Fraser, P. Transcription factories are nuclear subcompartments that remain in the absence of transcription. *Genes Dev*. **22**, 20-25 (2008).
25. Palstra, R.J., Simonis, M., Klous, P., Brasset, E., Eijkelkamp, B. & de Laat, W. Maintenance of long-range DNA interactions after inhibition of ongoing RNA polymerase II transcription. *PLoS ONE* **3**, e1661 (2008).
26. Ke, Y. et al. 3D chromatin structures of mature gametes and structural reprogramming during mammalian embryogenesis. *Cell* **170**, 367-381 (2017).
27. Barutcu, A.R., Blencowe, B.J. & Rinn, J.L. Differential contribution of steady-state RNA and active transcription in chromatin organization. *EMBO Rep*. **20**, e48068 (2019).
28. Brant, L. et al. Exploiting native forces to capture chromosome conformation in mammalian cell nuclei. *Mol. Syst. Biol*. **12**, 891 (2016).
29. El Khattabi, L. et al. A pliable Mediator acts as a functional rather than an architectural bridge between promoters and enhancers. *Cell* **178**, 1145-1158 (2019).
30. Jiang, Y. et al. Genome-wide analyses of chromatin interactions after the loss of Pol I, Pol II, and Pol III. *Genome Biol*. **21**, 158 (2020).
31. Sun, F., Sun, T., Kronenberg, M., Tan, X., Huang, C. & Carey, M.F. The Pol II preinitiation complex (PIC) influences Mediator binding but not promoter-enhancer looping. *Genes Dev*. **35**, 1175-1189 (2021).
32. Haarhuis, J.H.I. et al. A Mediator-cohesin axis controls heterochromatin domain formation. *Nat. Commun*. **13**, 754 (2022).
33. Hsieh, T.S. et al. Resolving the 3D landscape of transcription-linked mammalian chromatin folding. *Mol. Cell* **78**, 539-553 (2020).
34. Krietenstein, N. et al. Ultrastructural details of mammalian chromosome architecture. *Mol. Cell* **78**, 554-565 (2020).
35. Hua, P. et al. Defining genome architecture at base-pair resolution. *Nature* **595**, 125-129 (2021).
36. Cramer, P. Organization and regulation of gene transcription. *Nature* **573**, 45-54 (2019).
37. Ramasamy, S., Aljahani, A., Karpinska, M.A., Cao, T.B.N., Cruz, J.N. & Oudelaar, M.A. The Mediator complex regulates enhancer-promoter interactions. *bioRxiv* **doi**, 10.1101/2022.06.15.496245 (2022).
38. Nagashima, R. et al. Single nucleosome imaging reveals loose genome chromatin networks via active RNA polymerase II. *J. Cell Biol*. **218**, 1511-1530 (2019).
39. Zhang, S. et al. RNA polymerase II is required for spatial chromatin reorganization following exit from mitosis. *Sci. Adv*. **7**, eabg8205 (2021).
40. Buckle, A., Brackley, C.A., Boyle, S., Marenduzzo, D. & Gilbert, N. Polymer simulations of heteromorphic chromatin predict the 3D folding of complex genomic loci. *Mol. Cell* **72**, 786-797 (2018).
41. Fiorillo, L. et al. Inference of chromosome 3D structures from GAM data by a physics computational approach. *Methods* **181-182**, 70-79 (2020).
42. Busslinger, G.A. et al. Cohesin is positioned in mammalian genomes by transcription, CTCF and Wapl. *Nature* **544**, 503-507 (2017).
43. Heinz, S. et al. Transcription elongation can affect genome 3D structure. *Cell* **174**, 1522-1536 (2018).

44. Olan, I. et al. Transcription-dependent cohesin repositioning rewires chromatin loops in cellular senescence. *Nat. Commun*. **11**, 6049 (2020).
45. Zhu, Y., Denholtz, M., Lu, H. & Murre, C. Calcium signaling instructs NIPBL recruitment at active enhancers and promoters via distinct mechanisms to reconstruct genome compartmentalization. *Genes Dev*. **35**, 65-81 (2021).
46. Rinaldi, L. et al. The glucocorticoid receptor associates with the cohesin loader NIPBL to promote long-range gene regulation. *Sci. Adv*. **8**, eabj8360 (2022).
47. Rinzema, N.J. et al. Building regulatory landscapes reveals that an enhancer can recruit cohesin to create contact domains, engage CTCF sites and activate distant genes. *Nat. Struct. Mol. Biol*. **29**, 563-574 (2022).
48. Valton, A.L. et al. A cohesin traffic pattern genetically linked to gene regulation. *bioRxiv* **doi**, 10.1101/2021.07.29.454218 (2021).
49. Banigan, E.J. et al. Transcription shapes 3D chromatin organization by interacting with loop extrusion. *bioRxiv* **doi**, 10.1101/2022.01.07.475367 (2022).
50. Rosencrance, C.D. et al. Chromatin hyperacetylation impacts chromosome folding by forming a nuclear subcompartment. *Mol. Cell* **78**, 112-126 (2020).
51. Ferrai, C. et al. RNA polymerase II primes Polycomb-repressed developmental genes throughout terminal neuronal differentiation. *Mol. Syst. Biol*. **13**, 946 (2017).
52. Rhodes, J.D.P. et al. Cohesin disrupts polycomb-dependent chromosome interactions in embryonic stem cells. *Cell Rep*. **30**, 820-835 (2020).
53. Penagos-Puig, A. et al. RNA polymerase II pausing contributes to maintain chromatin organization in erythrocytes. *bioRxiv* **doi**, 10.1101/2022.06.16.496295 (2022).
54. Andersson, R., Sandelin, A. & Danko, C.G. A unified architecture of transcriptional regulatory elements. *Trends Genet*. **31**, 426-433 (2015).
55. Casa, V. Et al. edundant and specific roles of cohesin STAG subunits in chromatin looping and transcriptional control. *Genome Res*. **30**, 515-527 (2020).
56. Liu, N.Q. et al. WAPL maintains a cohesin loading cycle to preserve cell-type-specific distal gene regulation. *Nat. Genet*. **53**, 100-109 (2021).
57. Hakimi, M.A., et al. A chromatin remodelling complex that loads cohesin onto human chromosomes. *Nature* **418**, 994-998 (2002).
58. Kagey, M.H. et al. Mediator and cohesin connect gene expression and chromatin architecture. *Nature* **467**, 430-435 (2010).
59. Mattingly, M. et al. Mediator recruits the cohesin loader Scc2 to RNA Pol II-transcribed genes and promotes sister chromatid cohesion. *Curr Biol*. **32**, 2884-2896 (2022).

Acknowledgements

We thank Marieke Oudelaar, Kerstin Wendt, and all members of the Papantonis lab for discussions, and the Maeshima lab (NIG, Japan) for the DLD-1 mAID-RPB1 cells. **Funding:** Work in the lab of A.P. is funded by the Deutsche Forschungsgemeinschaft (DFG) via the SPP2202 (PA 2456/11-2) and SPP2191 Priority Programs (PA 2456/17-1), and the TRR81 TransRegio program (INST 160/697-1). S.Z. is supported by a China Scholarship Council fellowship. S.Z. and N.Ü. are further supported by the International Max Planck Research School for Genome Science. **Author contributions:** S.Z. performed bioinformatics analyses; N.Ü. performed experiments; M.B. performed computational modeling; A.P. conceived and supervised the study, and compiled the manuscript with input from all coauthors. **Competing interests:** The authors have no competing interests to declare.

Methods

Cell synchronization and sorting. mAID-POLR2A(RPB1)-mClover DLD-1 cells[38] were grown in RPMI-1640 medium supplemented with 10% FBS under 5% CO_2. Inducible depletion of RPB1 initiated via treatment with doxycycline for 24 h to induce *TIR1* expression, before addition of 500 μM indole-3-acetic acid solution ("auxin"; Sigma-Aldrich) for 14 h to induce RPB1 degradation. Cells treated with auxin were

harvested, resuspended in 1 µg/ml propidium iodide, and sorted to isolate G1 cells on a FACS Canto II flow cytometer (Becton Dickinson).

Micro-C and data analysis. Micro-C was performed using the Micro-C v1.0 kit in collaboration with Dovetail Genomics as per manufacturer's instructions. Micro-C libraries (at least 3 per each biological replicate) that passed QC criteria were pooled and paired-end sequenced on a NovaSeq6000 platform (Illumina) to >600 million read pairs per replicate (**Table S1**). Micro-C contact matrices were produced using Dovetail Genomics pipeline (https://micro-c.readthedocs.io/en/latest/fastq_to_bam.html). In brief, read pairs were mapped to human reference genome hg38 using BWA, after which low mapping quality (<40) reads and PCR duplicates were filtered out. Next, ICE-balanced *.cool* files and KR-balanced *.hic* files were generated and visualized via HiGlass or Juicebox. Decay plots were generated *cooltools* (https://cooltools.readthedocs.io/en/latest/notebooks/contacts_vs_distance.html). Subcompartment analysis was performed using CALDER[60] considered 50 kbp-resolution Micro-C data. For loop calling, we used a multi-tool (HiCCUPS, *cooltools*, and *mustache*) and multi-resolution (5- and 10-kbp) approach as previously described[33,34]. Loop lists derived from each tool were merged using *pgltools*[61] as follows: dots from both 10- and 5-kbp resolution are retained if they are supported by >10 read counts, and kept at native resolution. To further annotate loops as CTCF- or transcription-anchored, using CTCF, H3K27ac CUT&Tag peaks (from this work), as well as RNAPII peaks and nascent RNA-seq signal (RPKM >10; from ref. 39). All intersections were performed using *pgltools intersect1D* without any distance tolerance for CTCF anchors, and with a 10-kbp tolerance for enhancers and promoter anchors (annotated TSS±2 kbp) identified using *chipseeker*[62]. Note that promoters of all gene isoforms were considered, and "super-enhancers" called using the ROSE algorithm[63]. Finally, aggregate plots for loops and boundaries were generated using *coolpup.py*[64]. All the custom code used in this study is available at: https://github.com/shuzhangcourage/HiC-data-analysis.

Cleavage Under Targets and tagmentation (CUT&Tag). Following lifting from plates using accutase and FACS sorting, 0.5 million G1-phase DLD-1 cells were processed according to manufacturer's instructions (Active Motif). Samples were paired-end sequenced to obtain at least 10^7 reads. Reads were processed according to the standard CUT&Tag pipeline (https://yezhengstat.github.io/CUTTag_tutorial/). Briefly, paired-end reads were trimmed for adapter removal and mapped to human (hg38) and *E. coli* reference genomes (ASM584v2) using Bowtie 2[65]. *E. coli* mapped reads were quantified and used for calibrating human-mapped reads. Peak calling was performed using a multi-FDR-tryout method (FDR <0.01 to <0.1) and IgG controls for thresholding. Acceptable FDRs could vary between different datasets, but were always kept same for control and auxin-treated samples. Thus, for CTCF, an FDR <0.1 was selected and, for additional stringency, we only considered a CUT&Tag peak as CTCF-bound if it encompassed a canonical CTCF motif (assessed using FIMO[66]). For H3K27ac and H3K27me3, peaks were selected on the basis of FDR <0.025 and <0.01, respectively, while for SMC1A, an FDR <0.1 was used. Heatmaps were generated using Deeptools[67].

Chromatin fractionation and western blotting. For assessing protein abundance in different subcellular fractions, a protocol previously described was used[68]. Protein concentration in each fraction extract was determined using the Pierce BCA Protein Assay Kit (Thermo Fisher Scientific). Following separation on precast SDS-PAGE gels (BioRad), proteins were detected using antibodies against p-Ser5 RPB1 (Active Motif 61085; 1:2000), RPB1 (Abcam ab817; 1:500), NIPBL (Bethyl A301-779A; 1:10000), MED24 (Affinity Biosciences AF0346; 1:1000), Lamin B1 (Abcam ab16048; 1:10000), SMC1A (Abcam ab9262; 1:4000),

CTCF (Active Motif 61311; 1:2000), H3K27me3 (Active Motif 39155; 1:1000) and HSC70 (Santa Cruz sc-7298; 1:2000), and visualized using the Pierce SuperSignal WestPico ECL kit (ThermoFisher).

Simulations of chromatin folding. We performed Molecular Dynamics simulations via the multi-purpose EspressoMD package[69]. In our simulations, individual proteins are represented by ''beads'' interacting via phenomenological force fields and move according Langevin equation, and the chromatin fiber is represented as a chain of beads connected by bonds. The position of every bead in the system, either a protein or chromatin bead, evolves according to the Langevin differential equation that encodes Newton's laws in the case of thermal bath with the friction γ due to an implied solvent in presence of forces between beads encoded by energy potential functions *U*[40,70]. Langevin equations for all beads are simultaneously solved in EspressoMD using a standard Velocity-Verlet numerical algorithm. The potential connecting *i* and *i+1* beads of the fiber is a finitely extensible non-linear elastic (FENE) spring that adds up to a steric repulsion potential between non-adjacent sites of the polymer, the Weeks-Chandler-Andersen (WCA) potential:

$$U_{FENE} = -\frac{K_{FENE}R_0^2}{2} ln\left[1 - \left(\frac{r_{i,i+1} - r\_0}{R_0}\right)\right] \qquad (1)$$

$$U_{WCA} = \begin{cases} 4\epsilon\left[\left(\frac{\sigma}{r}\right)^{12} - \left(\frac{\sigma}{r}\right)^{6} + \frac{1}{4}\right] & if\ r < \sigma 2^{1/6} \\ 0 & otherwise \end{cases} \qquad (2)$$

where $r_{i,i+1}$ is the distance between consecutive beads, and σ is where the interaction from repulsive becomes attractive and can be interpreted as the diameter of the particles. This value is a natural length scale of the system. In FENE we fix parameters to have an equilibrium distance of 1.6 σ with maximum extension of 0.8 σ, and a bond energy of K_{FENE} = 30 k_BT. Since our fiber is resolved at 2 kbp, chromatin rigidity cannot be neglected (i.e. we are below the estimated persistence length). Bending rigidity of the polymer is introduced via the Kratky-Porod potential for every three adjacent chromatin beads where θ is the angle between three consecutive beads as given by:

$$U_{KP}(\theta) = K_{BEND}(1 - cos(\theta)) \qquad (3)$$

and K_{BEND} is the bending energy. The persistence length in units of σ is given by $L_p = K_{BEND}/k_BT$.
In order to model more complex aspects of transcription and loop extrusion, and the impact their interplay have on 3D chromatin organization, we encoded in the model: (i) full 3D loop extrusion by the interplay of cohesin dimers and CTCF; (ii) transcription by RNAPII particles. To simulate association between cohesin and RNAPII with the chromatin fiber, we employed a harmonic potential mimicking formation of a stable bond between two particles that fluctuate around an equilibrium distance d_0:

$$U_H = \frac{1}{2}K_H(r - d_0)^2 \qquad (4)$$

To regulate the lifetime of the above interaction, we introduced mechanisms of bond formation and removal according to cutoff distance *cd* below which a bond is formed with a certain probability rate of detachment in units of time τ_b=2 τ, τ the fundamental MD unit of time (see below). These are then set to approximate the experimentally observed range of RNAPII transcription and cohesin loop extrusion speeds and chromatin residence time. The above mechanics is added on top of the SBS model we previously employed[71]. The model encodes the association tendency of RNAPII with promoters by

means of the shifted, truncated Lennard-Jones (LJ) potential that allows spontaneous co-localization of beads with lifetime and stability properties depending on the depth of the energy well ϵ:

$$U_{LJ} = \begin{cases} 4\epsilon\left[\left(\frac{\sigma}{r}\right)^{12} - \left(\frac{\sigma}{r}\right)^{6} + \mathrm{c_{shift}}\right] & if\ r < r_{cut} \\ 0 & otherwise \end{cases} \qquad (2)$$

where r_{cut} = 2.5σ for all LJ potentials in the simulations, r is the separation of any two beads. This is a standard widely used in the field to simulate phenomenological course-grained affinities[40,70].

For RNAPII interactions and transcription, the polymerase is represented as a bead with LJ interaction with specific beads of the chromatin fiber representing promoters and enhancers with energy ϵ = 1.5 and 2 k_BT respectively. Such mild affinity helps to identify promoters as the correct sites where transcription initiation will take place (i.e., RNAPII forming stable bonds with promoter beads) before the elongation process on the gene body starts. LJ interactions were also introduced among RNAPII beads (ϵ=2.5k_BT) to simulate their tendency to form condensates acting as transcription hubs, as well as between RNAPII and cohesin (ϵ=3k_BT) to simulate the latter preferential loading at promoter/enhancer beads. RNAPII transcription dynamics are simulated as a four-step process: attachment to a promoter in an exclusive manner, elongation starts, elongation proceeds through the gene body, detachment at TES. A bond is formed if the beads are less distant in space than the cutoff 2.7σ. To simulate the tendency of RNAPII to reel in gene body beads, a secondary bond is formed with the next bead on the chromatin fiber in the direction of transcription (*i+1* bead, where *i* is the promoter coordinate on the fiber, and if transcription occurs in the sense direction; *i-1* in the antisense direction). In the next step, RNAPII moves on the next site by forming new bonds with *i+1* site and dissolving the old ones with *i*. This happens at a given rate (0.4 τ_b^{-1}) and only if the beads are found within the cutoff distance 1.05σ. These values are selected to obtain a RNAPII transcription speed approximately in the range of 1-10 kbp/min observed experimentally. Upon reaching the TES, RNAPII stops and becomes unbound with rate 0.2 τ_b^{-1}. Upon binding with promoters RNAPII loses its LJ interaction with promoters, since this is substituted by the bond itself. On the contrary RNAPII increases the LJ-affinity with enhancers (3 k_BT) to favor associations between actively transcribed segments. This preserves the stability of condensates/hubs during the process of transcription.

CTCF interacts via LJ interactions (ϵ=1.5k_BT) with specific sites of the chromatin fiber representing the oriented cognate binding motifs. Once a bond is formed (with rate 0.8 τ_b^{-1}) it is pair-exclusive (i.e., other CTCF cannot bind that same site). The bond dissolves at the rate $2x10^{-5}$ τ_b^{-1} and CTCF is again free to diffuse and search for other binding sites. Cohesin dimers are represented as bead pairs connected by one bond (r_0=1.6σ and K=8 k_BT). Extrusion has three steps: attachment, active extrusion, and detachment. For attachment, each cohesin monomer forms a bond with the chromatin fiber. Bonds form when a cohesin monomer and a chromatin site come within the cutoff distance 1.6σ with attachment rate 0.1 τ_b^{-1}. Only the case where both monomers simultaneously form bonds on adjacent chromatin beads is considered a successful attachment and the dimer is retained for the next step, otherwise bonds dissolve. If a promoter is already engaged in a bond with RNAPII, cohesin is forbidden to bind that promoter. Also, to favor cohesin loading in correspondence of active transcribing promoters, a 90% chance of binding has been introduced when a cohesin molecule is close to a promoter/enhancer and at the same time one RNAPII is close by as well (cutoff distance 1.5 σ), otherwise cohesin binding chance drops to 10%. The active extrusion and detachment steps follow the same mechanics as for RNAPII, with the difference that RNAPII can reel through cohesin-bound sites while the converse is not allowed. New bonds are formed if the distance is below 1.1σ. Such value

produces ranges of cohesin extruding speed of 15-30 kbp/min, which is within the range of experimentally observed values[6], as cohesin detachment occurs at the rate 10^{-4} τ_b^{-1} to fit its known chromatin residence time of 20 min. Finally, CTCF "loop anchors" are modeled so that cohesin cannot form new bonds with the next *i±1* site if the latter is already bound by CTCF, provided it has the binding motif in convergent orientation. This renders extrusion dependent on CTCF dynamics. Last, cohesin has LJ affinity with RNAPII both in the bound (ϵ=3 k_BT) and unbound state (ϵ=2 k_BT), higher affinity for bound RNAPII mimicking RNAPII suggested role in cohesin loading on chromatin[39].

RNAPII and LE dynamics are performed using a python script that drives the EspressoMD library. The polymer initializes as a random walk and its dynamics first evolves in the absence of extrusion and transcription to generate an equilibrium coil conformation. In the following step, both extrusion and transcription are switched on, and its dynamics evolve until a new steady-state conformation is obtained. Across all simulations, we used standard values for the friction coefficient (γ=0.5) and the time step (t=0.01), and we let the system evolve for up to 10^8 steps. As in previous studies, to connect our *in silico* space-time units with real distances and times of the biological process, we assumed that the concentration of DNA in the 3D simulation space is the same as that in a human nucleus. If we use a total DNA amount of 6 Gbp and a nucleus radius of 5 μm, we obtain the rough estimation of σ=65 nm. For time units, we consider the standard MD relation $\tau=\eta(6\pi\sigma^3/\epsilon)$. Assuming a viscosity ~0.25P, the fundamental time unit is τ=0.03 sec. By running simulations starting from independent configurations and by sampling periodically the system we obtain an ensemble of configurations up to 10^3 for the measurement of the quantities shown. Concentrations of CTCF, cohesin, and RNAPII are taken from physiological values and range from 10 to 50 nmol/l. The energy scale of the system is given by the Boltzmann factor k_B multiplied by the temperature of the system T=310 K.

Statistical analyses. *P*-values derived from the Fisher's exact test were calculated using GraphPad (http://graphpad.com/), those from the Wilcoxon-Mann-Whitney test using R. Unless otherwise stated, *P*-values <0.01 were deemed significant. For the comparison of Micro-C and simulated contact matrices distance-corrected Pearson's and stratum-adjusted correlation coefficients (SCC) from HiCRep[72] with h=5 were used as metrics.

References

60. Liu, Y. et al. Systematic inference and comparison of multi-scale chromatin sub-compartments connects spatial organization to cell phenotypes. *Nat. Commun*. **12**, 2439 (2021).
61. Greenwald, W.W., Li, H., Smith, E.N., Benaglio, P., Nariai, N. & Frazer, K.A. Pgltools: a genomic arithmetic tool suite for manipulation of Hi-C peak and other chromatin interaction data. *BMC Bioinformatics* **18**, 207 (2017).
62. Yu, G., Wang, L.G. & He, Q.Y. ChIPseeker: an R/Bioconductor package for ChIP peak annotation, comparison and visualization. *Bioinformatics* **31**, 2382-2383 (2015).
63. Whyte, W.A. et al. Master transcription factors and mediator establish super-enhancers at key cell identity genes. *Cell* **153**, 307-319 (2013).
64. Flyamer, I.M., Illingworth, R.S. & Bickmore, W.A. Coolpup.py: versatile pile-up analysis of Hi-C data. *Bioinformatics* **36**, 2980-2985 (2020).
65. Langmead, B. & Salzberg, S.L. Fast gapped-read alignment with Bowtie 2. *Nat. Methods* **9**, 357-359 (2012).
66. Grant, C.E., Bailey, T.L. & Noble, W.S. FIMO: scanning for occurrences of a given motif. *Bioinformatics* **27**, 1017-1018 (2011).
67. Ramírez, F., Dündar, F., Diehl, S., Grüning, B.A. & Manke, T. DeepTools: A flexible platform for exploring deep-sequencing data. *Nucleic Acids Res*. **42**, W187-191 (2014).

68. Watrin, E., Schleiffer, E., Tanaka, K., Eisenhaber, F., Nasmyth, K. & Peters, J.M. Human Scc4 is required for cohesin binding to chromatin, sister-chromatid cohesion, and mitotic progression. *Curr. Biol*. **16**, 863-874 (2006).
69. Reynwar, B.J., Illya, G., Harmandaris, V.A., Muller, M.M., Kremer, K. & Deserno, M. Aggregation and vesiculation of membrane proteins by curvature-mediated interactions. *Nature* **447**, 461-464 (2007).
70. Chiariello, A.M., Annunziatella, C., Bianco, S., Esposito, A. & Nicodemi, M. Polymer physics of chromosome large-scale 3D organisation. *Sci. Rep*. **6**, 29775 (2016).
71. Barbieri, M. et al. Active and poised promoter states drive folding of the extended HoxB locus in mouse embryonic stem cells. *Nat. Struct. Mol. Biol.* **24**, 515-524 (2017).
72. Yang, T. et al. HiCRep: assessing the reproducibility of Hi-C data using a stratum-adjusted correlation coefficient. *Genome Res*. **27**, 1939-1949 (2017).

Supplementary Material

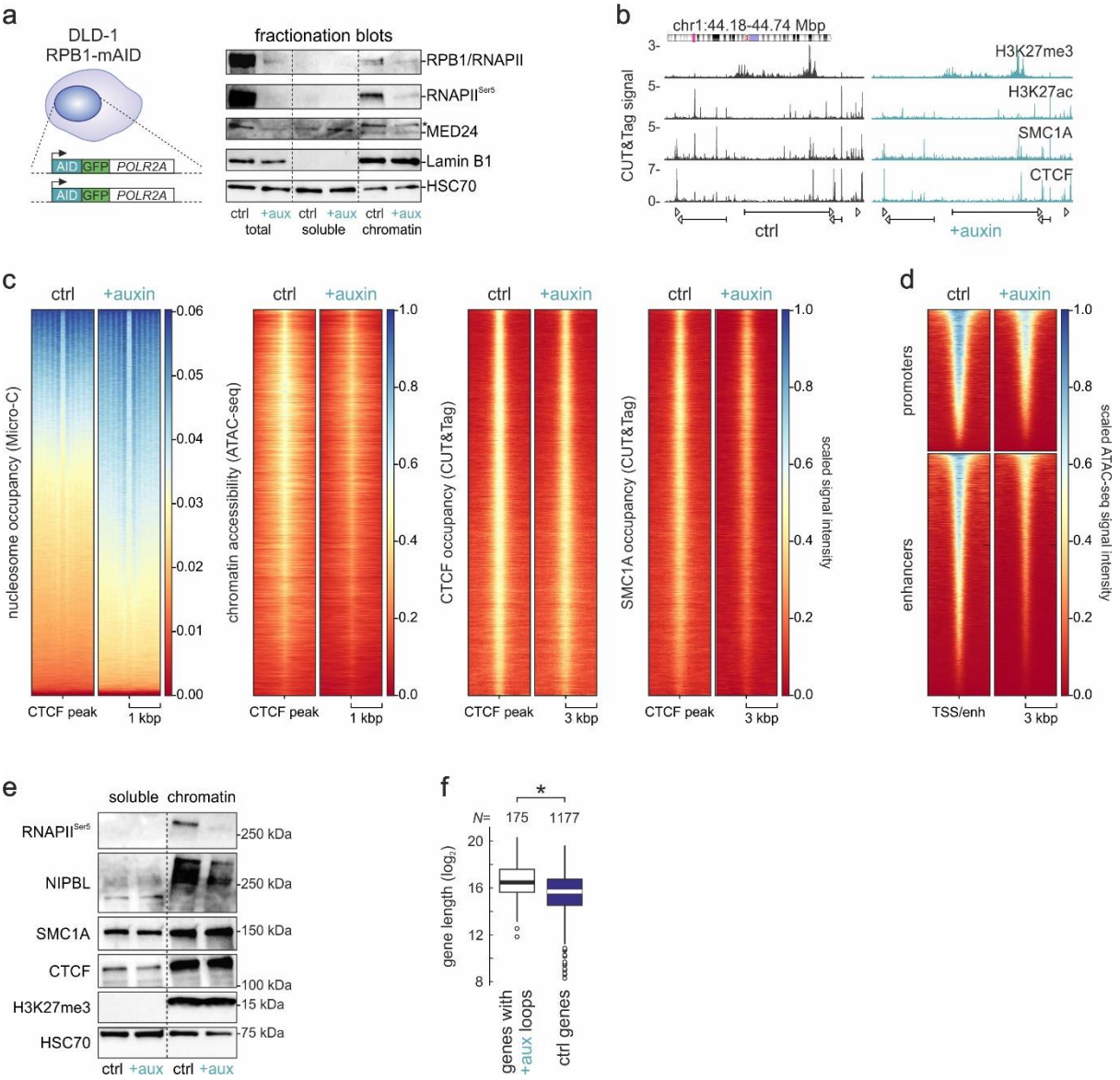

Fig. S1. Effects of RNAPII depletion on chromatin organization and protein levels. a, Left: Schematic of the biallelic tagging strategy in the endogenous *POLR2A* loci. Right: Fractionation blots showing the levels of RPB1 and Ser5-phosphorylated RNAPII, Mediator subunit 24, and Lamin B1 from DLD1-mAID-RBP1 cells treated or not with auxin to deplete RNAPII. HSC70 levels provide a control. **b,** Representative tracks of CUT&Tag signal for H3K27me3, H3K27ac, SMC1A, and CTCF from control (*black*) and auxin-treated DLD1-mAID-RBP1 cells (*green*) along 0.55 Mbp of chr1. **c,** Heatmaps of nucleosome occupancy deduced from Micro-C data, of chromatin accessibility deduced from ATAC-seq, and of CTCF and SMC1A occupancy deduced from CUT&Tag around CTCF loop anchors before (ctrl) and after RNAPII degradation (+auxin). **d,** As in panel c, but showing scaled ATAC-seq signal around gene promoters and enhancers. **e,** As in panel a, but for Ser5-phosphorylated RNAPII, NIPBL, SMC1A, CTCF, and H3K27me3 levels in the soluble and chromatin fractions of DLD-1 cells. HSC70 levels provide a control. **f,** Boxplots depicting the distribution of genes containing (genes with +aux loops) or not (ctrl genes) gained loop anchors upon RNAPII depletion. **P*<0.01, Wilcoxon-Mann-Whitney test.

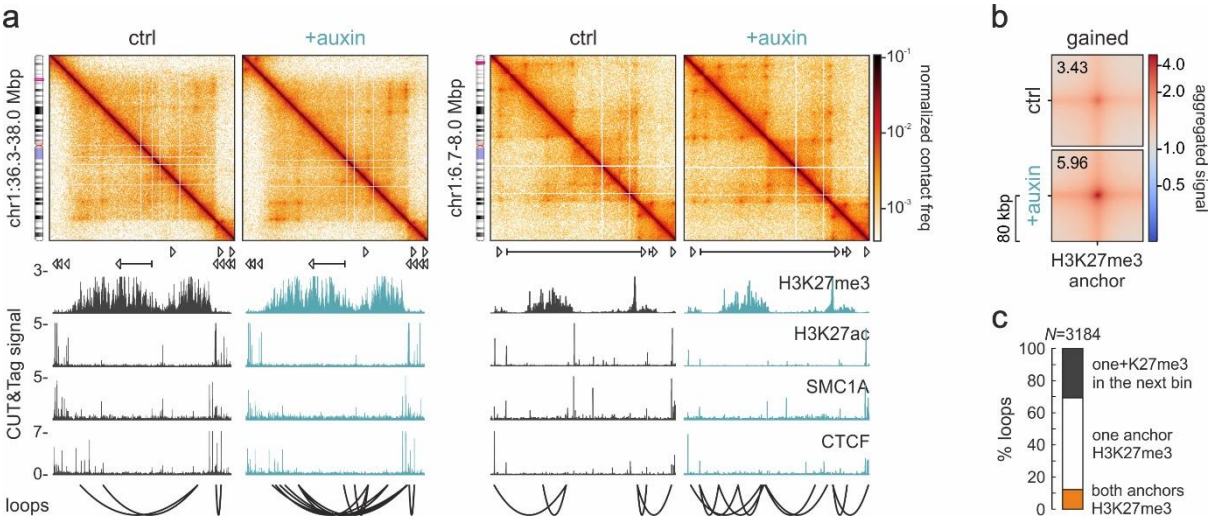

Fig. S2. Effects of RNAPII depletion on facultative heterochromatin 3D organization. a, Micro-C contact maps from control (left) and auxin-treated cells (right) in two exemplary genomic regions of chr1 at 2-kbp resolution aligned to H3K27me3, H3K27ac, CTCF, and SMC1A CUT&Tag signal tracks. Loops called for each region and condition are also shown by spider plots (bottom). **b,** Aggregate plots of all H3K27me3-anchored loops emerging in auxin-treated cells. **c,** Bar plot showing per cent of gained loops with one (white) or two H3K27me3 anchors (orange) or with H3K27me3 in the next-door genomic bin (i.e., within <10 kbp from the anchor).

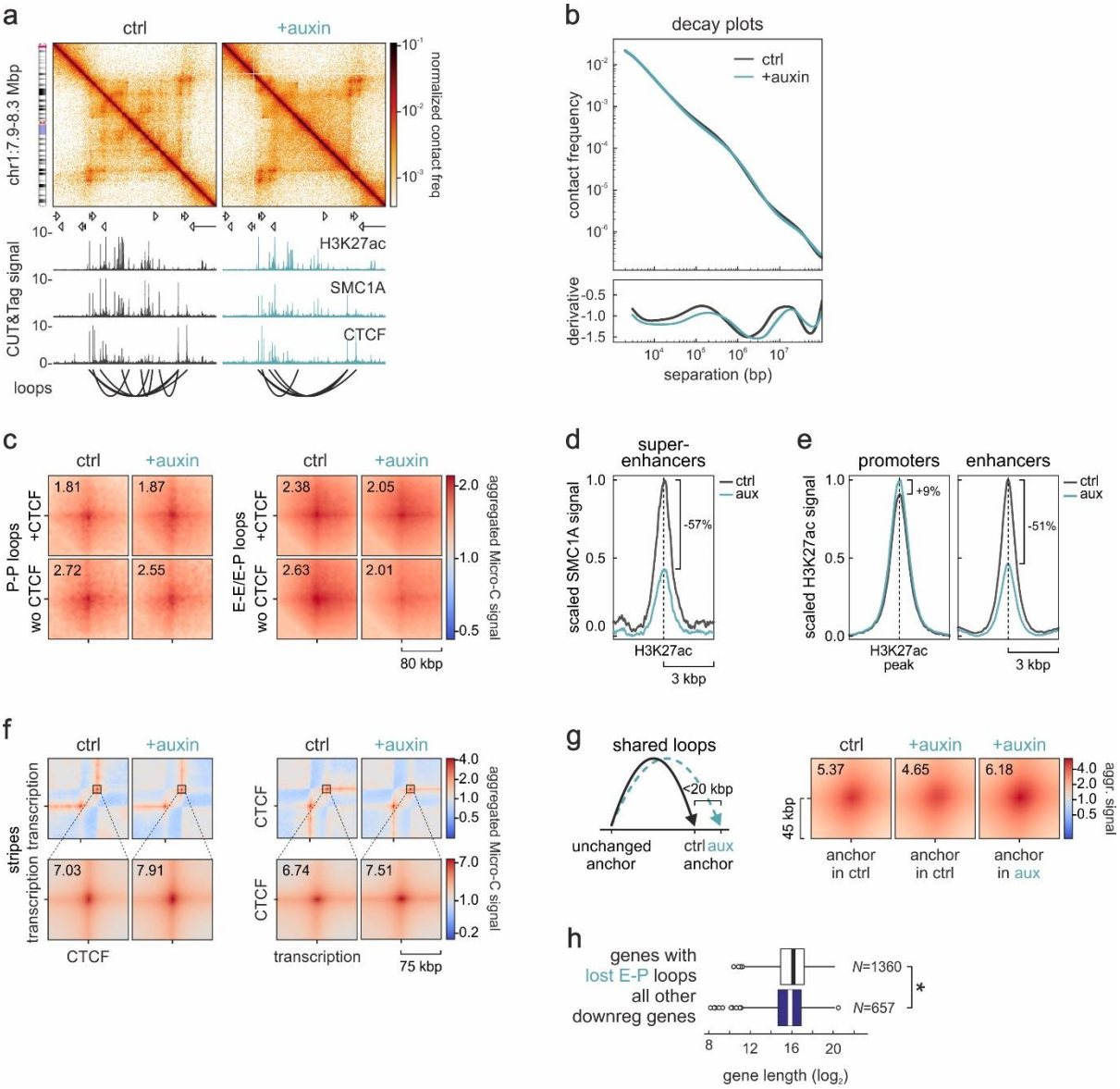

Fig. S3. Changes in loops and stripes following RNAPII depletion. a, Micro-C contact maps from control (left) and auxin-treated cells (right) in an exemplary genomic region on chr1 at 4-kbp resolution aligned to H3K27ac, CTCF, and SMC1A CUT&Tag signal tracks. Loops called for each region and condition are also shown by spider plots (bottom). **b,** Plots of interaction frequency decay as a function of genomic distance from control and auxin-treated cells (top) and their first derivative (bottom). **c,** Aggregate plots of gene promoter-(P-P) or enhancer-anchored loops (E-E/-P) in control and auxin-treated cells that involve (+CTCF) or not CTCF (wo CTCF) in at least one anchor. **d,** Line plot showing mean SMC1A CUT&Tag signal from control and auxin-treated cells in the 6 kbp around H3K27ac peaks from 590 super-enhancers. **e,** As in panel c, but for H3K27ac signal around active gene promoters or enhancers. **f,** Average plots showing mean signal of stripes with one CTCF and one transcriptional anchor before (ctrl) and after RNAPII depletion (+auxin). *Zoom-in*: Aggregate plots for loops at the end of the stripes. **g,** As in panel c, but for shared loops that rewire one anchor by <20 kbp (see cartoon). **h,** Boxplots depicting length distribution of genes downregulated upon RNAPII depletion that are linked (genes with lost E-P loops) or not (al other genes) to lost E-P loops. *: *P*<0.01, Wilcoxon-Mann-Whitney test.

Supplementary Table 1. Mapping, deduplication, and contact statistics from 4 merged replicates.

	Control DLD-1	%	+Auxin DLD-1	%
Total read pairs	2,727,166,750	100.0	2,698,337,998	100.0
Mapped read pairs	2,181,293,155	80.01	2,138,171,683	79.24
Duplicate pairs	895,400,630	32.80	877,684,142	32.52
Valid *trans* read pairs	144,654,584	5.30	149,856,062	5.56
Valid *cis* read pairs	1,141,237,941	88.75	1,110,631,479	88.10
Long-range contacts	790,299,199	61.50	753,737,258	59.79
Long-/short-contact ratio	2.26x	N/A	2.11x	N/A

Supplementary Table 2. Translocation speeds and loading in the different MD modeling scenarios.

	RNAP speed (kbp/min)	Cohesin speed (kbp/min)	Total cohesin loaded (per min)
Control	7.5	18.2	8.1
75% RNAP depletion	7.8	20.2	7.1
100% RNAP depletion	N/A	23.0	6.0
Toy model: control	8.9	20.2	3.4
Toy model: 100% RNAP depletion	N/A	28.4	1.9

4. Discussion

The eukaryotic genome is highly organised in a hierarchical manner. Despite an emerging picture of how the chromatin architecture is established its functional relevance we now only begin to untangle. Research to date assumes that the 3D organisation is a highly dynamic entity that changes between individual cells, different stages of the cell cycle and during development (Naumova *et al.*, 2013; Rao *et al.*, 2014; Wang *et al.*, 2016; Bonev *et al.*, 2017; Hug *et al.*, 2017; Nagano *et al.*, 2017; Gibcus *et al.*, 2018; Kaaij *et al.*, 2018). Thereby, the interplay of converging and opposing forces shape the chromatin structure in a dynamic manner. These forces have already been proposed before as compartmentalisation (Rao *et al.*, 2014), loop extrusion (Rao *et al.*, 2017; Nuebler *et al.*, 2018; de Wit and Nora, 2022) and active transcription (Papantonis and Cook, 2011; Rowley *et al.*, 2017). It has been shown that the chromatin structure reflects cellular activity and potentially impacts transcription (Tsukamoto *et al.*, 2000; Lieberman-Aiden *et al.*, 2009; Rowley *et al.*, 2017). However, the participation of transcription, and transcriptional components such as RNAPII, or the Mediator complex on the chromatin structure is heavily debated in the field of epigenetics.

In this thesis, I provide evidence for a central role of RNAPII in 3D genome organisation. By inducibly depleting the largest subunit RPB1 with the mAID system (Nagashima *et al.*, 2019; Yesbolatova *et al.*, 2019), I was able to address its implication in chromatin folding. *In situ* Hi-C and Micro-C performed in both asynchronous, and synchronised G1-sorted DLD1-mAID-mClover-RPB1 cells upon RNAPII depletion revealed an impact of RNAPII on all layers of chromatin organisation at the M-G1 transition.

4.1. Transcription-based 3D organisation in asynchronous G1 cells

The structure-to-function relationship of mammalian genomes is still not fully understood. The first question in this thesis sought to determine the relevance of RNAPII on the general 3D organisation. Hi-C performed in G1-sorted asynchronous cells revealed only minor changes at the compartment and TAD levels (Chapter 1, Fig 1C-E). A prior study by Jiang et al. showed similar results in mouse ES cells. In their study, short-term 2 hour depletion of RNAPII had minor effects on large-scale genome organisation (Jiang *et al.*, 2020). As a result, the large-scale chromatin structure has been declared very robust, and could not be disrupted even after nuclear volume swelling (Sanders *et al.*, 2022). Depletion of RNAPII for more than 6 hours showed reduced accessibility (Jiang *et al.*, 2020) which was concordant with our finding that accessibility was decreased at TSSs genome-wide (Chapter 1, Fig 1B). This reduced accessibility is in line with increased H3K27me3 signals indicating chromatin Heterochromatinization. Furthermore, transcription inhibition has been shown to deplete H3K27ac marks, which we also

observed upon auxin addition in our system (Chapter 1, Fig S1B) (Wang *et al.*, 2022). Increased chromatin compaction upon loss of RNAPII in this study is in line with earlier findings. Transcriptional inhibition (α-amanitin) has already been shown to result in compacted chromatin (Naughton *et al.*, 2013). Upon RNAPII inhibition with both actinomycin D and DRB, Croft et al. observed a compaction of the gene-rich chromosome 19. On the contrary, chromosome 18 which is supposed to be gene-poor did not change its space in the nuclear area (Croft *et al.*, 1999). The finding that loss of transcription leads to chromatin Heterochromatinization indicates a role of RNAPII or transcription in 3D chromatin organization. Furthermore, we observed stronger insulation of TAD boundaries and gain of loops (Chapter 1, Fig 1F,H). These new loops emerged in highly expressed regions, suggesting that active transcription counteracts loop extrusion. This does not correspond to the findings of Jiang et al. In Jiang's study neither were changes in TAD insulation observed nor were longer loops in the RNAPII-depleted cells detected. A possible explanation might be the difference in auxin-treatment duration to deplete RNAPII. Incomplete RNAPII depletion could already change its effects on 3D organisation. Upon short-term RNAPII degradation for two hours, we also did not detect any differences in TAD insulation, or loop length (Chapter 1, Fig S2J-K). This can be explained by incomplete degradation of RNAPII. The detected differences in RNAPII levels after two hours of degradation may be due to the antibody used to detect RNAPII levels in their study. The largest subunit of RNAPII has a CTD, which contains a Tyr-Ser-Pro-Thr-Ser-Pro-Ser repeated sequence. Phosphorylation of different Ser residues regulate different stages of the transcription cycle. In this context, Ser5P has been detected upon transcription initiation. After transcription initiation RNAPII Ser5P accumulates downstream of the TSS which was described as paused RNAPII (Buratowski, 2009; Fuda, Ardehali and Lis, 2009). Jiang et al. measured the whole protein level of RNAPII by using an antibody against the CTD region.

We also took a closer look at the whole RNAPII, as well as at paused RNAPII by applying a Ser5P antibody. Interestingly, RNAPII Ser5P remained partially bound to chromatin. In contrast, we were able to deplete the unbound RNAPII detected with an antibody against the CTD. Depletion for 14 hours resulted in decreased RNAPII Ser5P levels compared to the two hours treatment (Chapter 1, Fig S1A). Thus, chromatin-bound RNAPII might be more difficult to degrade and remains bound to the TSS, whereas unbound RNAPII is degraded more rapidly. A previous study observed remaining RNAPII at promoters upon blocking initiation, and elongation by Triptolide and Flavopiridol treatment, respectively (Buckley *et al.*, 2014). This agrees with the hypothesis that paused RNAPII is stably bound to promoters. Thus, the use of an antibody detecting the RNAPII Ser5P would be more reliable to quantify the depletion efficiency. This could potentially rule out remaining RNAPII at promoter regions in Jiang's study. Overall, we did not observe significant effects on 3D organization upon RNAPII depletion in asynchronous cells.

4.2. RNAPII reestablishes the spatial chromatin organisation at the M to G1 transition

During the cell cycle, the chromatin passes through dramatic structural rearrangements, which are accompanied by changes in transcription. At the beginning of mitosis, chromatin is in a highly compacted state and most chromatin-bound proteins are evicted. This also affects the gene regulatory machinery, and the disassociation in turn leads to declined transcription. Recent findings proposed that transcriptional silencing during mitosis is important to reset transcription and regulate gene expression throughout the cell cycle (Ramos-Alonso *et al.*, 2023). Following exit from mitosis, cohesin is reloaded onto chromatin and the 3D organisation is reestablished (Naumova *et al.*, 2013; Nagano *et al.*, 2017; Abramo *et al.*, 2019). At the same time transcription reaches its peak at the M-G1 transition (Hsiung *et al.*, 2016). This suggests that reloading of RNAPII upon mitotic exit is concomitant with the reestablishment of structural features.

The observed structural changes between control and auxin-treated cells could be explained by differences in cell cycle progression. It is possible that cells take longer to go through the cell cycle with reduced RNAPII levels. Thus, the observed 3D organisation changes could just depict an earlier cell cycle stage in auxin-treated cells compared to already reestablished control cells. However, I ruled out the possibility that RNAPII-depleted cells cycled slower compared to control cells via FACS analysis (data not shown). Furthermore, I verified similar cell cycle stages between control and auxin-treated cell by staining for different cell cycle markers (Chapter 1, Figure S3A).

We decided to look at the structural changes of cells at the M-G1 transition with *in situ* Hi-C. One drawback of 3C methods is that they are restricted to depict a population average in asynchronous cells. However, throughout the cell cycle different genome organisation-, and transcription-states have been identified (Naumova *et al.*, 2013; Nagano *et al.*, 2017; Yin Liu *et al.*, 2017; Abramo *et al.*, 2019). Despite of using G1-sorted cells, there are differences in genome organisation between the different G1 subphases (early-, mid-, late-G1-phase). Moreover, with a duration of around eleven hours the G1 phase is the longest cell cycle phase. Hence, there is a possibility we efficiently depleted RNAPII in cells after they went through M phase (Wang, 2021). By sorting G1 cells all the G1-subphases are included and averaged out in Hi-C maps (Zhang *et al.*, 2019). Thus, subphase-specific structural changes might be missed in the asynchronous setup. In order to minimise heterogeneity and thus blurred or missing information, we synchronised the cells at the G2/M transition (Vassilev, 2006) and released them through M until G1 phase with and without RNAPII. Synchronisation of the cells in combination with FACS sorting enabled the detection of specific G1-interactions.

In this setting, we observed dramatic changes in Hi-C maps across all layers of genome organisation. For instance, changes on the compartment level, included domain erosion with blurred compartment boundaries and compartment mixing in the absence of RNAPII (Chapter 1, Fig 2D,E). At the same time, inter-chromosomal contacts were increased (Chapter 1, Fig S3F,G). During mitosis, compartments are weak. They are reestablished in early G1 while progressively increasing their strength until G2 phase (Nagano *et al.*, 2017; Zhang *et al.*, 2019). Interestingly, it has been shown that there is a correlation between compartment identity and the transcriptional state. A compartments were defined as transcriptionally active, GC-rich, and accessible (Lieberman-Aiden *et al.*, 2009; Rowley *et al.*, 2017). Furthermore, A compartments containing early reactivated genes show a higher rate of compartmentalization in early G1 compared to compartments including later-expressed genes. Prior studies have noted that H3K27ac bookmarks promoters for rapid transcriptional reactivation (Pelham-Webb *et al.*, 2021). In interphase, distant acetylated chromatin regions interact with each other and form domains. Within these acetylated domains increased gene expression has been reported (Rosencrance *et al.*, 2020). Efficient transcription depends on E-P contacts, but enhancers are usually located far away from their promoter. However, enhancer regions are highly acetylated (Whyte *et al.*, 2013). Chromatin contacts anchored by H3K27ac were faster recovered in G1 than CTCF/cohesin anchored loops (Pelham-Webb *et al.*, 2021). Thus, the ability to form interactions between acetylated regions could rapidly reset E-P contacts and transcription in G1 reentry cells. Accordingly, loss of H3K27ac decreased transcription rates in both asynchronous and G1 reentry cells (Pelham-Webb *et al.*, 2021). We also observed reduced H3K27ac levels in asynchronous, as well in G1 reentry cells upon RNAPII depletion (Chapter 1, Fig S1B and Fig S3C). Inhibition of transcription initiation with Triptolide in *Drosophila melanogaster* resulted in decreased domains, but was less distinct compared to organisational changes upon heat shock (Rowley *et al.*, 2017). This can be explained by remains of chromatin-bound RNAPII upon Triptolide treatment, whereas heat shock has been shown to be more efficient to remove RNAPII from chromatin (Li *et al.*, 2015). These observations are in line with our detected domain erosion, which might directly depend on transcription itself, or indirectly on the transcription-mediated chromatin landscape. The transcriptional epigenetic state is characterised by open chromatin marked by active histone marks such as H3K27ac.

At a smaller scale, we observed loss of interactions within TADs and weakened TAD insulation following RNAPII depletion. These changes stood out due to fewer but larger TADs (Chapter 1, Fig 2F-I). TAD borders are conserved between interphase cells, but their insulation score varies throughout the cell cycle and peaks in G1 (Nagano *et al.*, 2017). TAD boundaries are usually demarcated by active histone marks and RNAPII (Chapter 1, Fig 2J). This association of TAD boundaries with active marks or expressed genes has been observed before (Ulianov *et al.*, 2016; El-Sharnouby *et al.*, 2017; Hug *et al.*, 2017). In addition, changes of TAD boundaries correlate with gene expression changes (Bonev *et al.*,

2017; Stadhouders *et al.*, 2018). In this context, transcriptional inactivation in *Drosophila* embryos already showed loss of TAD boundary insulation (Hug *et al.*, 2017). Taken together, TAD insulation culminates in G1 when transcription is highly active, which hint to a role of RNAPII in TAD insulation (Hsiung *et al.*, 2016; Nagano *et al.*, 2017). This suggests that RNAPII or the transcription machinery acts as boundary element to support insulation of transcriptionally active regions from inactive regions for proper gene expression regulation.

In line with generally stronger effects in synchronised cells compared to asynchronous cells, we observed more dramatic changes in loop formation in RNAPII-depleted cells. Namely, 1900 loops were lost, but more than 1100 new loops emerged (Chapter 1, Fig 2K-N). These rewired and longer loops were located in highly expressed regions. It is known that cohesin can extrude DNA to form loops at rates ranging from 0.5 - 2.36 kb/s (Kanke *et al.*, 2016; Busslinger *et al.*, 2017; Davidson *et al.*, 2019; Kim *et al.*, 2019; Golfier *et al.*, 2020) and remains bound to chromatin for 20 minutes (Hansen *et al.*, 2017). Another molecule known to move along DNA is RNAPII with an elongation rate of 3.1 kbp/min (Cho *et al.*, 2016). It has been proposed that cohesin can be positioned by RNAPII movements (Davidson *et al.*, 2016). Previous studies reported that cohesin accumulates between convergently transcribed genes and was repositioned by transcription in yeast (Glynn *et al.*, 2004; Lengronne *et al.*, 2004). Similar conclusions have been drawn in mammals, where cohesin was located at the TSS, or downstream of actively transcribed genes in the absence of WAPL, and CTCF. At regions containing converging genes with different expression levels, cohesin was located at the weaker expressed gene (Busslinger *et al.*, 2017). Additionally, elongating RNAPII has been shown to displace cohesin from CTCF sites, whereas inhibited elongation (Flavopiridol) favored the accumulation of cohesin at CTCF and transcription initiation sites (Heinz *et al.*, 2018). A recent study confirmed that cohesin and NIPBL accumulated at TSSs (Banigan *et al.*, 2022). This can be explained by the function of RNAPII as barrier for cohesin-mediated loop extrusion. Similar findings have been observed in RAS-induced senescent (RIS) cells where cohesin was repositioned and gene expression changed. Cohesin sites were highly enriched for RNAPII and H3K27ac. In addition, cohesin repositioning seems to be dependent on transcription due to the observation of cohesin accumulation at 3' ends of highly expressed genes (Olan *et al.*, 2020).

Likewise to cohesin, the movement of condensing was impaired by transcription in *Bacillus subtilis* (Wang *et al.*, 2017). Similarly, Brandão et al. showed that transcription affects condensin-mediated loop extrusion (Brandão *et al.*, 2021). Comparing the findings of cohesin and condensin suggests a model in which transcription relocates molecules along DNA. Accordingly, loop extruders can move by different forces acting on chromatin. On the one hand, cohesin can move along DNA through its motor activity. On the other hand, RNAPII can translocate cohesin. Apart from direct translocation of cohesin, physical barriers, such as protein complexes bound to chromatin also affected loop extrusion. Previously the MCM complex has been reported to act as an obstacle for cohesin-mediated loop

extrusion (Dequeker *et al.*, 2022). However, it has been suggested that SMC complexes can bypass physical barriers (Pradhan *et al.*, 2022). One explanation of how RNAPII could act as a barrier is direct binding to cohesin. It is well established that cohesin directly binds to CTCF. Recent data point to the interaction of CTCF with cohesin through the YDF motif spanning the amino acids 222-231 of CTCF. Additionally, MCM3 contains a YDF motif through which it directly interacts with the STAG2-RAD21 subunits of cohesin (Li *et al.*, 2020). Interestingly, the RPB2 subunit of RNAPII also contains the YDF motif. The motif is located in an outwards-facing loop, which makes it accessible for a potential interaction with cohesin (**Fig 8**). This motif is conserved in different eukaryotes such as *C. elegans*, *D. melanogaster*, *M. musculus* and *H. sapiens*. Notably, *S. cerevisiae* does not contain the YDF motif. In addition, the reversed FDY motif can be found in the RPB1 subunit, and the motif is only conserved between human and mouse. Whether these motifs are functionally relevant remains unclear and needs to be elucidated by mutagenesis experiments of the YDF motif.

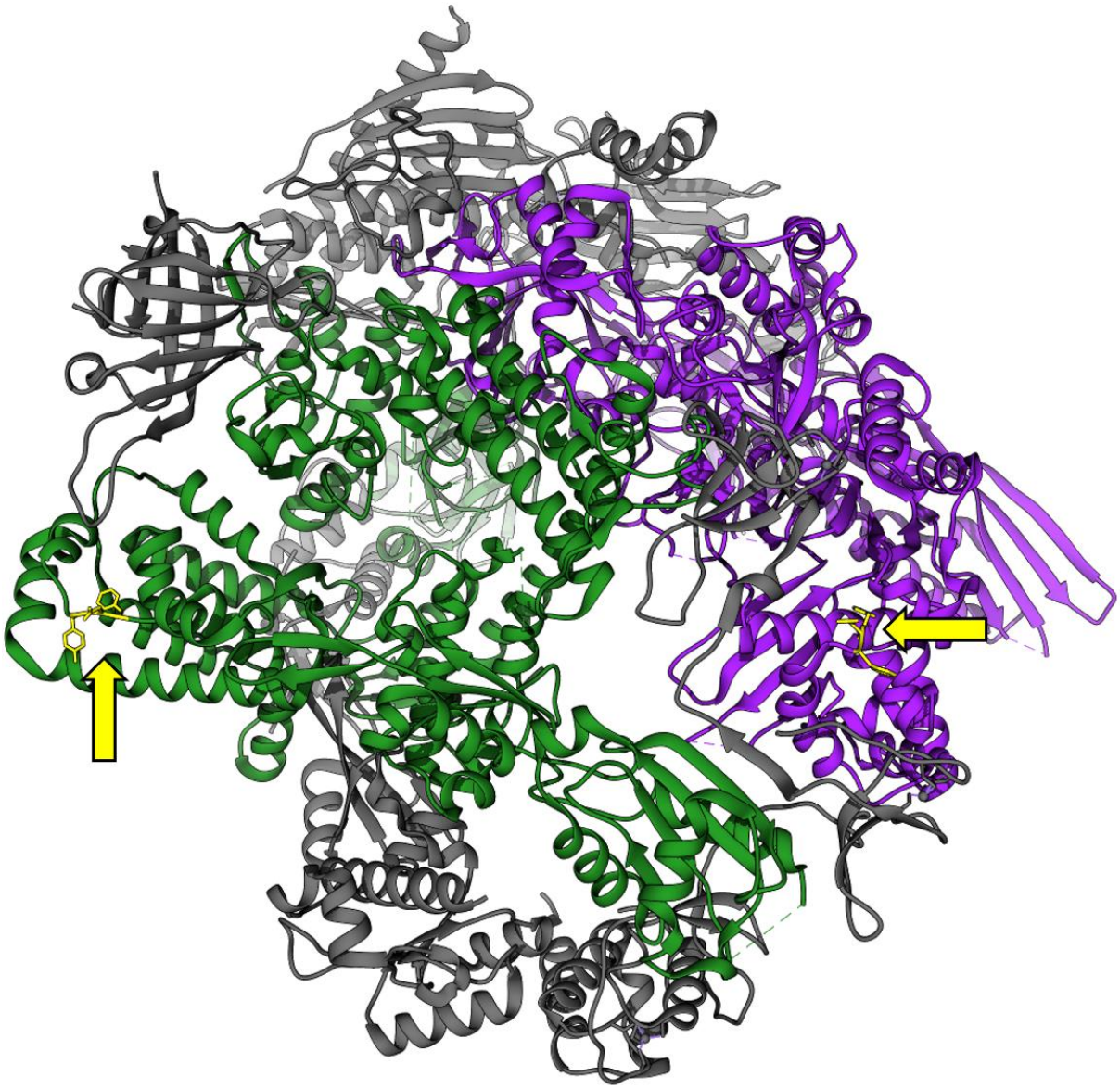

Figure 8: Structure of RNAPII. *The RPB2 subunit is depicted in purple containing an YDF motif (yellow, indicated by yellow arrow). The RPB1 subunit is depicted in green containing the reverse FDY motif (yellow, indicated by yellow arrow) (PDB: 7B7U,* Fianu *et al.*, 2021).

Taken together the interaction of cohesin with RNAPII could prevent its traverse, which eventually impedes loop extrusion. As a result, loss of RNAPII could reduce the number of obstacles along the DNA and leads to more efficient loop extrusion. This is consistent with the observed longer loops (Chapter 1, Fig 2K). Conclusively, RNAPII can act as either physical barrier for loop extrusion, or can translocate cohesin by the act of transcription, which explains the observed longer loops in RNAPII depleted cells.

Even though many new loops were detected, almost 1900 loops were lost upon auxin addition in our system. Additional 2443 loops were present in the control and in RNAPII-depleted cells, but weaker and with reduced insulation in the latter. It is important to note that CTCF and cohesin did not change

their chromatin-bound levels. Surprisingly, the cohesin loaders NIPBL and MAU2, as well as its unloader WAPL exhibited reduced chromatin-bound levels in RNAPII depleted cells upon G1 reentry (Chapter 1, Fig 3A). These results seem to be consistent with other research who found reduced NIPBL levels upon Mediator depletion (Mattingly *et al.*, 2022). However, decreased NIPBL and WAPL levels are not sufficient to explain differences in loop formation. Despite that WAPL knockout experiments resulted in increased loop length, decreased NIPBL or MAU2 levels resulted in shorter loops (Haarhuis *et al.*, 2017). Furthermore, it has been shown that decreased WAPL levels are sufficient to compensate phenotypes caused in Nipbl$^{+/-}$ mice (Kean *et al.*, 2022). I has been shown that co-depletion of NIPBL and WAPL restores physiological cohesin levels (Haarhuis *et al.*, 2017; Luppinoid *et al.*, 2022). The decreased NIPBL/MAU2, and WAPL levels are in line with the observed unchanged cohesin levels on chromatin, but cannot explain the changes in loop formation upon RNAPII depletion.

To analyse differences in the distribution of architectural proteins I performed CUT&Tag of CTCF and cohesin. Since CTCF and cohesin are important for loop formation a high overlap of their localisation is expected. One unanticipated finding was that a reduced fraction of cohesin overlapped with CTCF sites upon RNAPII depletion. The cohesin occupancy at TSSs has been decreased while it was increased at intergenic sites (Chapter 1, Fig 3D,E). In contrast, CTCF depletion resulted in accumulated cohesin at active TSSs, which could be the location where cohesin is loaded (Busslinger *et al.*, 2017; Valton *et al.*, 2022). Earlier studies reported binding of CTCF, cohesin, and the cohesin loader NIPBL close to enhancers, active promoter sites, and RNAPII-associated transcription factories (Kagey *et al.*, 2010; Dowen *et al.*, 2014; Muto *et al.*, 2014; Swain *et al.*, 2016; Kubo *et al.*, 2021). Therefore, it is reasonable to assume that a connection between transcription and cohesin loading exists, which would explain the differences in cohesin occupancy between control and RNAPII depleted cells. Besides, Co-Immunoprecipitation (Co-IP) revealed an interaction of RNAPII with NIPBL and WAPL (Chapter 1, Fig S5E), as well as with MAU2 (data not shown). These findings are in accordance with the identification of NIPBL and TBP as binding partners (data not shown). Furthermore, cohesin and Nipbl have been shown to interact with the mediator complex, which is localized at promoters and enhancers (Kagey *et al.*, 2010). A recent finding suggested that Mediator can recruit Scc2/Scc4 for efficient cohesin loading (human: NIPBL/MAU2) (Mattingly *et al.*, 2022). These data point to an interaction of the cohesin regulators with the transcription initiation complex. A possible scenario is a yet unexplored role of RNAPII or Mediator in recruiting NIPBL and WAPL to TSS, or a direct role in cohesin loading. Work by Rao et al. already showed efficient cohesin depletion in RAD21-mAID-mClover cells upon auxin addition and accordingly lost loops, which were recovered by auxin withdrawal. The faster recovery of loops in regions with active promoters, enhancers, or active histone marks supports the potential role of RNAPII in cohesin loading (Rao *et al.*, 2017). Moreover, combination of *Wapl* and *Ctcf* DKO with transcription inhibition lead to loss of cohesin, which was reversed by reactivating

transcription (Busslinger *et al.*, 2017). More recently *Wapl* and *CT* DKO showed cohesin accumulation at active genes together with NIPBL and MAU2 (Banigan *et al.*, 2022). Earlier work suggested that NIPBL binds at promoter regions (Zuin *et al.*, 2014; Busslinger *et al.*, 2017; Zhu *et al.*, 2021). These observations strengthen the hypothesis that cohesin is loaded at TSS, or enhancer regions where NIPBL is bound. Thus, in the absence of RNAPII cohesin is not loaded efficiently. Computational modelling of cohesin loading at TSSs by RNAPII, versus random loading of cohesin in RNAPII-depleted cells reconstructed the former Hi-C maps (Chapter 1, Fig 4A). Therefore, the observed changes in the 3D organisation can be explained by an interplay between transcription and loop extrusion. In general, this would be a smart solution how transcription restructures the 3D genome organisation to promote cis-regulatory contacts. Hence, a modified genomic landscape would support E-P interactions and thus maintains proper gene expression. However, we cannot rule out that cohesin accumulates at TSSs due to RNAPII acting as a barrier.

Strikingly, a big difference between asynchronous (Chapter 1, Fig 1B) and synchronised cells (Chapter 1, Fig 3G) was observed in ATAC-seq. While asynchronous cells showed decreased TSS accessibility, we observed increased accessibility at TSSs in synchronised RNAPII-depleted cells. This was in line with increased TBP- levels bound to chromatin in RNAPII-depleted cells (Chapter 1, Fig 3A), while cells arrested at G2/M did not show differences in TBP levels (Chapter 1, Fig S5B). Previously reported data revealed TBP as bookmarking factor for fast reactivation of genes (Teves *et al.*, 2018). Especially early-reactivated genes were marked by high accessibility, increased H3K27ac, and TBP (Pelham-Webb *et al.*, 2021). Furthermore, RNAPII binds to promoters in telophase (de Castro, Gokhan and Vagnarelli, 2016). This could reflect a mechanism by which increased accessibility at TSSs provides a basis to recruit the PIC and RNAPII for the transcription burst at the M-G1 transition. However, depletion of RNAPII leads to reduced transcription efficiency. As a feedback mechanism, TBP could mark accessible TSSs, which could compensate for reduced transcription to increase the probability to recruit the RNAPII. Moreover, already marked promoters with TBP cannot load RNAPII, which in turn leads to remaining TBP at these regions.

The invention of Hi-C was groundbreaking to gain insight into higher-order chromatin architecture. We identified structural changes in chromatin architecture at the compartment-, TAD-, and loop level in RNAPII depleted cells (see **Chapter 1**). However, Hi-C fails to address the 3D organisation at fine-scale resolution, which presumably displays direct RNAPII-mediated structures such as E-P interactions due to resolution limitations. The introduction of Micro-C increased the resolution to sub-kb scale (Hsieh *et al.*, 2015, 2016) and revealed numerous undetected loops (Hsieh *et al.*, 2020; Krietenstein *et al.*, 2020). Mostly, transcription-dependent interactions between promoters and *cis*-regulatory elements (P-P, E-P) have been identified. These RNAPII-dependent loops are highly dynamic. We discovered 23,735 new loops that were only detected by Micro-C, and 8,178 shared between Hi-C and Micro-C

(Chapter 2, Fig 1E). Similar to our previous study described in Chapter 1, we found both lost and gained loops. Especially loops harbouring RNAPII at their anchor were rewired (Chapter 2, Fig 2F). These lost or gained loops provide further support that RNAPII can act both as opposing and convergent force for loop extrusion, respectively. In accordance with RNAPII-dependent changes in 3D organisation at a smaller scale, transcriptional inhibition in *Bacillus subtilis* confirmed loss of short-range interactions (Wang *et al.*, 2017).

In this thesis, I found that active transcription can both converge but also counteracts loop extrusion. I observed structural changes across all layers of genome organisation upon RNAPII depletion. Overall, the results prove a role of RNAPII in higher-order and fine-scale chromatin structure reestablishment following exit from mitosis.

4.3. The role of cohesin in E-P interactions

Precise gene expression in a cell-type-specific manner depends on different E-P interactions. Enhancers are *cis*-regulatory elements that bind different TF combinations, which in turn recruit the Mediator complex. It is noteworthy that enhancers can be located distal of their promoters (Furlong and Levine, 2018). Another hallmark is that enhancers are highly enriched for H3K27ac marks (Whyte *et al.*, 2013). Usually, enhancers interact with promoters located within the same TAD, and TAD disruption can lead to aberrant gene expression (Lupiáñez *et al.*, 2015; Symmons *et al.*, 2016). How E-P contacts are established to control gene expression is not fully understood. Existing research recognises the critical role of RNAPII and the Mediator complex in E-P interactions. RNAPII and Mediator are known to colocalize in a transcription-dependent manner. It has been proposed that this interaction occurs first at enhancers followed by the binding to promoters. Thus, Mediator could serve as a physical bridge between the enhancer and the transcription machinery at promoters (Cho *et al.*, 2018). Loss of Mediator causes reduced gene expression and especially affects genes controlled by SEs (Kagey *et al.*, 2010; Whyte *et al.*, 2013; Jaeger *et al.*, 2020). In our findings, RNAPII depletion only slightly affected P-P loops. These results reflect those of Thiecke et al. who found maintained P-P interactions upon both transcriptional inhibition with Triptolide and cohesin depletion (Thiecke *et al.*, 2020). Surprisingly, we observed a more pronounced loss of around 900 enhancer-anchored loops in RNAPII-depleted cells (Chapter 2, Fig 3D), which was in conjunction with decreased cohesin-, and H3K27ac levels at E-P contacts (Chapter 2, Fig 3E and Fig S3E). SEs showed an even stronger reduction of cohesin (Chapter 2, Fig S3D). Typically, SEs also exhibit higher levels of Mediator binding compared to enhancers (Whyte *et al.*, 2013). In accordance with our findings, depletion of Mediator has been shown to reduce both E-P interactions, and the cohesin occupancy at enhancers (Ramasamy *et al.*, 2022). Thus, both RNAPII and Mediator seem to influence cohesin binding at enhancers. It has been

proposed that cohesin is loaded at accessible chromatin regions, or more specifically at lineage-specific enhancers (Barrington *et al.*, 2019). Previous cohesin depletion studies observed reduced and rewired E-P interactions which correlated with reduced, or changed gene expression, respectively (Thiecke *et al.*, 2020; Aljahani *et al.*, 2022). These results could reflect a role of cohesin in E-P communication. A previous study has shown that binding of cohesin as well as Mediator is important for functional E-P contacts. Therefore, it is not surprising that both Mediator and cohesin occupy promoter and enhancer sites. Moreover, the cohesin loader Nipbl was associated with the Mediator-cohesin complex but not with the CTCF-cohesin complex (Kagey *et al.*, 2010). Both Nipbl and Mediator have been shown to synergistically regulate gene expression by E-P interactions during limb development (Muto *et al.*, 2014). Here, I observed reduced NIPBL binding to chromatin upon RNAPII depletion (Chapter 2, Fig S1E). A recent finding suggested that Mediator can recruit Scc2/Scc4 (human: NIPBL/MAU2) to RNAPII transcribed genes (Mattingly *et al.*, 2022), which would explain a previously reported decreased cohesin occupancy upon Mediator depletion (Ramasamy *et al.*, 2022). According to these data, RNAPII and Mediator could recruit NIPBL in order to load cohesin onto enhancer regions. This is in line with the previously described Co-IP experiments that showed an interaction between the cohesin regulators and the transcription initiation complex (Chapter 1, Fig S5E). Another study reported that cohesin is especially important for long-range E-P interactions and gene expression. There, distal E-P interactions were highly affected by cohesin KD experiments compared to proximal E-P contacts. (Rinzema *et al.*, 2022). Similar findings have been observed in neuronal gene expression where long-range chromatin contacts were dependent on cohesin (Calderon *et al.*, 2022). In contrast, short-range E-P interactions are more likely to establish stochastically and are consequently less affected by loss of cohesin (Rinzema *et al.*, 2022). These results suggest that cohesin is recruited to enhancers to stimulate E-P looping. It is therefore likely that cohesin is loaded at enhancers, which would be in accordance with NIPBL recruitment to enhancers.

In my thesis, I showed that regulation of E-P interaction and cohesin recruitment to enhancers seems to be affected by RNAPII depletion. A simple interpretation of these results would be that the interplay between RNAPII, Mediator and cohesin contributes to cell-type specific E-P interactions. The thereby stabilised E-P loops are important to optimise gene expression. Thus, loss of the aforementioned proteins would result in reduced E-P contact efficiency.

5. Outlook

One major finding of this thesis is that RNAPII plays a role in reestablising the 3D chromatin organisation following exit from mitosis. However, the long duration of RNAPII depletion could affect the process of transcription, binding partners of RNAPII, and nascent RNA levels. Thus, the obtained findings could be partially the result of secondary effects. For example, it has been shown that CTCF depends on RNA binding to stabilize loops. Consequently, loss of the interaction between CTCF and RNA results in collapse of loops (Hansen *et al.*, 2017; Saldaña-Meyer *et al.*, 2019). It is challenging to determine the contribution of the individual factors separately. Therefore, future work is required to dissect the role of RNA, the process of transcription and the protein RNAPII on chromatin organisation. To analyse the impact of RNA on chromatin architecture a new RNAseL construct could be used to rapidly degrade RNA. It has already been shown that RNA degradation did not affect SEs (Decker *et al.*, 2022). However, the effect of RNA on all layers of genome organisation still needs to be elucidated.

How does RNAPII depletion effect cohesin loading and loop extrusion?

This thesis shed light into the relationship between loop extrusion and gene expression. I identified a dependency of cohesin loading on RNAPII. My Co-IP results verified the interaction between RNAPII, NIPBL/MAU2 and WAPL. How cohesin occupancy is affected by RNAPII remains unclear. Further research should be undertaken to investigate at which genomic positions cohesin is loaded. Recent evidence suggests that cohesin is loaded at accessible DNA regions. Another source of uncertainty is the exact mechanism of how loops are extruded. This is an important question for future work. I showed that upon RNAPII depletion longer loops emerged. My work suggests that RNAPII is a physical barrier to loop extrusion. This could be explained by direct interaction of RNAPII with cohesin. To elucidate whether and how RNAPII interacts with cohesin, the protein complex structure needs to be solved via cryo-EM.

How does RNAPII influence E-P interactions?

Furthermore, I made progress in understanding how E-P interactions are established. Here, I provided evidence for a role of RNAPII in E-P interactions. Another study already showed that Mediator depletion has a less strong effect on E-P contacts (Ramasamy *et al.*, 2022) that RNAPII depletion. In contrast, P-P interactions were maintained after RNAPII degradation. This suggests that hitherto unknown factors can mediate P-P contacts. (Factories?) Many more questions remain unanswered. Why did P-P interaction respond differently in the absence of RNAPII? The mechanism of how E-P contacts are established remains poorly understood.

How does the absence of RNAPII contribute to expanding Polycomb regions?

My experiments revealed increased H3K27me3 levels in RNAPII depleted cells. Accordingly, increased interactions between Polycomb-bound regions emerged upon RNAPII depletion. A prior study showed the disruption of polycomb interactions by cohesin (Rhodes *et al.*, 2020). Is the increased H3K27me3 signal influenced by changes in cohesin occupancy upon RNAPII depletion? Or is it directly affected by the absence of RNAPII or transcription?

Further research on these questions will elucidate the exact interplay of RNAPII, the transcription machinery, TFs, enhancers and cohesin. This will develop the full picture of the structure-to-function relationship of of mammalian genomes.

6. Literature

Abramo, K. *et al.* (2019) 'A chromosome folding intermediate at the condensin-to-cohesin transition during telophase', *Nature Cell Biology 2019 21:11*. Nature Publishing Group, 21(11), pp. 1393–1402. doi: 10.1038/s41556-019-0406-2.

Ahmadiyeh, N. *et al.* (2010) '8q24 prostate, breast, and colon cancer risk loci show tissue-specific long-range interaction with MYC', *Proceedings of the National Academy of Sciences of the United States of America*, 107(21), pp. 9742–9746. doi: 10.1073/PNAS.0910668107/-/DCSUPPLEMENTAL.

Aljahani, A. *et al.* (2022) 'Analysis of sub-kilobase chromatin topology reveals nano-scale regulatory interactions with variable dependence on cohesin and CTCF', *Nature Communications*. Springer US, 13(1), pp. 1–13. doi: 10.1038/s41467-022-29696-5.

Amano, T. *et al.* (2009) 'Chromosomal Dynamics at the Shh Locus: Limb Bud-Specific Differential Regulation of Competence and Active Transcription', *Developmental Cell*, 16(1), pp. 47–57. doi: 10.1016/J.DEVCEL.2008.11.011.

Arumugam, P. *et al.* (2003) 'ATP Hydrolysis Is Required for Cohesin's Association with Chromosomes', *Current Biology*. Cell Press, 13(22), pp. 1941–1953. doi: 10.1016/J.CUB.2003.10.036.

Banigan, E. J. *et al.* (2022) 'Transcription shapes 3D chromatin organization by interacting with loop-extruding cohesin complexes', *bioRxiv*, p. 2022.01.07.475367. Available at: https://www.biorxiv.org/content/10.1101/2022.01.07.475367v1%0Ahttps://www.biorxiv.org/content/10.1101/2022.01.07.475367v1.abstract.

Barrington, C. *et al.* (2019) 'Enhancer accessibility and CTCF occupancy underlie asymmetric TAD architecture and cell type specific genome topology', *Nature Communications*. Springer US, 10(1), pp. 1–14. doi: 10.1038/s41467-019-10725-9.

Beagan, J. A. *et al.* (2017) 'YY1 and CTCF orchestrate a 3D chromatin looping switch during early neural lineage commitment', *Genome Research*. Cold Spring Harbor Laboratory Press, 27(7), pp. 1139–1152. doi: 10.1101/GR.215160.116.

Beliveau, B. J. *et al.* (2012) 'Versatile design and synthesis platform for visualizing genomes with Oligopaint FISH probes', *Proceedings of the National Academy of Sciences of the United States of America*. National Academy of Sciences, 109(52), pp. 21301–21306. doi: 10.1073/PNAS.1213818110/SUPPL_FILE/SAPP.PDF.

Bell, A. C. and Felsenfeld, G. (2000) 'Methylation of a CTCF-dependent boundary controls imprinted expression of the Igf2 gene', *Nature 2000 405:6785*. Nature Publishing Group, 405(6785), pp. 482–485. doi: 10.1038/35013100.

Bermudez, V. P. *et al.* (2012) 'In vitro loading of human cohesin on DNA by the human Scc2-Scc4 loader complex', *Proceedings of the National Academy of Sciences of the United States of America*. Proc Natl Acad Sci U S A, 109(24), pp. 9366–9371. doi: 10.1073/PNAS.1206840109/-/DCSUPPLEMENTAL/PNAS.201206840SI.PDF.

Black, K. L. *et al.* (2016) 'Chromatin proteins and RNA are associated with DNA during all phases of mitosis', *Cell Discovery*. Nature Publishing Group, 2. doi: 10.1038/celldisc.2016.38.

Bondeson, D. P. *et al.* (2018) 'Lessons in PROTAC Design from Selective Degradation with a Promiscuous Warhead', *Cell Chemical Biology*. Cell Press, 25(1), pp. 78-87.e5. doi: 10.1016/J.CHEMBIOL.2017.09.010.

Bonev, B. *et al.* (2017) 'Multiscale 3D Genome Rewiring during Mouse Neural Development', *Cell*. Cell Press, 171(3), pp. 557-572.e24. doi: 10.1016/J.CELL.2017.09.043.

Bonev, B. and Cavalli, G. (2016) 'Organization and function of the 3D genome', *Nature Reviews Genetics 2016 17:11*. Nature Publishing Group, 17(11), pp. 661–678. doi: 10.1038/nrg.2016.112.

Van Bortle, K. *et al.* (2014) 'Insulator function and topological domain border strength scale with architectural protein occupancy', *Genome biology*. BioMed Central, 15(6), p. R82. doi: 10.1186/GB-2014-15-5-R82/FIGURES/6.

Boyle, S. *et al.* (2011) 'Fluorescence in situ hybridization with high-complexity repeat-free oligonucleotide probes generated by massively parallel synthesis', *Chromosome Research*. Springer, 19(7), pp. 901–909. doi: 10.1007/S10577-011-9245-0/FIGURES/3.

Brackley, C. A. *et al.* (2018) 'Extrusion without a motor: A new take on the loop extrusion model of genome organization', *Nucleus*. Taylor & Francis, 9(1), pp. 95–103. doi: 10.1080/19491034.2017.1421825.

Bradbury, E. M., Inglis, R. J. and Matthews, H. R. (1974) 'Control of Cell Division by Very Lysine Rich Histone (F1) Phosphorylation', *Nature 1974 247:5439*. Nature Publishing Group, 247(5439), pp. 257–261. doi: 10.1038/247257a0.

Brandão, H. B. *et al.* (2021) 'DNA-loop-extruding SMC complexes can traverse one another in vivo', *Nature Structural and Molecular Biology*. Springer US, 28(8), pp. 642–651. doi: 10.1038/s41594-021-00626-1.

Buckley, M. S. *et al.* (2014) 'Kinetics of promoter Pol II on Hsp70 reveal stable pausing and key insights into its regulation', *Genes & Development*. Cold Spring Harbor Laboratory Press, 28(1), pp. 14–19. doi: 10.1101/GAD.231886.113.

Buratowski, S. (2009) 'Progression through the RNA Polymerase II CTD Cycle', *Molecular Cell*. Cell Press, 36(4), pp. 541–546. doi: 10.1016/J.MOLCEL.2009.10.019.

Busslinger, G. A. *et al.* (2017) 'Cohesin is positioned in mammalian genomes by transcription, CTCF and Wapl', *Nature*. Nature Publishing Group, 544(7651), pp. 503–507. doi: 10.1038/NATURE22063.

Calderon, L. *et al.* (2022) 'Cohesin-dependence of neuronal gene expression relates to chromatin loop length', *eLife*. eLife Sciences Publications Ltd, 11. doi: 10.7554/eLife.76539.

Caravaca, J. M. *et al.* (2013) 'Bookmarking by specific and nonspecific binding of FoxA1 pioneer factor to mitotic chromosomes', *Genes and Development*, 27(3), pp. 251–260. doi: 10.1101/gad.206458.112.

de Castro, I. J., Gokhan, E. and Vagnarelli, P. (2016) 'Resetting a functional G1 nucleus after mitosis', *Chromosoma*. Chromosoma, 125(4), pp. 607–619. doi: 10.1007/s00412-015-0561-6.

Chen, X. *et al.* (2021) 'Structural insights into preinitiation complex assembly on core promoters', *Science*. American Association for the Advancement of Science, 372(6541). doi: 10.1126/SCIENCE.ABA8490/SUPPL_FILE/ABA8490S31.MP4.

Cho, W. K. *et al.* (2016) 'RNA Polymerase II cluster dynamics predict mRNA output in living cells', *eLife*. eLife Sciences Publications Ltd, 5(MAY2016). doi: 10.7554/ELIFE.13617.

Cho, W. K. *et al.* (2018) 'Mediator and RNA polymerase II clusters associate in transcription-dependent condensates', *Science*, 361(6400), pp. 412–415. doi: 10.1126/science.aar4199.

Ciosk, R. *et al.* (2000) 'Cohesin's binding to chromosomes depends on a separate complex consisting of Scc2 and Scc4 proteins', *Molecular cell*. Mol Cell, 5(2), pp. 243–254. doi: 10.1016/S1097-2765(00)80420-7.

Clark, D. J. and Kimura, T. (1990) 'Electrostatic mechanism of chromatin folding', *Journal of molecular biology*. J

Mol Biol, 211(4), pp. 883–896. doi: 10.1016/0022-2836(90)90081-V.

Cong, L. *et al.* (2013) 'Multiplex genome engineering using CRISPR/Cas systems', *Science*. American Association for the Advancement of Science, 339(6121), pp. 819–823. doi: 10.1126/SCIENCE.1231143/SUPPL_FILE/PAPV2.PDF.

Cremer, T. and Cremer, C. (2001) 'Chromosome territories, nuclear architecture and gene regulation in mammalian cells', *Nature Reviews Genetics 2001 2:4*. Nature Publishing Group, 2(4), pp. 292–301. doi: 10.1038/35066075.

Croft, J. A. *et al.* (1999) 'Differences in the localization and morphology of chromosomes in the human nucleus', *Journal of Cell Biology*, 145(6), pp. 1119–1131. doi: 10.1083/jcb.145.6.1119.

Dahmus, M. E. (1995) 'Phosphorylation of the C-terminal domain of RNA polymerase II', *Biochimica et biophysica acta*. Biochim Biophys Acta, 1261(2), pp. 171–182. doi: 10.1016/0167-4781(94)00233-S.

Davidson, I. F. *et al.* (2016) 'Rapid movement and transcriptional re-localization of human cohesin on DNA', *The EMBO Journal*. John Wiley & Sons, Ltd, 35(24), pp. 2671–2685. doi: 10.15252/EMBJ.201695402.

Davidson, I. F. *et al.* (2019) 'DNA loop extrusion by human cohesin', *Science*. American Association for the Advancement of Science, 366(6471), pp. 1338–1345. doi: 10.1126/science.aaz3418.

Decker, C. J. *et al.* (2022) 'RNA is required for the integrity of multiple nuclear and cytoplasmic membrane-less RNP granules', *The EMBO Journal*. John Wiley & Sons, Ltd, 41(9), p. e110137. doi: 10.15252/EMBJ.2021110137.

Dekker, J. *et al.* (2002) 'Capturing chromosome conformation', *Science*, 295(5558), pp. 1306–1311. doi: 10.1126/SCIENCE.1067799.

Dequeker, B. J. H. *et al.* (2022) 'MCM complexes are barriers that restrict cohesin-mediated loop extrusion', *Nature*. Springer US, 606(7912), pp. 197–203. doi: 10.1038/s41586-022-04730-0.

Diebold-Durand, M. L. *et al.* (2017) 'Structure of Full-Length SMC and Rearrangements Required for Chromosome Organization', *Molecular Cell*. Cell Press, 67(2), pp. 334-347.e5. doi: 10.1016/J.MOLCEL.2017.06.010.

Dixon, J. R. *et al.* (2012) 'Topological domains in mammalian genomes identified by analysis of chromatin interactions', *Nature*. Nature Publishing Group, 485(7398), pp. 376–380. doi: 10.1038/nature11082.

Dowen, J. M. *et al.* (2014) 'Control of cell identity genes occurs in insulated neighborhoods in mammalian chromosomes', *Cell*. Elsevier Inc., 159(2), pp. 374–387. doi: 10.1016/j.cell.2014.09.030.

Egli, D. *et al.* (2007) 'Developmental reprogramming after chromosome transfer into mitotic mouse zygotes', *Nature*. Nature Publishing Group, 447(7145), pp. 679–685. doi: 10.1038/NATURE05879.

El-Sharnouby, S. *et al.* (2017) 'Regions of very low H3K27me3 partition the Drosophila genome into topological domains', *PLOS ONE*. Public Library of Science, 12(3), p. e0172725. doi: 10.1371/JOURNAL.PONE.0172725.

Elbashir, S. M. *et al.* (2001) 'Duplexes of 21-nucleotide RNAs mediate RNA interference in cultured mammalian cells', *Nature*. Nature, 411(6836), pp. 494–498. doi: 10.1038/35078107.

Esnault, C. *et al.* (2008) 'Mediator-Dependent Recruitment of TFIIH Modules in Preinitiation Complex', *Molecular Cell*. Cell Press, 31(3), pp. 337–346. doi: 10.1016/J.MOLCEL.2008.06.021.

Feaver, W. J. *et al.* (1994) 'Relationship of CDK-activating kinase and RNA polymerase II CTD kinase TFIIH/TFIIK', *Cell*, 79(6), pp. 1103–1109. doi: 10.1016/0092-8674(94)90040-X.

Festuccia, N. *et al.* (2016) 'Mitotic binding of Esrrb marks key regulatory regions of the pluripotency network', *Nature Cell Biology*, 18(11), pp. 1139–1148. doi: 10.1038/ncb3418.

Festuccia, N. *et al.* (2017) 'Mitotic bookmarking in development and stem cells', *Development (Cambridge)*, 144(20), pp. 3633–3645. doi: 10.1242/dev.146522.

Fianu, I. *et al.* (2021) 'Cryo-EM structure of mammalian RNA polymerase II in complex with human RPAP2', *Communications Biology 2021 4:1*. Nature Publishing Group, 4(1), pp. 1–7. doi: 10.1038/s42003-021-02088-z.

Flavahan, W. A. *et al.* (2015) 'Insulator dysfunction and oncogene activation in IDH mutant gliomas', *Nature 2015 529:7584*. Nature Publishing Group, 529(7584), pp. 110–114. doi: 10.1038/nature16490.

Fuda, N. J., Ardehali, M. B. and Lis, J. T. (2009) 'Defining mechanisms that regulate RNA polymerase II transcription in vivo', *Nature 2009 461:7261*. Nature Publishing Group, 461(7261), pp. 186–192. doi: 10.1038/nature08449.

Fudenberg, G. *et al.* (2016) 'Formation of Chromosomal Domains by Loop Extrusion', *Cell Reports*. Elsevier B.V., 15(9), pp. 2038–2049. doi: 10.1016/J.CELREP.2016.04.085.

Furlong, E. E. M. and Levine, M. (2018) 'Developmental enhancers and chromosome topology', *Science*. American Association for the Advancement of Science, 361(6409), pp. 1341–1345. doi: 10.1126/SCIENCE.AAU0320/ASSET/412087A1-DE48-433F-BC76-9CA9B70B9A1B/ASSETS/GRAPHIC/361_1341_F4.JPEG.

Gandhi, R., Gillespie, P. J. and Hirano, T. (2006) 'Human Wapl Is a Cohesin-Binding Protein that Promotes Sister-Chromatid Resolution in Mitotic Prophase', *Current Biology*. Cell Press, 16(24), pp. 2406–2417. doi: 10.1016/J.CUB.2006.10.061.

Gasperini, M. *et al.* (2019) 'A Genome-wide Framework for Mapping Gene Regulation via Cellular Genetic Screens', *Cell*. Cell Press, 176(1–2), pp. 377-390.e19. doi: 10.1016/J.CELL.2018.11.029.

Gassler, J. *et al.* (2017) 'A mechanism of cohesin-dependent loop extrusion organizes zygotic genome architecture', *The EMBO Journal*. EMBO, 36(24), pp. 3600–3618. doi: 10.15252/embj.201798083.

Gebara, M. M., Sayre, M. H. and Corden, J. L. (1997) 'Phosphorylation of the carboxy-terminal repeat domain in RNA polymerase II by cyclin-dependent kinases is sufficient to inhibit transcription', *Journal of cellular biochemistry*. J Cell Biochem, 64(3), pp. 390–402. doi: 10.1002/(SICI)1097-4644(19970301)64:3<390::AID-JCB6>3.0.CO;2-Q.

Gerguri, T. *et al.* (2021) 'Comparison of loop extrusion and diffusion capture as mitotic chromosome formation pathways in fission yeast', *Nucleic Acids Research*. Oxford Academic, 49(3), pp. 1294–1312. doi: 10.1093/NAR/GKAA1270.

Gerlich, D. *et al.* (2006) 'Live-cell imaging reveals a stable cohesin-chromatin interaction after but not before DNA replication', *Current biology : CB*. Curr Biol, 16(15), pp. 1571–1578. doi: 10.1016/J.CUB.2006.06.068.

Gibcus, J. H. *et al.* (2018) 'A pathway for mitotic chromosome formation', *Science*. American Association for the Advancement of Science, 359(6376). doi: 10.1126/SCIENCE.AAO6135/SUPPL_FILE/AAO6135S1.MP4.

Gligoris, T. G. *et al.* (2014) 'Closing the cohesin ring: Structure and function of its Smc3-kleisin interface', *Science*. American Association for the Advancement of Science, 346(6212), pp. 963–967. doi: 10.1126/SCIENCE.1256917/SUPPL_FILE/GLIGORIS-SM.PDF.

Glynn, E. F. *et al.* (2004) 'Genome-Wide Mapping of the Cohesin Complex in the Yeast Saccharomyces cerevisiae', *PLOS Biology*. Public Library of Science, 2(9), p. e259. doi: 10.1371/JOURNAL.PBIO.0020259.

Golfier, S. *et al.* (2020) 'Cohesin and condensin extrude DNA loops in a cell-cycle dependent manner', *eLife*. eLife Sciences Publications Ltd, 9, pp. 1–34. doi: 10.7554/ELIFE.53885.

Gomes, N. P. and Espinosa, J. M. (2010) 'Gene-specific repression of the p53 target gene PUMA via intragenic CTCF–Cohesin binding', *Genes & Development*. Cold Spring Harbor Laboratory Press, 24(10), pp. 1022–1034. doi: 10.1101/GAD.1881010.

Gottesfeld, J. M. and Forbes, D. J. (1997) 'Mitotic repression of the transcriptional machinery', *Trends in biochemical sciences*. Trends Biochem Sci, 22(6), pp. 197–202. doi: 10.1016/S0968-0004(97)01045-1.

Guacci, V., Koshland, D. and Strunnikov, A. (1997) 'A direct link between sister chromatid cohesion and chromosome condensation revealed through the analysis of MCD1 in S. cerevisiae', *Cell*. Cell, 91(1), pp. 47–57. doi: 10.1016/S0092-8674(01)80008-8.

Guo, Y. *et al.* (2015) 'CRISPR Inversion of CTCF Sites Alters Genome Topology and Enhancer/Promoter Function', *Cell*. Cell Press, 162(4), pp. 900–910. doi: 10.1016/J.CELL.2015.07.038.

Haarhuis, J. H. I. *et al.* (2017) 'The Cohesin Release Factor WAPL Restricts Chromatin Loop Extension', *Cell*, 169(4), pp. 693-707.e14. doi: 10.1016/j.cell.2017.04.013.

Haering, C. H. *et al.* (2004) 'Structure and stability of cohesin's Smc1-kleisin interaction', *Molecular cell*. Mol Cell, 15(6), pp. 951–964. doi: 10.1016/J.MOLCEL.2004.08.030.

Halley-Stott, R. P. *et al.* (2014) 'Mitosis Gives a Brief Window of Opportunity for a Change in Gene Transcription', *PLoS Biology*, 12(7), pp. 1–13. doi: 10.1371/journal.pbio.1001914.

Hansen, A. S. *et al.* (2017) 'CTCF and cohesin regulate chromatin loop stability with distinct dynamics', *eLife*. eLife Sciences Publications Ltd, 6. doi: 10.7554/ELIFE.25776.001.

Heinz, S. *et al.* (2018) 'Transcription Elongation Can Affect Genome 3D Structure', *Cell*. Cell, 174(6), pp. 1522-1536.e22. doi: 10.1016/J.CELL.2018.07.047.

Hildebrand, E. M. and Dekker, J. (2020) 'Mechanisms and Functions of Chromosome Compartmentalization', *Trends in Biochemical Sciences*. Elsevier Current Trends, 45(5), pp. 385–396. doi: 10.1016/J.TIBS.2020.01.002.

Hirano, T. (2002) 'The ABCs of SMC proteins: two-armed ATPases for chromosome condensation, cohesion, and repair', *Genes & Development*. Cold Spring Harbor Laboratory Press, 16(4), pp. 399–414. doi: 10.1101/GAD.955102.

Hirano, T. (2006) 'At the heart of the chromosome: SMC proteins in action', *Nature Reviews Molecular Cell Biology 2006 7:5*. Nature Publishing Group, 7(5), pp. 311–322. doi: 10.1038/nrm1909.

Hirano, T. (2015) 'Chromosome dynamics during mitosis', *Cold Spring Harbor Perspectives in Biology*, 7(6), pp. 1–15. doi: 10.1101/cshperspect.a015792.

Hnisz, D. *et al.* (2016) 'Activation of proto-oncogenes by disruption of chromosome neighborhoods', *Science*. American Association for the Advancement of Science, 351(6280), pp. 1454–1458. doi: 10.1126/SCIENCE.AAD9024/SUPPL_FILE/HNISZ.SM.PDF.

Hopfner, K. P. *et al.* (2000) 'Structural biology of Rad50 ATPase: ATP-driven conformational control in DNA double-strand break repair and the ABC-ATPase superfamily', *Cell*. Elsevier B.V., 101(7), pp. 789–800. doi: 10.1016/S0092-8674(00)80890-9.

Hou, C. *et al.* (2012) 'Gene Density, Transcription, and Insulators Contribute to the Partition of the Drosophila Genome into Physical Domains', *Molecular Cell*, 48(3), pp. 471–484. doi: 10.1016/J.MOLCEL.2012.08.031.

Hsieh, T. H. S. *et al.* (2015) 'Mapping Nucleosome Resolution Chromosome Folding in Yeast by Micro-C', *Cell*. Elsevier Inc., 162(1), pp. 108–119. doi: 10.1016/j.cell.2015.05.048.

Hsieh, T. H. S. *et al.* (2016) 'Micro-C XL: assaying chromosome conformation from the nucleosome to the entire genome', *Nature Methods 2016 13:12*. Nature Publishing Group, 13(12), pp. 1009–1011. doi: 10.1038/nmeth.4025.

Hsieh, T. H. S. *et al.* (2020) 'Resolving the 3D Landscape of Transcription-Linked Mammalian Chromatin Folding', *Molecular Cell*. Cell Press, 78(3), pp. 539-553.e8. doi: 10.1016/J.MOLCEL.2020.03.002/ATTACHMENT/B7BC90D2-D699-4286-BF95-A8B6E1B645C3/MMC10.XLSX.

Hsiung, C. C. S. *et al.* (2016) 'A hyperactive transcriptional state marks genome reactivation at the mitosis-G1 transition', *Genes and Development*, 30(12), pp. 1423–1439. doi: 10.1101/gad.280859.116.

Hua, P. *et al.* (2021) 'Defining genome architecture at base-pair resolution', *Nature 2021 595:7865*. Nature Publishing Group, 595(7865), pp. 125–129. doi: 10.1038/s41586-021-03639-4.

Huang, C. E., Milutinovich, M. and Koshland, D. (2005) 'Rings, bracelet or snaps: fashionable alternatives for Smc complexes', *Philosophical Transactions of the Royal Society B: Biological Sciences*. The Royal SocietyLondon, 360(1455), pp. 537–542. doi: 10.1098/RSTB.2004.1609.

Hug, C. B. *et al.* (2017) 'Chromatin Architecture Emerges during Zygotic Genome Activation Independent of Transcription', *Cell*. Cell Press, 169(2), pp. 216-228.e19. doi: 10.1016/J.CELL.2017.03.024.

Huis In't Veld, P. J. *et al.* (2014) 'Characterization of a DNA exit gate in the human cohesin ring', *Science (New York, N.Y.)*. Science, 346(6212), pp. 968–972. doi: 10.1126/SCIENCE.1256904.

Jaeger, M. G. *et al.* (2020) 'Selective Mediator dependence of cell-type-specifying transcription', *Nature Genetics*. Springer US, 52(7), pp. 719–727. doi: 10.1038/s41588-020-0635-0.

Javasky, E. *et al.* (2018) 'Study of mitotic chromatin supports a model of bookmarking by histone modifications and reveals nucleosome deposition patterns', *Genome Research*, 28(10), pp. 1455–1466. doi: 10.1101/gr.230300.117.

Jeronimo, C. and Robert, F. (2014) 'Kin28 regulates the transient association of Mediator with core promoters', *Nature Structural & Molecular Biology 2014 21:5*. Nature Publishing Group, 21(5), pp. 449–455. doi: 10.1038/nsmb.2810.

Jiang, Y. *et al.* (2020) 'Genome-wide analyses of chromatin interactions after the loss of Pol I, Pol II, and Pol III', *Genome Biology*. Genome Biol, 21(1), p. 158. doi: 10.1186/s13059-020-02067-3.

Kaaij, L. J. T. *et al.* (2018) 'Systemic Loss and Gain of Chromatin Architecture throughout Zebrafish Development', *Cell Reports*. Cell Press, 24(1), pp. 1-10.e4. doi: 10.1016/J.CELREP.2018.06.003.

Kadauke, S. *et al.* (2012) 'Tissue-Specific Mitotic Bookmarking by Hematopoietic Transcription Factor GATA1', *Cell*, 150(4), pp. 725–737. doi: 10.1016/j.cell.2012.06.038.

Kadauke, S. and Blobel, G. A. (2013) 'Mitotic bookmarking by transcription factors', *Epigenetics and Chromatin*, 6(1), pp. 6–10. doi: 10.1186/1756-8935-6-6.

Kagey, M. H. *et al.* (2010) 'Mediator and cohesin connect gene expression and chromatin architecture', *Nature*. Nature Publishing Group, 467(7314), pp. 430–435. doi: 10.1038/nature09380.

Kang, H. *et al.* (2020) 'Dynamic regulation of histone modifications and long-range chromosomal interactions during postmitotic transcriptional reactivation', *Genes and Development*. Cold Spring Harbor Laboratory Press, 34(13–14), pp. 1–18. doi: 10.1101/GAD.335794.119.

Kanke, M. *et al.* (2016) 'Cohesin acetylation and Wapl-Pds5 oppositely regulate translocation of cohesin along

DNA', *The EMBO Journal*. John Wiley & Sons, Ltd, 35(24), pp. 2686–2698. doi: 10.15252/EMBJ.201695756.

Kean, C. M. *et al.* (2022) 'Decreasing Wapl dosage partially corrects embryonic growth and brain transcriptome phenotypes in Nipbl+/− embryos', *Science Advances*. American Association for the Advancement of Science, 8(48). doi: 10.1126/SCIADV.ADD4136.

El Khattabi, L. *et al.* (2019) 'A Pliable Mediator Acts as a Functional Rather Than an Architectural Bridge between Promoters and Enhancers', *Cell*. Cell, 178(5), pp. 1145-1158.e20. doi: 10.1016/J.CELL.2019.07.011.

Khoury, A. *et al.* (2020) 'Constitutively bound CTCF sites maintain 3D chromatin architecture and long-range epigenetically regulated domains', *Nature Communications*. Springer US, 11(1). doi: 10.1038/s41467-019-13753-7.

Kikuchi, S. *et al.* (2016) 'Crystal structure of the cohesin loader Scc2 and insight into cohesinopathy', *Proceedings of the National Academy of Sciences of the United States of America*. Proc Natl Acad Sci U S A, 113(44), pp. 12444–12449. doi: 10.1073/PNAS.1611333113.

Kim, T. H. *et al.* (2007) 'Analysis of the Vertebrate Insulator Protein CTCF-Binding Sites in the Human Genome', *Cell*. Elsevier B.V., 128(6), pp. 1231–1245. doi: 10.1016/j.cell.2006.12.048.

Kim, Y. *et al.* (2019) 'Human cohesin compacts DNA by loop extrusion', *Science*. American Association for the Advancement of Science, 366(6471), pp. 1345–1349. doi: 10.1126/SCIENCE.AAZ4475/SUPPL_FILE/PAPV2.PDF.

Kim, Y. J. *et al.* (1994) 'A multiprotein mediator of transcriptional activation and its interaction with the C-terminal repeat domain of RNA polymerase II', *Cell*, 77(4), pp. 599–608. doi: 10.1016/0092-8674(94)90221-6.

Koch, F. *et al.* (2008) 'Genome-wide RNA polymerase II: not genes only!', *Trends in Biochemical Sciences*. Elsevier Current Trends, 33(6), pp. 265–273. doi: 10.1016/J.TIBS.2008.04.006.

Krietenstein, N. *et al.* (2020) 'Ultrastructural Details of Mammalian Chromosome Architecture', *Molecular Cell*. Cell Press, 78(3), pp. 554-565.e7. doi: 10.1016/J.MOLCEL.2020.03.003.

Kruhlak, M. J. *et al.* (2001) 'Regulation of Global Acetylation in Mitosis through Loss of Histone Acetyltransferases and Deacetylases from Chromatin', *Journal of Biological Chemistry*. Elsevier, 276(41), pp. 38307–38319. doi: 10.1074/JBC.M100290200.

Kubo, N. *et al.* (2021) 'Promoter-proximal CTCF binding promotes distal enhancer-dependent gene activation', *Nature Structural and Molecular Biology*. Springer US, 28(2), pp. 152–161. doi: 10.1038/s41594-020-00539-5.

Kueng, S. *et al.* (2006) 'Wapl controls the dynamic association of cohesin with chromatin', *Cell*. Cell, 127(5), pp. 955–967. doi: 10.1016/J.CELL.2006.09.040.

Lengronne, A. *et al.* (2004) 'Cohesin relocation from sites of chromosomal loading to places of convergent transcription.', *Nature*, 430(6999), pp. 573–8. doi: 10.1038/nature02742.

Leresche, A., Wolf, V. J. and Gottesfeld, J. M. (1996) 'Repression of RNA Polymerase II and III Transcription during M Phase of the Cell Cycle', *Experimental Cell Research*. Academic Press, 229(2), pp. 282–288. doi: 10.1006/EXCR.1996.0373.

Li, L. *et al.* (2015) 'Widespread rearrangement of 3D chromatin organization underlies polycomb-mediated stress-induced silencing', *Molecular cell*. Mol Cell, 58(2), pp. 216–231. doi: 10.1016/J.MOLCEL.2015.02.023.

Li, Y. *et al.* (2020) 'The structural basis for cohesin–CTCF-anchored loops', *Nature*. Springer US, 578(7795), pp. 472–476. doi: 10.1038/s41586-019-1910-z.

Liang, K. *et al.* (2015) 'Mitotic Transcriptional Activation: Clearance of Actively Engaged Pol II via Transcriptional

Elongation Control in Mitosis', *Molecular Cell*. Cell Press, 60(3), pp. 435–445. doi: 10.1016/J.MOLCEL.2015.09.021.

Lieberman-Aiden, E. *et al.* (2009) 'Comprehensive Mapping of Long-Range Interactions Reveals Folding Principles of the Human Genome', *Science*, 326(5950), pp. 289–293. doi: 10.1126/science.1181369.

Liu, N. Q. *et al.* (2021) 'WAPL maintains a cohesin loading cycle to preserve cell-type-specific distal gene regulation', *Nature Genetics*. Nature Research, 53(1), pp. 100–109. doi: 10.1038/S41588-020-00744-4.

Liu, Yin *et al.* (2017) 'Transcriptional landscape of the human cell cycle', *Proceedings of the National Academy of Sciences of the United States of America*, 114(13), pp. 3473–3478. doi: 10.1073/pnas.1617636114.

Liu, Yiyuan *et al.* (2017) 'Widespread Mitotic Bookmarking by Histone Marks and Transcription Factors in Pluripotent Stem Cells', *Cell Reports*. Elsevier B.V., 19(7), pp. 1283–1293. doi: 10.1016/J.CELREP.2017.04.067.

Liu, Z. *et al.* (2022) 'An overview of PROTACs: a promising drug discovery paradigm', *Molecular Biomedicine 2022 3:1*. Springer, 3(1), pp. 1–26. doi: 10.1186/S43556-022-00112-0.

Lopez-Serra, L. *et al.* (2014) 'The Scc2-Scc4 complex acts in sister chromatid cohesion and transcriptional regulation by maintaining nucleosome-free regions', *Nature Genetics*. Nature Publishing Group, 46(10), pp. 1147–1151. doi: 10.1038/ng.3080.

Löwe, J., Cordell, S. C. and Van Den Ent, F. (2001) 'Crystal structure of the SMC head domain: An ABC ATPase with 900 residues antiparallel coiled-coil inserted', *Journal of Molecular Biology*. Academic Press, 306(1), pp. 25–35. doi: 10.1006/jmbi.2000.4379.

Lu, H. *et al.* (1991) 'The nonphosphorylated form of RNA polymerase II preferentially associates with the preinitiation complex', *Proceedings of the National Academy of Sciences of the United States of America*. Proc Natl Acad Sci U S A, 88(22), pp. 10004–10008. doi: 10.1073/PNAS.88.22.10004.

Lu, J. *et al.* (2015) 'Hijacking the E3 Ubiquitin Ligase Cereblon to Efficiently Target BRD4', *Chemistry & Biology*. Cell Press, 22(6), pp. 755–763. doi: 10.1016/J.CHEMBIOL.2015.05.009.

Lubischer, J. L. (2007) 'The Cell Cycle, Principles of Control. David O. Morgan.', *Integrative and Comparative Biology*. Oxford Academic, 47(5), pp. 794–795. doi: 10.1093/icb/icm066.

Luger, K. *et al.* (1997) 'Crystal structure of the nucleosome core particle at 2.8 Å resolution', *Nature 1997 389:6648*. Nature Publishing Group, 389(6648), pp. 251–260. doi: 10.1038/38444.

Lupiáñez, D. G. *et al.* (2015) 'Disruptions of topological chromatin domains cause pathogenic rewiring of gene-enhancer interactions', *Cell*, 161(5), pp. 1012–1025. doi: 10.1016/j.cell.2015.04.004.

Luppinoid, J. M. *et al.* (2022) 'Co-depletion of NIPBL and WAPL balance cohesin activity to correct gene misexpression'. doi: 10.1371/journal.pgen.1010528.

Mali, P. *et al.* (2013) 'RNA-guided human genome engineering via Cas9', *Science*. American Association for the Advancement of Science, 339(6121), pp. 823–826. doi: 10.1126/SCIENCE.1232033/SUPPL_FILE/MALI.SM.PDF.

Marko, J. F. *et al.* (2019) 'DNA-segment-capture model for loop extrusion by structural maintenance of chromosome (SMC) protein complexes', *Nucleic Acids Research*. Oxford Academic, 47(13), pp. 6956–6972. doi: 10.1093/NAR/GKZ497.

Martínez-Balbás, M. A. *et al.* (1995) 'Displacement of sequence-specific transcription factors from mitotic chromatin.', *Cell*, 83(1), pp. 29–38. doi: 10.1016/0092-8674(95)90231-7.

Matityahu, A. and Onn, I. (2022) 'It's all in the numbers: Cohesin stoichiometry', *Frontiers in Molecular*

Biosciences. Frontiers Media S.A., 9, p. 1170. doi: 10.3389/FMOLB.2022.1010894/BIBTEX.

Mattingly, M. *et al.* (2022) 'Mediator recruits the cohesin loader Scc2 to RNA Pol II-transcribed genes and promotes sister chromatid cohesion', *Current Biology*, pp. 1–13. doi: 10.1016/j.cub.2022.05.019.

Meister, P. *et al.* (2010) 'The spatial dynamics of tissue-specific promoters during C. elegans development', *Genes & development*. Genes Dev, 24(8), pp. 766–782. doi: 10.1101/GAD.559610.

Merkenschlager, M. and Nora, E. P. (2016) 'CTCF and Cohesin in Genome Folding and Transcriptional Gene Regulation', *Annual Review of Genomics and Human Genetics*, 17, pp. 17–43. doi: 10.1146/annurev-genom-083115-022339.

Michaelis, C., Ciosk, R. and Nasmyth, K. (1997) 'Cohesins: Chromosomal Proteins that Prevent Premature Separation of Sister Chromatids', *Cell*. Cell Press, 91(1), pp. 35–45. doi: 10.1016/S0092-8674(01)80007-6.

Michelotti, E. F., Sanford, S. and Levens, D. (1997) 'Marking of active genes on mitotic chromosomes', *Nature*, 388(6645), pp. 895–899. doi: 10.1038/42282.

Millán-Zambrano, G. *et al.* (2022) 'Histone post-translational modifications — cause and consequence of genome function', *Nature Reviews Genetics 2022 23:9*. Nature Publishing Group, 23(9), pp. 563–580. doi: 10.1038/s41576-022-00468-7.

Moore, J. M. *et al.* (2012) 'Loss of Maternal CTCF Is Associated with Peri-Implantation Lethality of Ctcf Null Embryos', *PLOS ONE*. Public Library of Science, 7(4), p. e34915. doi: 10.1371/JOURNAL.PONE.0034915.

Müller, W. G. *et al.* (2001) 'Large-scale chromatin decondensation and recondensation regulated by transcription from a natural promoter', *Journal of Cell Biology*. The Rockefeller University Press, 154(1), pp. 33–48. doi: 10.1083/JCB.200011069.

Murayama, Y. and Uhlmann, F. (2014) 'Biochemical reconstitution of topological DNA binding by the cohesin ring', *Nature*, 505(7483), pp. 367–371. doi: 10.1038/nature12867.

Muto, A. *et al.* (2014) 'Nipbl and Mediator Cooperatively Regulate Gene Expression to Control Limb Development', *PLoS Genetics*, 10(9). doi: 10.1371/journal.pgen.1004671.

Nagano, T. *et al.* (2017) 'Cell-cycle dynamics of chromosomal organization at single-cell resolution', *Nature*. Nature Publishing Group, 547(7661), pp. 61–67. doi: 10.1038/nature23001.

Nagashima, R. *et al.* (2019) 'Single nucleosome imaging reveals loose genome chromatin networks via active RNA polymerase II', *The Journal of cell biology*. J Cell Biol, 218(5), pp. 1511–1530. doi: 10.1083/JCB.201811090.

Narendra, V. *et al.* (2015) 'CTCF establishes discrete functional chromatin domains at the Hox clusters during differentiation', *Science (New York, N.Y.)*. Science, 347(6225), pp. 1017–1021. doi: 10.1126/SCIENCE.1262088.

Natsume, T. *et al.* (2016) 'Rapid Protein Depletion in Human Cells by Auxin-Inducible Degron Tagging with Short Homology Donors', *Cell Reports*. Elsevier B.V., 15(1), pp. 210–218. doi: 10.1016/j.celrep.2016.03.001.

Natsume, T. and Kanemaki, M. T. (2017) 'Conditional Degrons for Controlling Protein Expression at the Protein Level', *Annual Review of Genetics*. Annual Reviews Inc., 51, pp. 83–102. doi: 10.1146/ANNUREV-GENET-120116-024656.

Naughton, C. *et al.* (2013) 'Transcription forms and remodels supercoiling domains unfolding large-scale chromatin structures', *Nature Structural & Molecular Biology 2013 20:3*. Nature Publishing Group, 20(3), pp. 387–395. doi: 10.1038/nsmb.2509.

Naumova, N. *et al.* (2013) 'Organization of the mitotic chromosome', *Science*, 342(6161), pp. 948–953. doi:

10.1126/science.1236083.

Nichols, M. H. and Corces, V. G. (2018) 'A tethered-inchworm model of SMC DNA translocation', *Nature Structural & Molecular Biology 2018 25:10*. Nature Publishing Group, 25(10), pp. 906–910. doi: 10.1038/s41594-018-0135-4.

Nishimura, K. *et al.* (2009) 'An auxin-based degron system for the rapid depletion of proteins in nonplant cells', *Nature Methods*. Nature Publishing Group, 6(12), pp. 917–922. doi: 10.1038/nmeth.1401.

Nora, E. P. *et al.* (2012) 'Spatial partitioning of the regulatory landscape of the X-inactivation centre', *Nature 2012 485:7398*. Nature Publishing Group, 485(7398), pp. 381–385. doi: 10.1038/nature11049.

Nora, E. P. *et al.* (2017) 'Targeted Degradation of CTCF Decouples Local Insulation of Chromosome Domains from Genomic Compartmentalization', *Cell*, 169(5), pp. 930-944.e22. doi: 10.1016/j.cell.2017.05.004.

Nuebler, J. *et al.* (2018) 'Chromatin organization by an interplay of loop extrusion and compartmental segregation', *Proceedings of the National Academy of Sciences of the United States of America*, 115(29), pp. E6697–E6706. doi: 10.1073/pnas.1717730115.

Olan, I. *et al.* (2020) 'Transcription-dependent cohesin repositioning rewires chromatin loops in cellular senescence', *Nature Communications 2020 11:1*. Nature Publishing Group, 11(1), pp. 1–14. doi: 10.1038/s41467-020-19878-4.

Ono, T. *et al.* (2003) 'Differential contributions of condensin I and condensin II to mitotic chromosome architecture in vertebrate cells', *Cell*. Elsevier B.V., 115(1), pp. 109–121. doi: 10.1016/S0092-8674(03)00724-4.

Oomen, M. E. *et al.* (2019) 'CTCF sites display cell cycle-dependent dynamics in factor binding and nucleosome positioning', *Genome Research*. Cold Spring Harbor Laboratory Press, 29(2), pp. 236–249. doi: 10.1101/GR.241547.118/-/DC1.

Oudet, P., Gross-Bellard, M. and Chambon, P. (1975) 'Electron microscopic and biochemical evidence that chromatin structure is a repeating unit', *Cell*. Cell, 4(4), pp. 281–300. doi: 10.1016/0092-8674(75)90149-X.

Palozola, K. C. *et al.* (2017) 'Mitotic transcription and waves of gene reactivation during mitotic exit', *Science*. American Association for the Advancement of Science, 358(6359), pp. 119–122. doi: 10.1126/SCIENCE.AAL4671/SUPPL_FILE/AAL4671_SUPPLEMENTAL_TABLES.ZIP.

Palstra, R.-J. *et al.* (2008) 'Maintenance of Long-Range DNA Interactions after Inhibition of Ongoing RNA Polymerase II Transcription', *PLOS ONE*. Edited by L. Tora. Public Library of Science, 3(2), p. e1661. doi: 10.1371/JOURNAL.PONE.0001661.

Papantonis, A. and Cook, P. R. (2011) 'Fixing the model for transcription', *Transcription*, 2(1), pp. 41–44. doi: 10.4161/trns.2.1.14275.

Papantonis, A. and Cook, P. R. (2013) 'Transcription factories: Genome organization and gene regulation', *Chemical Reviews*. American Chemical Society, 113(11), pp. 8683–8705. doi: 10.1021/CR300513P/ASSET/IMAGES/MEDIUM/CR-2012-00513P_0016.GIF.

Parelho, V. *et al.* (2008) 'Cohesins Functionally Associate with CTCF on Mammalian Chromosome Arms', *Cell*, 132(3), pp. 422–433. doi: 10.1016/j.cell.2008.01.011.

Parsons, G. G. and Spencer, C. A. (1997) 'Mitotic repression of RNA polymerase II transcription is accompanied by release of transcription elongation complexes', *Molecular and Cellular Biology*. American Society for Microbiology, 17(10), pp. 5791–5802. doi: 10.1128/MCB.17.10.5791.

Paulson, J. R. and Laemmli, U. K. (1977) 'The structure of histone-depleted metaphase chromosomes', *Cell*. Elsevier, 12(3), pp. 817–828. doi: 10.1016/0092-8674(77)90280-X.

Pelham-Webb, B. *et al.* (2021) 'H3K27ac bookmarking promotes rapid post-mitotic activation of the pluripotent stem cell program without impacting 3D chromatin reorganization', *Molecular Cell*. Cell Press, 81(8), pp. 1732-1748.e8. doi: 10.1016/J.MOLCEL.2021.02.032.

Petela, N. J. *et al.* (2018) 'Scc2 Is a Potent Activator of Cohesin's ATPase that Promotes Loading by Binding Scc1 without Pds5', *Molecular Cell*. Cell Press, 70(6), pp. 1134-1148.e7. doi: 10.1016/J.MOLCEL.2018.05.022.

Petrenko, N. *et al.* (2016) 'Mediator Undergoes a Compositional Change during Transcriptional Activation', *Molecular Cell*. Elsevier Inc., 64(3), pp. 443–454. doi: 10.1016/j.molcel.2016.09.015.

Pradhan, B. *et al.* (2022) 'SMC Complexes Can Traverse Physical Roadblocks Bigger Than Their Ring Size', *SSRN Electronic Journal*, pp. 1–17. doi: 10.2139/ssrn.4046136.

Prasanth, K. V. *et al.* (2003) 'Sequential entry of components of gene expression machinery into daughter nucleiv', *Molecular Biology of the Cell*. The American Society for Cell Biology , 14(3), pp. 1043–1057. doi: 10.1091/MBC.E02-10-0669/ASSET/IMAGES/LARGE/MK0332152009.JPEG.

Rada-Iglesias, A., Grosveld, F. G. and Papantonis, A. (2018) 'Forces driving the three-dimensional folding of eukaryotic genomes', *Molecular Systems Biology*, 14(6), pp. 1–12. doi: 10.15252/msb.20188214.

Ramasamy, S. *et al.* (2022) 'The Mediator complex regulates enhancer-promoter interactions', *bioRxiv*. Cold Spring Harbor Laboratory, p. 2022.06.15.496245. doi: 10.1101/2022.06.15.496245.

Ramos-Alonso, L. *et al.* (2023) 'Mitotic chromosome condensation resets chromatin to safeguard transcriptional homeostasis during interphase', *Proceedings of the National Academy of Sciences*, 120(4). doi: 10.1073/PNAS.2210593120.

Rao, S. S. P. *et al.* (2014) 'A 3D map of the human genome at kilobase resolution reveals principles of chromatin looping', *Cell*. Elsevier Inc., 159(7), pp. 1665–1680. doi: 10.1016/j.cell.2014.11.021.

Rao, S. S. P. *et al.* (2017) 'Cohesin Loss Eliminates All Loop Domains', *Cell*. Cell Press, 171(2), pp. 305-320.e24. doi: 10.1016/j.cell.2017.09.026.

Rhodes, J. *et al.* (2017) 'Scc2/Nipbl hops between chromosomal cohesin rings after loading', *eLife*. eLife Sciences Publications Ltd, 6. doi: 10.7554/ELIFE.30000.

Rhodes, J. D. P. *et al.* (2020) 'Cohesin Disrupts Polycomb-Dependent Chromosome Interactions in Embryonic Stem Cells', *Cell Reports*, 30(3), pp. 820-835.e10. doi: 10.1016/j.celrep.2019.12.057.

Richart, L. *et al.* (2021) 'STAG2 loss-of-function affects short-range genomic contacts and modulates the basal-luminal transcriptional program of bladder cancer cells', *Nucleic Acids Research*, 49(19), pp. 11005–11021. doi: 10.1093/nar/gkab864.

Rinzema, N. J. *et al.* (2022) 'Building regulatory landscapes reveals that an enhancer can recruit cohesin to create contact domains, engage CTCF sites and activate distant genes', *Nature Structural and Molecular Biology*. Springer US, 29(6), pp. 563–574. doi: 10.1038/s41594-022-00787-7.

Rosencrance, C. D. *et al.* (2020) 'Chromatin Hyperacetylation Impacts Chromosome Folding by Forming a Nuclear Subcompartment', *Molecular cell*. Mol Cell, 78(1), pp. 112-126.e12. doi: 10.1016/J.MOLCEL.2020.03.018.

Roth, S. Y. and Allis, C. D. (1992) 'Chromatin condensation: does histone H1 dephosphorylation play a role?', *Trends in Biochemical Sciences*. Elsevier Current Trends, 17(3), pp. 93–98. doi: 10.1016/0968-0004(92)90243-3.

Rowley, M. J. *et al.* (2017) 'Evolutionarily Conserved Principles Predict 3D Chromatin Organization', *Molecular Cell*. Elsevier Inc., 67(5), pp. 837-852.e7. doi: 10.1016/j.molcel.2017.07.022.

Rowley, M. J. and Corces, V. G. (2018) 'Organizational principles of 3D genome architecture', *Nature Reviews Genetics*. Springer US, 19(12), pp. 789–800. doi: 10.1038/s41576-018-0060-8.

van Ruiten, M. S. *et al.* (2022) 'The cohesin acetylation cycle controls chromatin loop length through a PDS5A brake mechanism', *Nature Structural & Molecular Biology*. Springer US, 29(6), pp. 586–591. doi: 10.1038/s41594-022-00773-z.

Ryu, J. K. *et al.* (2020) 'The condensin holocomplex cycles dynamically between open and collapsed states', *Nature Structural & Molecular Biology 2020 27:12*. Nature Publishing Group, 27(12), pp. 1134–1141. doi: 10.1038/s41594-020-0508-3.

Sakamoto, K. M. *et al.* (2001) 'Protacs: chimeric molecules that target proteins to the Skp1-Cullin-F box complex for ubiquitination and degradation', *Proceedings of the National Academy of Sciences of the United States of America*. Proc Natl Acad Sci U S A, 98(15), pp. 8554–8559. doi: 10.1073/PNAS.141230798.

Saldaña-Meyer, R. *et al.* (2019) 'RNA Interactions Are Essential for CTCF-Mediated Genome Organization', *Molecular Cell*. Cell Press, 76(3), pp. 412-422.e5. doi: 10.1016/j.molcel.2019.08.015.

Sanborn, A. L. *et al.* (2015) 'Chromatin extrusion explains key features of loop and domain formation in wild-type and engineered genomes', *Proceedings of the National Academy of Sciences of the United States of America*. Proc Natl Acad Sci U S A, 112(47), pp. E6456–E6465. doi: 10.1073/PNAS.1518552112.

Sanders, J. T. *et al.* (2022) 'Loops, topologically associating domains, compartments, and territories are elastic and robust to dramatic nuclear volume swelling.', *Scientific Reports*. Nature Research, 12(1), pp. 4721–4721. doi: 10.1038/S41598-022-08602-5.

de Santa, F. *et al.* (2010) 'A large fraction of extragenic RNA Pol II transcription sites overlap enhancers', *PLoS Biology*, 8(5). doi: 10.1371/journal.pbio.1000384.

Schalbetter, S. A. *et al.* (2017) 'SMC complexes differentially compact mitotic chromosomes according to genomic context', *Nature Cell Biology 2017 19:9*. Nature Publishing Group, 19(9), pp. 1071–1080. doi: 10.1038/ncb3594.

Schwarzer, W. *et al.* (2017a) 'Two independent modes of chromatin organization revealed by cohesin removal', *Nature*. Nature Publishing Group, 551(7678), pp. 51–56. doi: 10.1038/nature24281.

Schwarzer, W. *et al.* (2017b) 'Two independent modes of chromatin organization revealed by cohesin removal', *Nature*, 551(7678), pp. 51–56. doi: 10.1038/nature24281.

Sedeño Cacciatore, Á. and Rowland, B. D. (2019) 'Loop formation by SMC complexes: turning heads, bending elbows, and fixed anchors', *Current Opinion in Genetics and Development*, 55(Figure 1), pp. 11–18. doi: 10.1016/j.gde.2019.04.010.

Segil, N. *et al.* (1996) 'Mitotic regulation of TFIID: inhibition of activator-dependent transcription and changes in subcellular localization', *Genes & development*. Genes Dev, 10(19), pp. 2389–2400. doi: 10.1101/GAD.10.19.2389.

Seitan, V. C. *et al.* (2013) 'Cohesin-Based chromatin interactions enable regulated gene expression within preexisting architectural compartments', *Genome Research*, 23(12), pp. 2066–2077. doi: 10.1101/gr.161620.113.

Sexton, T. *et al.* (2012) 'Three-dimensional folding and functional organization principles of the Drosophila genome', *Cell*. Cell, 148(3), pp. 458–472. doi: 10.1016/J.CELL.2012.01.010.

Shi, Z. *et al.* (2020) 'Cryo-EM structure of the human cohesin-NIPBL-DNA complex', *Science*. American Association for the Advancement of Science, 368(6498), pp. 1454–1459. doi: 10.1126/SCIENCE.ABB0981/SUPPL_FILE/ABB0981S3.MOV.

Sofueva, S. *et al.* (2013) 'Cohesin-mediated interactions organize chromosomal domain architecture', *EMBO Journal*. Nature Publishing Group, 32(24), pp. 3119–3129. doi: 10.1038/emboj.2013.237.

Søgaard, T. M. M. and Svejstrup, J. Q. (2007) 'Hyperphosphorylation of the C-terminal Repeat Domain of RNA Polymerase II Facilitates Dissociation of Its Complex with Mediator', *Journal of Biological Chemistry*. Elsevier, 282(19), pp. 14113–14120. doi: 10.1074/JBC.M701345200.

Spicuglia, S. *et al.* (2002) 'Promoter Activation by Enhancer-Dependent and -Independent Loading of Activator and Coactivator Complexes', *Molecular Cell*. Cell Press, 10(6), pp. 1479–1487. doi: 10.1016/S1097-2765(02)00791-8.

Stadhouders, R. *et al.* (2018) 'Transcription factors orchestrate dynamic interplay between genome topology and gene regulation during cell reprogramming', *Nature genetics*. Nat Genet, 50(2), pp. 238–249. doi: 10.1038/S41588-017-0030-7.

Stedman, W. *et al.* (2008) 'Cohesins localize with CTCF at the KSHV latency control region and at cellular c-myc and H19/Igf2 insulators', *The EMBO Journal*. John Wiley & Sons, Ltd, 27(4), pp. 654–666. doi: 10.1038/EMBOJ.2008.1.

Strunnikov, A. V., Larionov, V. L. and Koshland, D. (1993) 'SMC1: an essential yeast gene encoding a putative head-rod-tail protein is required for nuclear division and defines a new ubiquitous protein family.', *Journal of Cell Biology*. The Rockefeller University Press, 123(6), pp. 1635–1648. doi: 10.1083/jcb.123.6.1635.

Sun, F. *et al.* (2021) 'The Pol II preinitiation complex (PIC) influences Mediator binding but not promoter-enhancer looping', *Genes and Development*. Cold Spring Harbor Laboratory Press, 35(15–16), pp. 1175–1189. doi: 10.1101/GAD.348471.121/-/DC1.

Swain, A. *et al.* (2016) 'Drosophila TDP-43 RNA-Binding Protein Facilitates Association of Sister Chromatid Cohesion Proteins with Genes, Enhancers and Polycomb Response Elements', *PLOS Genetics*. Public Library of Science, 12(9), p. e1006331. doi: 10.1371/JOURNAL.PGEN.1006331.

Symmons, O. *et al.* (2016) 'The Shh Topological Domain Facilitates the Action of Remote Enhancers by Reducing the Effects of Genomic Distances', *Developmental Cell*. Cell Press, 39(5), pp. 529–543. doi: 10.1016/J.DEVCEL.2016.10.015.

Talbert, P. B. and Henikoff, S. (2016) 'Histone variants on the move: substrates for chromatin dynamics', *Nature Reviews Molecular Cell Biology 2016 18:2*. Nature Publishing Group, 18(2), pp. 115–126. doi: 10.1038/nrm.2016.148.

Tan, X. *et al.* (2007) 'Mechanism of auxin perception by the TIR1 ubiquitin ligase', *Nature*. Nature Publishing Group, 446(7136), pp. 640–645. doi: 10.1038/NATURE05731.

Tanaka, T. *et al.* (2000) 'Cohesin ensures bipolar attachment of microtubules to sister centromeres and resists their precocious separation', *Nature Cell Biology 2000 2:8*. Nature Publishing Group, 2(8), pp. 492–499. doi: 10.1038/35019529.

Tedeschi, A. *et al.* (2013) 'Wapl is an essential regulator of chromatin structure and chromosome segregation', *Nature 2013 501:7468*. Nature Publishing Group, 501(7468), pp. 564–568. doi: 10.1038/nature12471.

Teves, S. S. *et al.* (2016) 'A dynamic mode of mitotic bookmarking by transcription factors', *eLife*, 5(NOVEMBER2016), pp. 1–24. doi: 10.7554/eLife.22280.

Teves, S. S. *et al.* (2018) 'A stable mode of bookmarking by TBP recruits RNA polymerase II to mitotic chromosomes', *eLife*. eLife Sciences Publications Ltd, 7. doi: 10.7554/ELIFE.35621.

Thiecke, M. J. *et al.* (2020) 'Cohesin-Dependent and -Independent Mechanisms Mediate Chromosomal Contacts between Promoters and Enhancers', *Cell Reports*. Cell Press, 32(3), p. 107929. doi: 10.1016/J.CELREP.2020.107929.

Tolhuis, B. *et al.* (2002) 'Looping and interaction between hypersensitive sites in the active β-globin locus', *Molecular Cell*, 10(6), pp. 1453–1465. doi: 10.1016/S1097-2765(02)00781-5.

Tonkin, E. T. *et al.* (2004) 'NIPBL, encoding a homolog of fungal Scc2-type sister chromatid cohesion proteins and fly Nipped-B, is mutated in Cornelia de Lange syndrome', *Nature genetics*. Nat Genet, 36(6), pp. 636–641. doi: 10.1038/NG1363.

Tsukamoto, T. *et al.* (2000) 'Visualization of gene activity in living cells', *Nature Cell Biology 2000 2:12*. Nature Publishing Group, 2(12), pp. 871–878. doi: 10.1038/35046510.

Tumbar, T., Sudlow, G. and Belmont, A. S. (1999) 'Large-Scale Chromatin Unfolding and Remodeling Induced by VP16 Acidic Activation Domain', *Journal of Cell Biology*. The Rockefeller University Press, 145(7), pp. 1341–1354. doi: 10.1083/JCB.145.7.1341.

Ulianov, S. V. *et al.* (2016) 'Active chromatin and transcription play a key role in chromosome partitioning into topologically associating domains', *Genome research*. Genome Res, 26(1), pp. 70–84. doi: 10.1101/GR.196006.115.

Valton, A. L. *et al.* (2022) 'A cohesin traffic pattern genetically linked to gene regulation', *Nature Structural & Molecular Biology 2022 29:12*. Nature Publishing Group, 29(12), pp. 1239–1251. doi: 10.1038/s41594-022-00890-9.

Vassilev, L. T. (2006) 'Cell cycle synchronization at the G2/M phase border by reversible inhibition of CDK1', *Cell Cycle*, 5(22), pp. 2555–2556. doi: 10.4161/cc.5.22.3463.

Vermunt, M. W., Zhang, D. and Blobel, G. A. (2019) 'The interdependence of gene-regulatory elements and the 3D genome', *Journal of Cell Biology*. The Rockefeller University Press, 218(1), pp. 12–26. doi: 10.1083/JCB.201809040.

Vian, L. *et al.* (2018) 'The Energetics and Physiological Impact of Cohesin Extrusion', *Cell*. Cell Press, 173(5), pp. 1165-1178.e20. doi: 10.1016/J.CELL.2018.03.072.

Vietri Rudan, M. *et al.* (2015) 'Comparative Hi-C Reveals that CTCF Underlies Evolution of Chromosomal Domain Architecture', *Cell Reports*. Elsevier B.V., 10(8), pp. 1297–1309. doi: 10.1016/j.celrep.2015.02.004.

Wang, H., Han, M. and Qi, L. S. (2021) 'Engineering 3D genome organization', *Nature Reviews Genetics 2021 22:6*. Nature Publishing Group, 22(6), pp. 343–360. doi: 10.1038/s41576-020-00325-5.

Wang, S. *et al.* (2016) 'Spatial organization of chromatin domains and compartments in single chromosomes', *Science*. American Association for the Advancement of Science, 353(6299), pp. 598–602. doi: 10.1126/SCIENCE.AAF8084/SUPPL_FILE/WANG-SM.PDF.

Wang, X. *et al.* (2017) 'Bacillus subtilis SMC complexes juxtapose chromosome arms as they travel from origin to terminus', *Science*. American Association for the Advancement of Science, 355(6324), pp. 524–527. doi:

10.1126/science.aai8982.

Wang, Z. (2021) 'Regulation of Cell Cycle Progression by Growth Factor-Induced Cell Signaling', *Cells 2021, Vol. 10, Page 3327*. Multidisciplinary Digital Publishing Institute, 10(12), p. 3327. doi: 10.3390/CELLS10123327.

Wang, Z. *et al.* (2022) 'Prediction of histone post-translational modification patterns based on nascent transcription data', *Nature Genetics*. Springer US, 54(3), pp. 295–305. doi: 10.1038/s41588-022-01026-x.

Watrin, E. *et al.* (2006) 'Human Scc4 is required for cohesin binding to chromatin, sister-chromatid cohesion, and mitotic progression', *Current biology : CB*. Curr Biol, 16(9), pp. 863–874. doi: 10.1016/J.CUB.2006.03.049.

Wei, Y. *et al.* (1999) 'Phosphorylation of histone H3 is required for proper chromosome condensation and segregation', *Cell*. Cell, 97(1), pp. 99–109. doi: 10.1016/S0092-8674(00)80718-7.

Weintraub, A. S. *et al.* (2017) 'YY1 Is a Structural Regulator of Enhancer-Promoter Loops', *Cell*. Elsevier Inc., 171(7), pp. 1573-1588.e28. doi: 10.1016/j.cell.2017.11.008.

Weiss, W. A., Taylor, S. S. and Shokat, K. M. (2007) 'Recognizing and exploiting differences between RNAi and small-molecule inhibitors', *Nature chemical biology*. NIH Public Access, 3(12), p. 739. doi: 10.1038/NCHEMBIO1207-739.

Wendt, K. S. *et al.* (2008) 'Cohesin mediates transcriptional insulation by CCCTC-binding factor', *Nature*, 451(7180), pp. 796–801. doi: 10.1038/nature06634.

Whyte, W. A. *et al.* (2013) 'Master transcription factors and mediator establish super-enhancers at key cell identity genes', *Cell*. Elsevier Inc., 153(2), pp. 307–319. doi: 10.1016/j.cell.2013.03.035.

Widom, J. (1986) 'Physicochemical studies of the folding of the 100 Å nucleosome filament into the 300 Å filament: Cation dependence', *Journal of Molecular Biology*. Academic Press, 190(3), pp. 411–424. doi: 10.1016/0022-2836(86)90012-4.

Wilkins, B. J. *et al.* (2014) 'A cascade of histone modifications induces chromatin condensation in mitosis', *Science*. American Association for the Advancement of Science, 343(6166), pp. 77–80. doi: 10.1126/SCIENCE.1244508/SUPPL_FILE/WILKINS.SM.PDF.

Winter, G. E. *et al.* (2015) 'Phthalimide conjugation as a strategy for in vivo target protein degradation', *Science*. American Association for the Advancement of Science, 348(6241), pp. 1376–1381. doi: 10.1126/SCIENCE.AAB1433/SUPPL_FILE/AAB1433TABLES4.PDF.

de Wit, E. *et al.* (2015) 'CTCF Binding Polarity Determines Chromatin Looping', *Molecular Cell*. Cell Press, 60(4), pp. 676–684. doi: 10.1016/J.MOLCEL.2015.09.023.

de Wit, E. and Nora, E. P. (2022) 'New insights into genome folding by loop extrusion from inducible degron technologies', *Nature reviews. Genetics*. Nat Rev Genet. doi: 10.1038/S41576-022-00530-4.

Wong, K. H., Jin, Y. and Struhl, K. (2014) 'TFIIH Phosphorylation of the Pol II CTD Stimulates Mediator Dissociation from the Preinitiation Complex and Promoter Escape', *Molecular Cell*. Cell Press, 54(4), pp. 601–612. doi: 10.1016/J.MOLCEL.2014.03.024.

Wutz, G. *et al.* (2017) 'Topologically associating domains and chromatin loops depend on cohesin and are regulated by CTCF, WAPL, and PDS5 proteins', *The EMBO Journal*, 36(24), pp. 3573–3599. doi: 10.15252/embj.201798004.

Yamada, N. A. *et al.* (2011) 'Visualization of fine-scale genomic structure by oligonucleotide-based high-resolution FISH', *Cytogenetic and genome research*. Cytogenet Genome Res, 132(4), pp. 248–254. doi:

10.1159/000322717.

Yesbolatova, A. *et al.* (2019) 'Generation of conditional auxin-inducible degron (AID) cells and tight control of degron-fused proteins using the degradation inhibitor auxinole', *Methods*. Academic Press, 164–165, pp. 73–80. doi: 10.1016/J.YMETH.2019.04.010.

Yesbolatova, A. *et al.* (2020) 'The auxin-inducible degron 2 technology provides sharp degradation control in yeast, mammalian cells, and mice', *Nature Communications*. Nature Research, 11(1). doi: 10.1038/S41467-020-19532-Z.

Yudkovsky, N., Ranish, J. A. and Hahn, S. (2000) 'A transcription reinitiation intermediate that is stabilized by activator', *Nature*, 408(6809), pp. 225–229. doi: 10.1038/35041603.

Zhang, H. *et al.* (2019) 'Chromatin structure dynamics during the mitosis-to-G1 phase transition', *Nature*. Nature Research, 576(7785), pp. 158–162. doi: 10.1038/S41586-019-1778-Y.

Zhu, X. *et al.* (2006) 'Genome-Wide Occupancy Profile of Mediator and the Srb8-11 Module Reveals Interactions with Coding Regions', *Molecular Cell*. Cell Press, 22(2), pp. 169–178. doi: 10.1016/J.MOLCEL.2006.03.032.

Zhu, Y. *et al.* (2021) 'Calcium signaling instructs NIPBL recruitment at active enhancers and promoters via distinct mechanisms to reconstruct genome compartmentalization', *Genes and Development*, 35(1), pp. 65–81. doi: 10.1101/GAD.343475.120.

Zuin, J. *et al.* (2014) 'Cohesin and CTCF differentially affect chromatin architecture and gene expression in human cells', *Proceedings of the National Academy of Sciences of the United States of America*. National Academy of Sciences, 111(3), pp. 996–1001. doi: 10.1073/pnas.1317788111.

Acknowledgements

With these words my PhD journey is almost over. The last four years were marked by mostly good moments and I don't want to miss these memories. I am very grateful that this time broadened my horizon. I learned a lot about science, how to be a good boss and about life.

First, I need to thank Akis for the opportunity to join his lab. You are a smart, helpful, kind and respectful mentor. I was very lucky that you guided me through this journey and I am thankful you gave me a second chance for science. You encourage people, you make sure everyone is their best self and your door is always open. All this in combination with your curious and supportive character make you a great supervisor.

I am very grateful to Spiro. We started this journey together and we are also ending it together. It was very helpful to have you around since the beginning. We could support each other, shared many nice moments, and went through the same issues. It is always nice to have someone to talk to discuss about science, but also about life. Thanks for everything!

Sia, thank you so much for being in the lab and taking care of everyone. Whenever there was a problem you tried to solve it.

In general, I am happy to be part of this group. During the years I met many different people. Without my colleagues, this journey would not have been so exciting. Thanks to all other lab members for the nice and supportive work environment. We always had a good atmosphere, which alleviated failed experiments. Special thanks go to Adi, Ioanna, and Ilia. Without you the PhD experience would not have been the same. It is nice to know that there are new, great PhD students to continue the work and keep the lab a nice place to be. Sorry that I cannot write about everyone individually.

Also a big thank you goes to my TAC members Ufuk and Matthias for the scientific inputs during our meetings. I would also like to thank Dr. Marieke Oudelaar, Prof. Heidi Hahn and Prof. Elisabeth Hessmann for agreeing to be on my examination board committee.

Of course, this journey would not have been possible without the IMPRS-GS program. I enjoyed the interdisciplinary people, and would also like to thank for the financial support to go to Oxford. Special thanks go to Henriette and Frauke. You are always kind and supportive. Whenever anyone had a problem we could talk to you. This is an exceptional graduate school because of you both.

I am also very grateful for my old and new friendships. My friends contributed a lot to feel Göttingen as my home. I enjoyed all the time with everyone especially Manu, Eileen, Miri and Pat. Thanks to my best friends Eddie and Kathi who are always listening to me. Also special thanks to Christina. All of you were supporting me throughout this journey and hopefully beyond.

Papa, ohne dich wäre ich nie hierhergekommen. Du hast immer an mich geglaubt und mich unterstützt. Dafür bin ich dir sehr dankbar.

Und zum Schluss vielen Dank an Basti. Du hast die Zeit in Göttingen zu etwas Besonderem gemacht. Ohne dich wäre es nur halb so schön und ich bin froh, dass du damals auch nach Göttingen gekommen bist. Vielen Dank für all die Unterstützung und die schöne gemeinsame Zeit. Nach all dem Stress freue ich mich auf neue Abenteuer mit dir.